The Steered Auxiliary Beam Canceller for Interference Cancellation in a Phased Array

Andrew H. Zai

Thesis submitted to the faculty of the Virginia Polytechnic Institute and State University
in partial fulfillment of the requirements for the degree of

Master of Science
In
Electrical Engineering

Lamine M. Mili, Chair
Timothy Pratt
Amir I. Zaghloul

July 21, 2011
Falls Church, VA

Keywords: Steered Auxiliary Beam Canceller, Phased Array, Interference Cacnellation

The Steered Auxiliary Beam Canceller for
Interference Cancellation in a Phased Array

Andrew H. Zai

ABSTRACT

A common problem encountered in phased array signal processing is how to remove sources of interference from a desired signal. Two existing methods to accomplish this are the Linearly Constrained Minimum Variance (LCMV) beamformer and the Side-Lobe Canceller (SLC). LCMV provides better performance than SLC, but comes with much higher computational costs.

The Steered Auxiliary Beam Canceller (SABC) presented in this thesis is a new algorithm developed to improve the performance of SLC without the computational costs of LCMV. SABC performs better than SLC because it uses high-gain auxiliary channels for cancellation. This new technique is now possible because digital arrays allow for direction finding algorithms such as Estimation of Signal Parameters via Rotational Invariance Techniques (ESPRIT) to estimate the directions of the interference sources. With this added knowledge, high gain beams similar to the main beam may be used as auxiliaries instead of low-gain antenna elements.

Another contribution is a method introduced to calculate the computational complexity of LCMV, SLC, and SABC much more accurately than existing methods which only provide order-of-magnitude estimates. The final contribution is a derivation of the signal loss experienced by SLC and SABC and simulations that verify the performance of LCMV, SLC, and SABC.

Acknowledgements

Lindsey and my family

Dr. Lamine Mili

Dr. Timothy Pratt

Dr. Amir Zaghloul

Dr. Salvador Talisa

My other coworkers at
The Johns Hopkins University
Applied Physics Laboratory

Table of Contents

List of Figures

List of Tables

CHAPTER 1

INTRODUCTION

1.1 PROBLEM STATEMENT

This thesis addresses the problem of how to remove interference from a signal using adaptive spatial beamforming techniques. It includes an investigation of the best way to preserve a signal coming from one direction, while minimizing the effects of interfering signals coming from different directions. This is a fairly common problem in phased array signal processing, and radar in particular, with several well known solutions. Among these are the Side-Lobe Canceller (SLC) [33] and the Linearly Constrained Minimum Variance (LCMV) beamformer [21].

A phased array works by forming a beam with an array of antenna elements in a certain direction, thus causing high gain on the signal of interest. SLC consists of a low-gain auxiliary channel with a near uniform gain pattern over the steerable range of the main beam. With this configuration, any interference in the side lobe of the main beam may be subtracted out of the desirable signal in the main beam using the information in the auxiliary channel [33]. Of course the signal of interest will also be present in this auxiliary channel and some signal loss will occur when subtracting from the main beam. This loss is expected to be small because the gain in the main beam is much higher than that of the auxiliary channel.

In contrast to SLC, LCMV beamformer is a method for calculating the beamforming weights of an array. In conventional beamforming, the typical weights are

just those that will introduce a progressive time delay to each unit such that the array is steered to a certain direction. LCMV adaptively computes weights that will still steer the array in the desired direction but also have nulls in the directions of interference while minimizing main beam losses. It achieves the same objective as SLC, removing interference, but it also minimizes the losses to signal of interest [21].

Both techniques were first introduced a couple decades ago; however, SLC has been the only algorithm feasible for implementation in large systems with hundreds of elements due to the computational cost of LCMV [35]. While it may be more practical for implementation, SLC does not perform as well as LCMV because it causes signal loss and does not work well for main-beam interference as its name suggests. Computing hardware is much more mature today than when these algorithms were first proposed, making the implementation of LCMV more realizable in practice. Nevertheless, LCMV presents significant computational challenges when the array has many elements and for signals with wide bandwidth [31].

1.2 LITERATURE REVIEW

The ideas behind adaptive arrays for interference cancellation are not new. In fact, the first papers on the concept started to appear in the mid 1960's by its pioneers, some of whom were Widrow, Reed, Mallett, and Brennan [28][38][50]. A full text book was written on the subject in 1980 by Monzingo and Miller [34]. The implementation of the technology has lagged its conceptualization by several decades because the computing power did not exist at the time; however, there has been a major resurgence on the topic in the last decade because of advances in the required computational equipment.

Adaptive Filter Theory by Simon Haykin [21] is a widely referenced text and this paper will be no exception. Haykin provides a very pedagogical explanation of LCMV as well as a generalized side-lobe canceller. *Statistical and Adaptive Signal Processing* by Manolakis, Ingle, and Kogon [34] covers many of the same topics as Haykin, but also covers several direction of arrival algorithms as well as a side-lobe canceller using auxiliary channels. There is even a brief section about using formed beams for adaptive cancellation, but only when steered to directions with a priori information about the interference location and it does not apply direction of arrival algorithms to steer these beams [34].

Work has been done at Virginia Tech in the field of interference cancellation by Picciolo [54], Mathews[55], and Shoenig[56]. Mathews wrote a master's thesis which involved solving the LCMV weights without having to invert a covariance matrix. This is related to the problem of computational complexity but approaches it in a different manner than we do. Picciolo and Shoenig wrote dissertations about how to robustly estimate the covariance matrix used in adaptive processing. The covariance matrix in traditional adaptive processing assumes white, Gaussian interference. Adaptive algorithms break quickly when these assumptions are violated and both of these authors made significant contributions to help overcome this problem.

1.3 CONTRIBUTIONS OF THE AUTHOR

To overcome the weaknesses of SLC mentioned earlier, we propose a new method that allows for improvements in SLC performance while maintaining its relative computational simplicity. This method is termed the Steered Auxiliary Beam Canceller

(SABC). SABC operates in a fashion very similar to SLC; however, it uses high-gain beams steered in the direction of the interference instead of low gain auxiliary channels. This method reduces the signal loss because the amount of signal present in the high-gain auxiliary channel is much lower than the amount of interference, as would be the case with a low-gain auxiliary channel. Therefore, when the auxiliary channel is subtracted from the main beam, a significantly smaller amount of signal is lost.

The obvious requirement of SABC is that one must know the direction of the interference sources. The main enabler of SABC which was not available when SLC was introduced is digital array architecture. The traditional phased array used when SLC was introduced applies the required time delays for beamforming with analog equipment and adds the channels together, and then the sum is processed by the receiver. A digital array samples the signal received by each element and thus saves much more information about the environment in which the array is operating. One can implement direction-finding algorithms, such as Estimation of Signal Parameters via Rotational Invariance Techniques (ESPRIT) [11][34][40], on the digitized array data to determine the direction where interference sources are arriving from. This information may then be input to SABC, providing the required information for cancellation.

Another contribution is our characterization of LCMV, SLC, and SABC in terms of floating point operations, similar to Golub's [19] methodology for his algorithms. This is important because knowing the amount of operations required within a time budget will help to develop hardware requirements. Although the order of these problems is well understood [35], it is very general in that it only describes the growth of the

algorithms. Our method can describe the computations required for a very specific system.

Our final contribution is a derivation of the signal loss in SLC and SABC as well as simulations of LCMV, SLC, and SABC. This derivation mathematically shows why SABC performs better than SLC. Additionally, it shows why SABC calculates its adaptive weights better than SLC in the presence of noise. The simulations show that SABC outperforms SLC and as well as LCMV in certain circumstances.

1.4 OUTLINE OF THESIS

This thesis reviews the current interference cancellation methods and evaluates their computational cost and performance. It then introduces the new SABC techniques and compares it to the existing methods using the same metrics. Chapter 2 includes an overview of array beam steering and adaptive interference cancellation. Specifically, we define the geometric characteristics of the problem and explain the mathematics involved with both conventional beamforming and adaptive beamforming. Chapter 2 starts with a treatment of the simpler narrow-band problem and then extends the techniques to wide-band signals where the narrow-band assumptions break down. Chapter 3 provides an analysis of the existing techniques presented in Chapter 2. The computational cost and the performance in terms of interference cancellation and signal loss are addressed. In Chapter 4, we introduce the new SABC technique and investigate the computational and performance compromises it makes. Chapter 4 also includes a side-by-side comparison of all techniques discussed. Chapter 5 presents some simulation results that evaluate the performances of the proposed procedures and compare them to those of the current

methods. Finally, some concluding remarks are made and areas for future study are outlined. The narrow-band assumption and ESPRIT algorithm are reviewed in the appendices.

CHAPTER 2

BACKGROUND ON ARRAY BEAM FORMING

This chapter provides a background in array beamforming, both fixed and adaptive. First, it presents the geometrical formulation of beamforming that will be used throughout this thesis. Then, it reviews the assumptions applicable to narrow-band signals assumptions and examines the conditions under which the narrow-band assumption does not hold. Finally, it ends with a performance analysis of the adaptive beamforming for both narrow-band and wide-band situations.

2.1 GEOMETRICAL FORMULATION FOR BEAMFORMING

Consider a stationary planar phased array. The elements of this array are uniformly spaced and are restricted to the X-Y plane; therefore, any element in the array will have a displacement vector $\mathbf{r}_e = x_e\hat{\mathbf{i}} + y_e\hat{\mathbf{j}} + 0\hat{\mathbf{k}}$, where $\hat{\mathbf{i}}, \hat{\mathbf{j}}, and\ \hat{\mathbf{k}}$ are unit vectors in the x, y, and z directions, respectively, and the center of the array is located at the origin.

A desired signal source position will be specified in terms of its range, azimuth, and elevation by the symbols $|\mathbf{r}_d|$, θ_d, and ϕ_d, respectively. This is shown schematically in Figure 2-1.

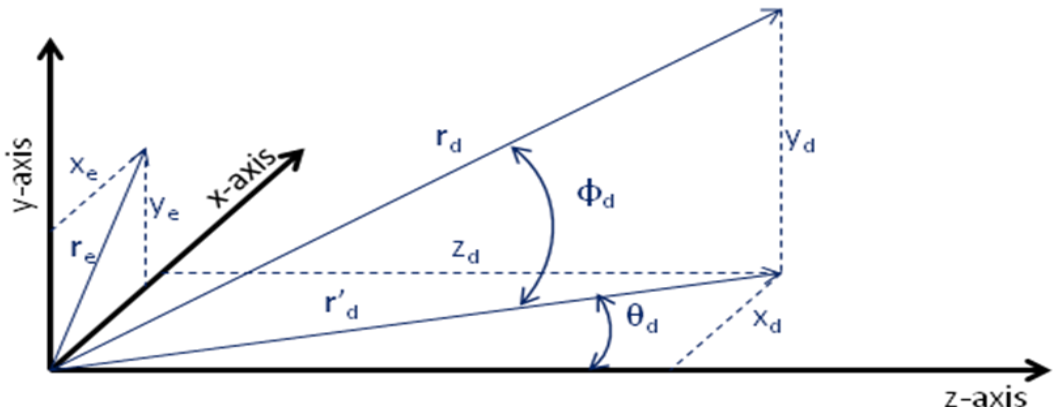

Figure 2-1 – Definitions of a desired signal vector, $\mathbf{r}_d$, and an element vector, $\mathbf{r}_e$.

It will be useful later to solve for the x, y, and z positions of a signal source. This can be done as follows:

$$|\mathbf{r}_d'| = |\mathbf{r}_d|\cos(\phi_d) \tag{2.1}$$

$$x_d = |\mathbf{r}_d'|\sin(\theta_d) = |\mathbf{r}_d|\cos(\phi_d)\sin(\theta_d) \tag{2.2}$$

$$y_d = |\mathbf{r}_d|\sin(\phi_d) \tag{2.3}$$

$$z_d = |\mathbf{r}_d'|\cos(\theta_d) = |\mathbf{r}_d|\cos(\phi_d)\cos(\theta_d) \tag{2.4}$$

Therefore, a desired signal source will have a displacement vector $\mathbf{r}_d = x_d\hat{\mathbf{i}} + y_d\hat{\mathbf{j}} + z_d\hat{\mathbf{k}}$.

2.2 FIXED BEAMFORMING

The process of forming beams in the direction of the desired signal source may be divided into two cases, depending on the bandwidth of the signal. This section shows

how a beam may be formed for both the narrow-band and wide-band cases. This section assumes the desired signal has an elevation of zero degrees.

2.2.1 Narrowband Beamforming

Consider the uniformly-spaced, M-element, linear array in Figure 2-2. A signal, x(t), is impinging upon the array from an azimuth angle, θ. The source of the signal is assumed to be far enough away that the rays of the signal approach as a plane wave.

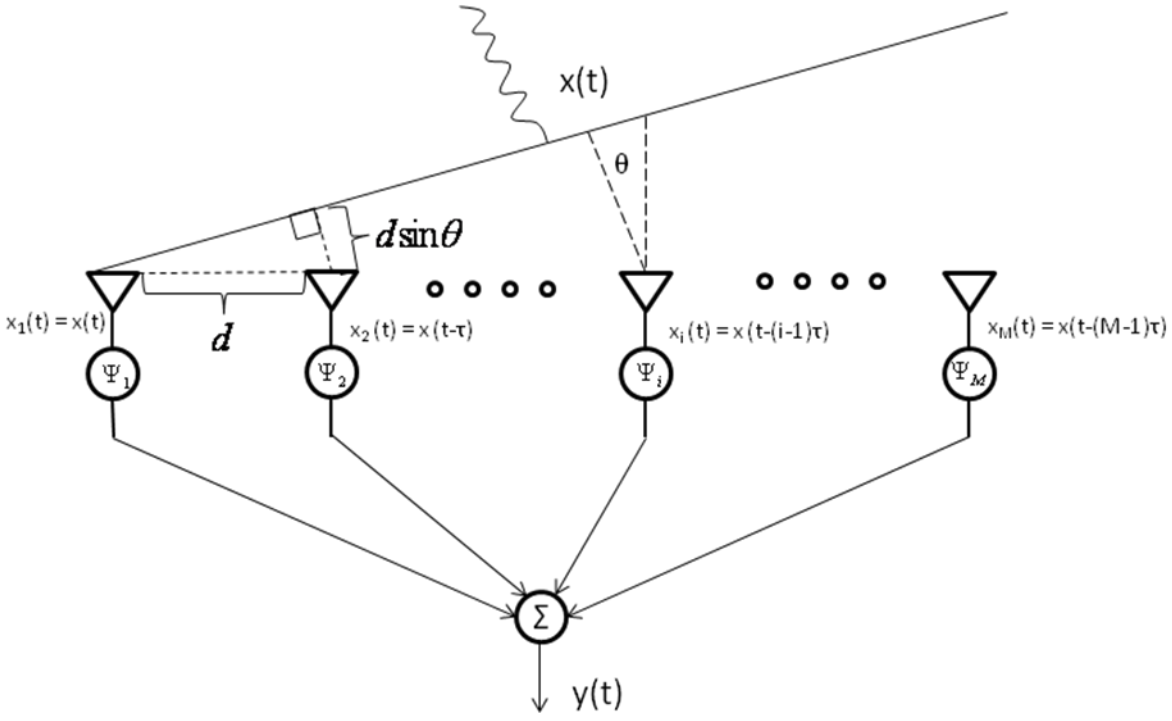

Figure 2-2 – The arrangement of a narrow-band uniform linear array. The array contains M elements with a uniform distance, d, between them. The signal, x(t), is arriving from an azimuth of θ relative to the boresight of the array. The symbol, Ψ, represents the phase shift applied to each element.

Since the elements are equally spaced by a distance d, there is a progressive time delay on x(t) received in each element. This time delay in the i[th] element can be represented by $x_i(t) = x_1(t-(i-1)\tau)$, where $\tau = \frac{d}{c}\sin(\theta)$ and c is the speed that the signal travels, or the speed of light in free space electromagnetic applications [39]. The signals in the elements may be modeled as shown below.

$$x_1(t) = e^{j2\pi f_0 t} \tag{2.5}$$

$$\begin{aligned} x_i(t) &= x_1(t-(i-1)\tau) \\ &= e^{j2\pi f_0 (t-(i-1)\tau)} \\ &= x_1(t)e^{-j2\pi f_0 (i-1)\tau} \end{aligned} \tag{2.6}$$

One can see from the result in (2.6) that the delay in the i[th] element manifests itself as a phase shift shown below.

$$\Psi_i(t) = e^{-j2\pi f_0 (i-1)\tau} \tag{2.7}$$

An array can take advantage of the fact that the signal received at each element is a delayed version of the signal of interest to coherently add them and increase the signal-to-noise ratio. Equation (2.8) shows that an array output, y(t), may be solved to increase the received signal voltage by a factor of M when each element is multiplied by the complex conjugate of its phase delay.

$$\begin{aligned} y(t) &= \sum_{i=1}^{M} x_i(t-(i-1)\tau) * e^{j2\pi f_0 (i-1)\tau} \\ &= \sum_{i=1}^{M} x(t)e^{-j2\pi f_0 (i-1)\tau} e^{j2\pi f_0 (i-1)\tau} = Mx(t) \end{aligned} \tag{2.8}$$

The notation in (2.8) may be simplified into vector notation as follows:

$$y(t) = \mathbf{w}_f(\theta_0)^H x(t)\mathbf{s}(\theta_0) \tag{2.9}$$

where $\mathbf{w}_f = \begin{bmatrix} 1 & e^{-j2\pi f_0 \tau} & \cdots & e^{-j2\pi f_0 (M-1)\tau} \end{bmatrix}^T$ is the weight vector of the array, $x(t)$ is the signal, $\mathbf{s}(\theta_0) = \begin{bmatrix} 1 & e^{-j2\pi f_0 \tau} & \cdots & e^{-j2\pi f_0 (M-1)\tau} \end{bmatrix}^T$ is the steering vector for the signal, and $\mathbf{a}^H$ represents the conjugate transpose of a vector [39]. The weight vector can also have a non-uniform magnitude taper applied to if for side-lobe control, but this thesis uses a uniform taper.

The result from (2.9) is what is known as fixed beamforming because the array is forming an antenna pattern that is focused in the direction of θ_0. The gain of the array will be highest for a signal coming from a direction of θ_0 because the inner product of the steering vector and weight vector's conjugate will be M and results in an M-times gain of the signal. The gain of a signal from any direction may be solved by taking this inner product using that signal's steering vector. It is well known that the pattern for these gains takes the shape of a sinc function known as the array factor [39][42]. Equation 2.10 shows the well known equation for calculating the array factor of a narrowband array where λ_0 is the wavelength of the carrier wave.

$$AF(\theta) = \frac{\sin\left[M\pi \frac{d}{\lambda_0}\left(\sin\theta - \sin\theta_0\right)\right]}{M\sin\left[\pi \frac{d}{\lambda_0}\left(\sin\theta - \sin\theta_0\right)\right]} \tag{2.10}$$

2.2.2 Wideband Beamforming

Up to this point it was assumed that the signal was narrow-band, meaning that it consisted of only one frequency, and had infinite duration. These assumptions may be relaxed to include a signal with a small bandwidth relative to the carrier frequency and a long duration relative to the size of the array. The breakdown point of the bandwidth assumption is discussed in Appendix A.

Once these assumptions are no longer valid, it is not possible to imitate a delay using a phase shift. Instead, the elements that receive the signal first must have their responses delayed to line up with the elements that receive the signal later. Current systems implement this time delay using analog delay lines. While this works reasonably well, they take up a lot of space, are costly, and only allow for a finite number of predesigned steering angles. In digital arrays, the appropriate delay can be synthesized digitally at each element with high resolution.

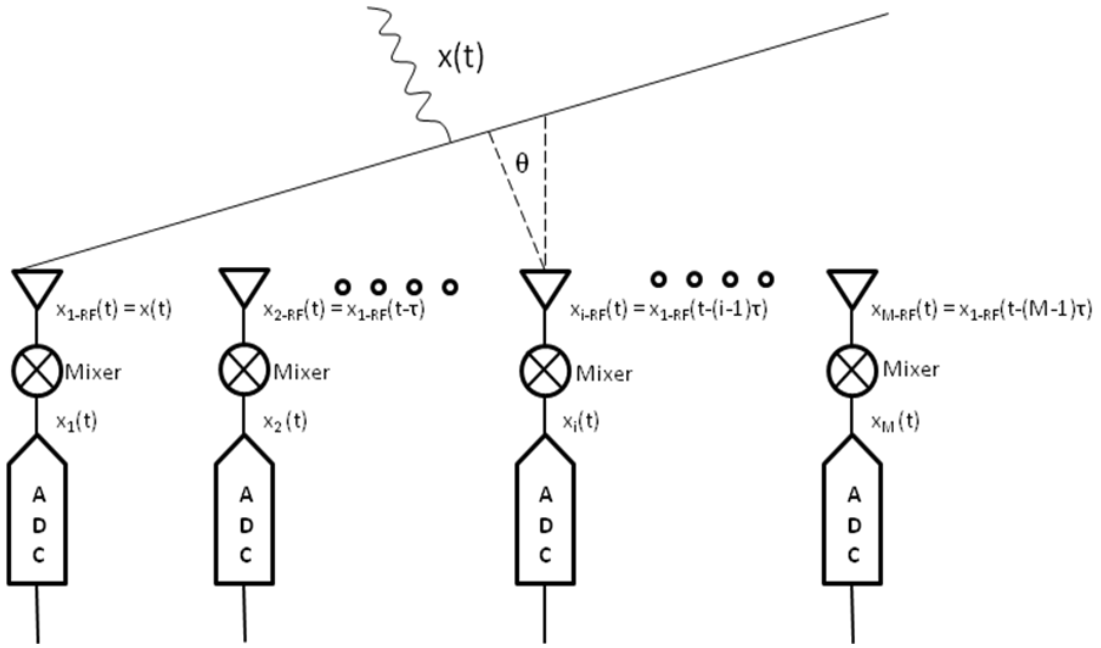

Figure 2-3 – The arrangement of a digital uniform linear array. The array contains M elements with a uniform distance, d, between them. The signal, x(t), is arriving from an azimuth of θ. The signal received by each element is down-converted by a mixer and sampled by an analog-to-digital converter (ADC).

Figure 2-3 shows the architecture for a digital array. Each element of the array receives a wide-band signal at a radio frequency. It is necessary to down-convert these radio frequencies to baseband frequencies so that the analog-to-digital converters don't need such a high sampling rate. Once the element's signals are digitized, they may be processed with computing hardware to implement the delays required for beamforming.

In order to understand how to delay the i^{th} signal, it will again be compared to various signals in the array. The signal received by the first element is:

$$\begin{aligned} x_1(t) &= x_{1-RF}(t)e^{-j2\pi f_{RF}t} \\ &= x(t)e^{j2\pi f_{RF}t}e^{-j2\pi f_{RF}t} = x(t) \end{aligned} \tag{2.11}$$

and the signal received by the i^{th} element is:

$$\begin{aligned} x_i(t) &= x_{i-RF}(t-(i-1)\tau)e^{-j2\pi f_{RF}t} \\ &= x(t-(i-1)\tau)e^{j2\pi f_{RF}(t-(i-1)\tau)}e^{-j2\pi f_{RF}t} \\ &= x(t-(i-1)\tau)e^{-j2\pi f_{RF}(i-1)\tau} \end{aligned} \tag{2.12}$$

These signals may be analyzed in the frequency domain to understand how to implement the delay [37].

$$X_1(f) = F\{x(t)\} = X(f) \tag{2.13}$$

$$\begin{aligned} X_i(f) &= F\{x_i(t)\} \\ &= F\left\{x_1(t-(i-1)\tau)e^{-j2\pi f_{RF}(i-1)\tau}\right\} \\ &= X(f)e^{-j2\pi f(i-1)\tau}e^{-j2\pi f_{RF}(i-1)\tau} \\ &= X(f)e^{-j2\pi(f+f_{RF})(i-1)\tau} \end{aligned} \tag{2.14}$$

One can see in (2.14) that the result is the same as (2.13) with a frequency dependent phase shift. If the narrowband assumptions are no longer valid, one must find a way to simulate the frequency dependent multiplication of (2.14).

The time delay modeled in (2.12) can be implemented using frequency domain processing [37]. This requires that the ADCs in Figure 2-3 save the information for a period of time and perform batch processing on the data. For the purposes of this paper, the ADCs sample the signal at a rate of f_s Hertz and save K samples T_s seconds apart. Once the K samples are saved into a [K x 1] vector, a Fourier Transform is performed upon it and it is multiplied by the appropriate frequency dependent complex weights as shown below:

$$\mathbf{x}_i = \begin{bmatrix} x_i(t-(K-1)T_s \\ \vdots \\ x_i(t-T_s) \\ x_i(t) \end{bmatrix} \tag{2.15}$$

$$\mathbf{x}_{i-delayed} = F^{-1}\left\{ \begin{bmatrix} X_i(0) \\ X_i(\frac{f_s}{K}) \\ X_i(\frac{2f_s}{K}) \\ \vdots \\ X_i(\frac{f_s}{2}) \\ X_i(-\frac{f_s}{2}+\frac{f_s}{K}) \\ \vdots \\ X_i(\frac{-f_s}{K}) \end{bmatrix} \odot \begin{bmatrix} e^{-j2\pi(0+f_{RF})(i-1)\tau} \\ e^{-j2\pi(\frac{f_s}{K}+f_{RF})(i-1)\tau} \\ e^{-j2\pi(\frac{2f_s}{K}+f_{RF})(i-1)\tau} \\ \vdots \\ e^{-j2\pi(\frac{f_s}{2}+f_{RF})(i-1)\tau} \\ e^{-j2\pi(-\frac{f_s}{2}+\frac{f_s}{K}+f_{RF})(i-1)\tau} \\ \vdots \\ e^{-j2\pi(\frac{-f_s}{K}+f_{RF})(i-1)\tau} \end{bmatrix} \right\} \tag{2.16}$$

where $X_i(k)$ is the k[th] frequency component of the Fourier transform of vector $\mathbf{x}_{i-t}$ and $\odot$ is the operator for element wise vector multiplication. This operation can be done on M-1 elements so that they all have the same delay as the M[th] element. From there, they may all be added together to form a beam in the direction corresponding to the delay τ. One thing to note is that a wideband array does not remove the delay of the last element by shifting it forward; instead, it delays the first elements to receive the signal until they are even in time with the last element. This is done because it is a causal system and cannot operate on future signal values.

2.2.3 Delays in a Planar Array

The last two sections have assumed that the array is a linear one where all of the elements lie on the x-axis. The ideas just presented can be extended to a planar array with all the elements lying in the x-y plane. In a planar array, the delay will be a function of the distance between two elements along the x-axis and y-axis. To be exact, $\tau = \Delta x \sin(\theta)\cos(\phi) + \Delta y \sin(\phi)$, with Δx and Δy being the spacing between the i^{th} element and the last element to receive the signal in the x-dimension and y-dimension respectively.

2.3 ADAPTIVE INTERFERENCE CANCELLATION

Up until this point, only the concept of fixed beamforming has been considered, in which the progressive delay at each array element is set to maximize a signal coming from a certain direction. In adaptive beam forming, one is interested in maximizing a signal from a certain direction while minimizing the effects of interference from other angles. The discussion will start with LCMV, and then move to SLC. Once again, the discussion will start with the narrowband case then extend the solution to a wideband scenario.

2.3.1 The Linearly Constrained Minimum Variance Beamformer

Equation (2.9) showed that the fixed weights needed for an M-times improvement in signal voltage were simply the steering vector of the signal of interest. This result gives the maximum gain that can be experienced by the array for a signal with that steering vector; however, it does not take into account the interference caused by signals

from other directions. A better weighting may be applied to the elements of the array, known as LCMV.

As the name implies, LCMV is found by minimizing the variance of the output signal, y(t), and thus minimizing the noise power in y(t). The trivial way to solve this problem would be to apply a weight of zero to each element of the array and thus have y(t) = 0. This is of no interest because while there may be no noise, there is also no signal. For this reason, at least one constraint must be imposed on the optimization.

It was shown by Frost [14] that the output of a beamformer with weights, **w**, will have an output variance of:

$$E\left\{\left|y(t)\right|^2\right\} = \mathbf{w}^H R\mathbf{w} \tag{2.17}$$

where

$$R = E\left\{\mathbf{x}(t)\mathbf{x}(t)^H\right\} \tag{2.18}$$

is the correlation matrix for the array's element signals. LCMV problem is solved by finding the weights that minimize the output variance subject to constraints chosen by the designer [21]. This is formulated in the equation below.

$$\mathbf{w} = \arg\min_{\mathbf{w}} \mathbf{w}^H R\mathbf{w} \quad subject\ to \quad \mathbf{s}(\theta)^H \mathbf{w} = G_0^* \tag{2.19}$$

The constraint in (2.19) is that the inner product of a chosen steering vector and the weight vector is equal to a complex value, G_0^*. The value of G_0^* can be any complex value, but the derivation is simplest when one solves for the constraint as unity. By

constraining the weights in this manner, one ensures that the signal of interest will incur minimal losses. With this constraint, (2.19) is reformulated as:

$$\mathbf{w} = \arg\min_{\mathbf{w}} \mathbf{w}^H R\mathbf{w} \quad subject\ to \quad \mathbf{s}(\theta_0)^H \mathbf{w} = 1 \tag{2.20}$$

Equation (2.20) may be solved using the method of Lagrange multipliers [21]. This is done as shown below by creating a cost function, $J(\mathbf{w})$, and solving for its minimum.

$$J(\mathbf{w}) = \mathbf{w}^H R\mathbf{w} + \lambda^* \left[\mathbf{w}^H \mathbf{s}(\theta_0) - 1\right] + \lambda \left[\mathbf{s}(\theta_0)^H \mathbf{w} - 1\right] \tag{2.21}$$

In (2.21), λ is the Lagrange multiplier. The cost function may be minimized by differentiating with respect to $\mathbf{w}^*$, λ, and λ^* then solving for the weights where the derivative is zero as shown below [21].

$$\frac{\partial}{\partial \mathbf{w}^*} J(\mathbf{w}) = R\mathbf{w} + \lambda^* \mathbf{s}(\theta_0) = 0 \tag{2.22}$$

$$\mathbf{w} = -\lambda^* R^{-1} \mathbf{s}(\theta_0) \tag{2.23}$$

The value of λ is unknown, so it must be solved as shown below.

$$-\lambda^* = \mathbf{s}(\theta_0)^H \mathbf{w} (\mathbf{s}(\theta_0)^H R^{-1} \mathbf{s}(\theta_0))^{-1} \tag{2.24}$$

When (2.21) is differentiated with respect to λ and set equal to zero, one finds that $\mathbf{s}(\theta_0)^H \mathbf{w} = 1$, which is the constraint. This may be used to solve for λ and (2.23) can be simplified to:

$$\mathbf{w} = \frac{R^{-1}\mathbf{s}(\theta_0)}{\mathbf{s}(\theta_0)^H R^{-1}\mathbf{s}(\theta_0)} \tag{2.25}$$

Equation (2.25) states that the adaptive weights are simply the inverse of the interference correlation matrix multiplied by the steering vector towards an angle of interest and normalized by the term in the denominator. This solution will ensure that a signal coming from an angle θ_0 will be preserved while all other sources of interference are minimized. It is shown through simulation in Chapter 5 that LCMV is very effective for side-lobe cancellation; however, it suffers losses as the interference moves into the main beam. It will be shown in Chapter 3 that this may not be a practical solution because of computational considerations. For this reason, another approach to interference cancelation will be introduced in the next section.

It should be emphasized that the correlations matrices used in the adaptive interference cancellation algorithms represented the true correlation matrices not known to a practical system. The true value is a mathematical construct that must be estimated in real systems. This may be done by using training samples of the interference. The more samples used to estimate the correlation matrix, the more accurate this estimate will be; however, it is very important that the signal of interest is not included in the training data for it will cause further errors.

2.3.2 The Side Lobe Canceller

LCMV requires the use of a digital array with the goal of solving an adaptive weight for each element such that interference is minimized. SLC takes a different

approach with the goal of saving on computational costs but sacrificing performance and does not require a digital array. For an SLC, one only needs to digitize the main beam and the auxiliary channels. This results in fewer channels to process and is the reason why SLC is less complex than LCMV. The architecture for SLC is shown below in Figure 2-4 [33].

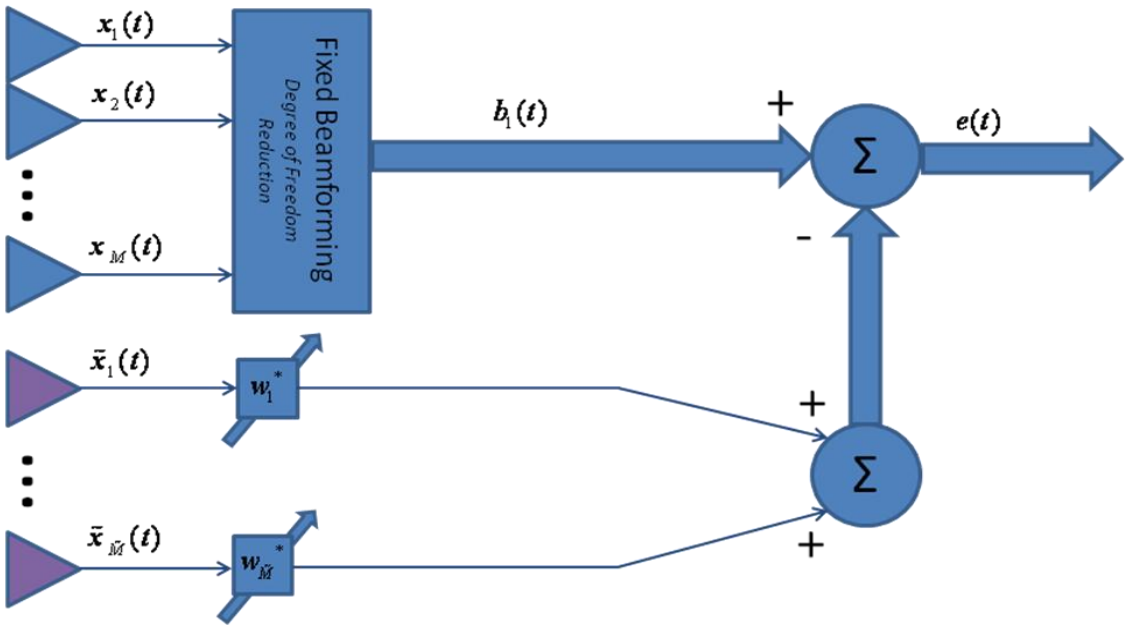

Figure 2-4 – The architecture for a side lobe canceller consists of a main array of M elements which form the beam, b(t), using a fixed beamformer. The array also has $\tilde{M}$ auxiliary channels which are weighted and subtracted from the main beam.

The architecture shown in this figure has two parts: the main array and auxiliary elements denoted with the tilde. The elements of the main array are weighted with the fixed weights of (2.9) to form beams in directions of interest. The auxiliary channels are each composed of only one element and thus have a much lower gain than a main beam. Each

auxiliary element is weighted with an adaptive weight and then subtracted out of the main beam to form an error signal. The goal of the side lobe canceller is to solve the weights that will minimize the error signal, e(t). In this arrangement, the error is the difference between the main beam and the weighted auxiliary channels. If it happens that there is an interfering signal in both the main beam and the auxiliary channels, minimizing the error will effectively subtract the interference out of the main beam. The first step in minimizing the error signal is to again create a cost function as shown below.

$$\begin{aligned} J &= E\left[e(t)e(t)^* \right] \\ &= E\left[\left(b(t) - \sum_{m=1}^{\tilde{M}} w_m{}^* \tilde{x}_m(t) \right) \left(b(t) - \sum_{m=1}^{\tilde{M}} w_m{}^* \tilde{x}_m(t) \right)^* \right] \\ &= \sigma_b^2 - \mathbf{w}^H E\left[\tilde{\mathbf{x}}(t) b(t)^* \right] - \mathbf{w}^T E\left[\tilde{\mathbf{x}}(t)^* b(t) \right] + \mathbf{w}^H E\left[\tilde{\mathbf{x}}(t) \tilde{\mathbf{x}}(t)^H \right] \mathbf{w} \\ &= \sigma_b^2 - \mathbf{w}^H \mathbf{r}_{bx} - \mathbf{w}^T \mathbf{r}_{bx}{}^* + \mathbf{w}^H R_a \mathbf{w} \end{aligned} \tag{2.26}$$

In (2.26), $\mathbf{r}_{bx} = E\left[\tilde{\mathbf{x}}(t) b(t)^* \right]$ is the correlation vector between the beam and the auxiliary channels and $R_a = E\left[\tilde{\mathbf{x}}(t) \tilde{\mathbf{x}}(t)^H \right]$ is the correlation matrix of the auxiliary channels. In order to minimize the cost function one must take the derivative with respect to the conjugate of the adaptive weight vector.

$$\begin{aligned} &\frac{\partial}{\partial \mathbf{w}^*} J(\mathbf{w}) = -\mathbf{r}_{bx} + R_a \mathbf{w} = 0 \\ &\mathbf{w} = R_a{}^{-1} \mathbf{r}_{bx} \end{aligned} \tag{2.27}$$

The output of the canceller is given by $y(t) = b(t) - \mathbf{w}^H \tilde{\mathbf{x}}(t)$. For a single instance in time y(t) is the same as e(t), but y(t) is the output of SLC whereas e(t) is used only for solving

the auxiliary weights. Equation (2.27) shows that the adaptive weights for the auxiliaries may be solved by multiplying the inverse of the auxiliary correlation matrix by the correlation vector. This structure is similar to a Weiner filter [21] where the beam of SLC acts as the desired signal in the Weiner filter.

SLC will remove the $\tilde{M}$ strongest signals that are present in both the main and auxiliary channels. If it so happens that there are more auxiliary channels than interference sources, and a desired signal is present in the training data, the desired signal will also be filtered out. This is why it is very important to make sure that the desired signal is masked or not present in the training data for (2.27).

2.4 WIDEBAND ADAPTIVE INTERFERENCE CANCELATION

The previous section was addressing the problem of cancelling an interference source while preserving a signal of interest. This was done by either finding the weights that formed an antenna pattern with nulls in the directions of the interference, or by finding the weight for an auxiliary channel that would subtract out the contribution of the interference. However, both of these solutions assumed that the signal of interest and the interference fulfilled the narrowband assumption and could be handled with weightings that were mere phase shifts. Much like with a fixed weight beamformer, each channel whether an auxiliary or main, requires more than one weight for a wideband situation. The two methods to implement wideband adaptive interference cancelation are with sub-bands or temporal taps for each channel. These two methods are discussed in the next few sections.

2.4.1 Wideband LCMV with Time Delay Units

The first option for adaptive wide-band beamforming is to use the LCMV structure with several complex weights applied to each element instead of just one [31]. The weights are applied to the N most recent samples of $x_i(t)$ as shown in Figure 2-5. This effectively places a finite impulse response filter after each element to implement the frequency response required of them for an adaptive response that emphasizes a desired wide-band signal and rejects wide-band interference.

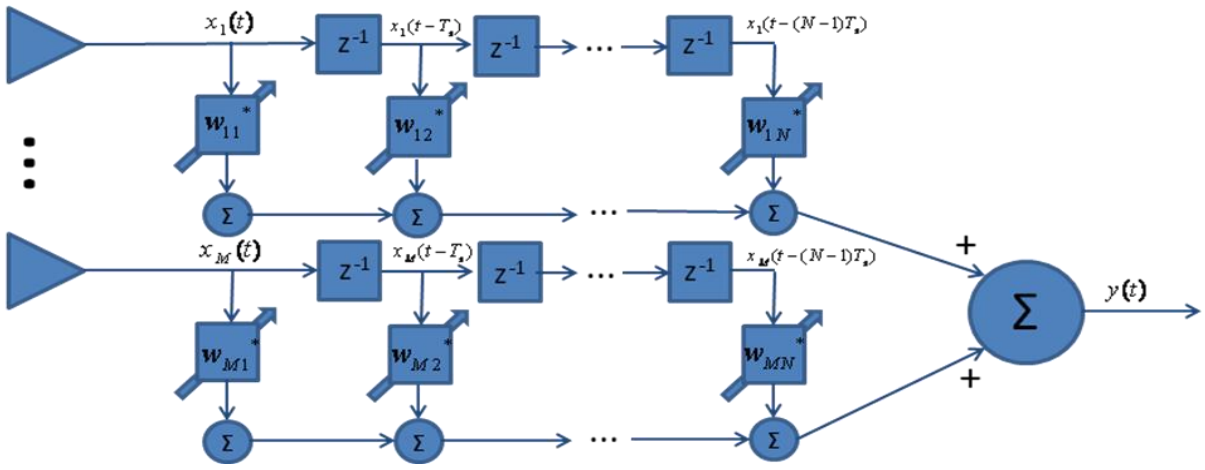

Figure 2-5 – LCMV with time taps. The output, y(t), is the weighted sum of N taps of M elements.

With the addition of the taps, the weight vector now takes the form of $\mathbf{w} = \begin{bmatrix} w_{11} & w_{21} & \cdots & w_{M1} & w_{12} & \cdots & w_{MN} \end{bmatrix}^T$. The delay that is needed to be removed by any weight is now a function of the steering angle and how many time delay units the signal has experienced. Instead of the delay seen previously, the delay is now $\tau = \frac{d}{c}\sin(\theta_0) + (n-1)T_s$ where n is the second number in the weight's subscript. With

this structure, a steering vector for a signal will be dependent on frequency and angle of arrival as shown:

$$\mathbf{s}(\theta_0, f_0) = \begin{bmatrix} 1 \\ e^{-j2\pi f_0(\frac{d}{c}\sin\theta_0)} \\ \vdots \\ e^{-j2\pi f_0(\frac{d}{c}(M-1)\sin\theta_0)} \\ e^{-j2\pi f_0(T_s)} \\ e^{-j2\pi f_0(\frac{d}{c}\sin\theta_0+T_s)} \\ \vdots \\ e^{-j2\pi f_0(\frac{d}{c}(M-1)\sin\theta_0+(N-1)T_s)} \end{bmatrix} \tag{2.28}$$

Notice that a wide-band signal cannot be described by a single steering vector because of its frequency dependence.

Now that the weight vector and steering vector are defined, the weights may be solved for an adaptive wideband array. Equation (2.20) is a starting point for the design of the weights, but since a range of frequencies must now be constrained a new equation is now necessary. Equation (2.29) is this new optimization where $C = \left[\mathbf{s}(\theta_0, f_1) \quad \cdots \quad \mathbf{s}(\theta_0, f_F)\right]$ is the constraint matrix and $\mathbf{g} = \left[1 \quad \cdots \quad 1\right]^T$ is the constraint vector.

$$\mathbf{w} = \arg\min_{\mathbf{w}} \mathbf{w}^H R\mathbf{w} \quad \textit{subject to} \quad C^H\mathbf{w} = \mathbf{g} \tag{2.29}$$

If the method of Lagrange multipliers is again used to solve this equation a result similar to (2.25) is found and is as follows:

$$\mathbf{w} = R^{-1}C\left(C^H R^{-1}C\right)\mathbf{g} \tag{2.30}$$

An important part of the result in (2.30) is how many frequencies, F, are used in the constraint matrix. Any signal consisting of more than one exact frequency is going to contain an infinite number of frequency components, but the constraint matrix can only contain a finite number in practice. For this reason, it is reasonable to segment the frequency range of the signal into portions that satisfy the narrowband assumption and use their steering vectors to build the constraint matrix. By making the narrowband assumption, there are portions of the signal band that are distorted; however, one may still achieve very good performance with this method.

2.4.2 The Sub-banded LCMV Beamformer

The next way to processes a wideband problem is to break it up into several independent problems, each of them satisfying the narrowband assumption. Figure 2-6 shows this process. The signal received by each of the M elements is passed through a filter bank and results in N band-pass signals, for a total of MN signals.

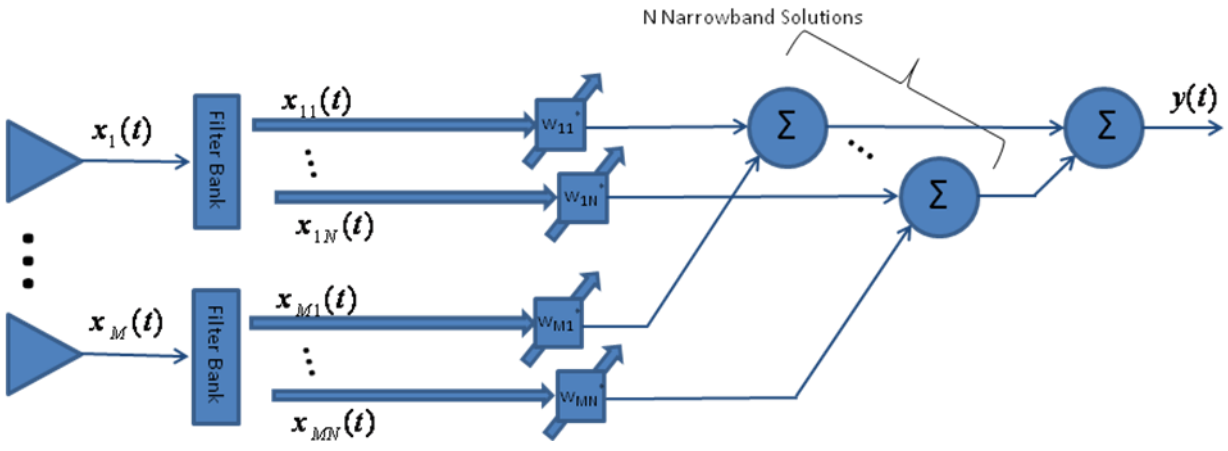

Figure 2-6 – LCMV split into sub-bands. The output, y(t), is the weighted sum of MxN channels. Each channel is a band-pass portion of the signal received by an element.

Once split into band-pass signals, the portions that share the same frequency are processed together using (2.25). The spacing of the array is fixed so each band-pass portion will have its own steering angle. Equation (2.31) shows how to solve the weights for each of the sub-bands.

$$\mathbf{w}_n = \frac{R_n^{-1}\mathbf{s}(\theta_{0-n})}{\mathbf{s}(\theta_{0-n})^H R_n^{-1}\mathbf{s}(\theta_{0-n})} \quad for\ n = 1, 2, ..., N \tag{2.31}$$

Much like before $\mathbf{s}(\theta_{0-n}) = \begin{bmatrix} 1 & e^{-j2\pi f_n \tau} & \cdots & e^{-j2\pi f_n (M-1)\tau} \end{bmatrix}^T$ with the steering vector being dependent on the center frequency for each sub-band. The resulting signal is the summation of the sub-bands with these adaptive weights applied is as follows:

$$y(t) = \sum_{n=1}^{N} \mathbf{w}_n{}^H \mathbf{x}_n(t) \tag{2.32}$$

with $\mathbf{w}_n = \begin{bmatrix} w_{1n} & w_{2n} & \cdots & w_{Mn} \end{bmatrix}^T$ and $\mathbf{x}_n(t) = \begin{bmatrix} \mathbf{x}_{1n}(t) & \mathbf{x}_{2n}(t) & \cdots & \mathbf{x}_{Mn}(t) \end{bmatrix}^T$.

2.4.3 Wideband Side Lobe Cancellation with Time Delay Units

SLC also has two approaches to wideband cancellation similar to those of LCMV. The first approach is to use time delay units in the auxiliary channels as shown in Figure 2-7. This architecture assumes that a main channel beam is formed using wideband fixed beamforming with the weights of the auxiliary channels being solved to minimize the error signal coming out of the canceller.

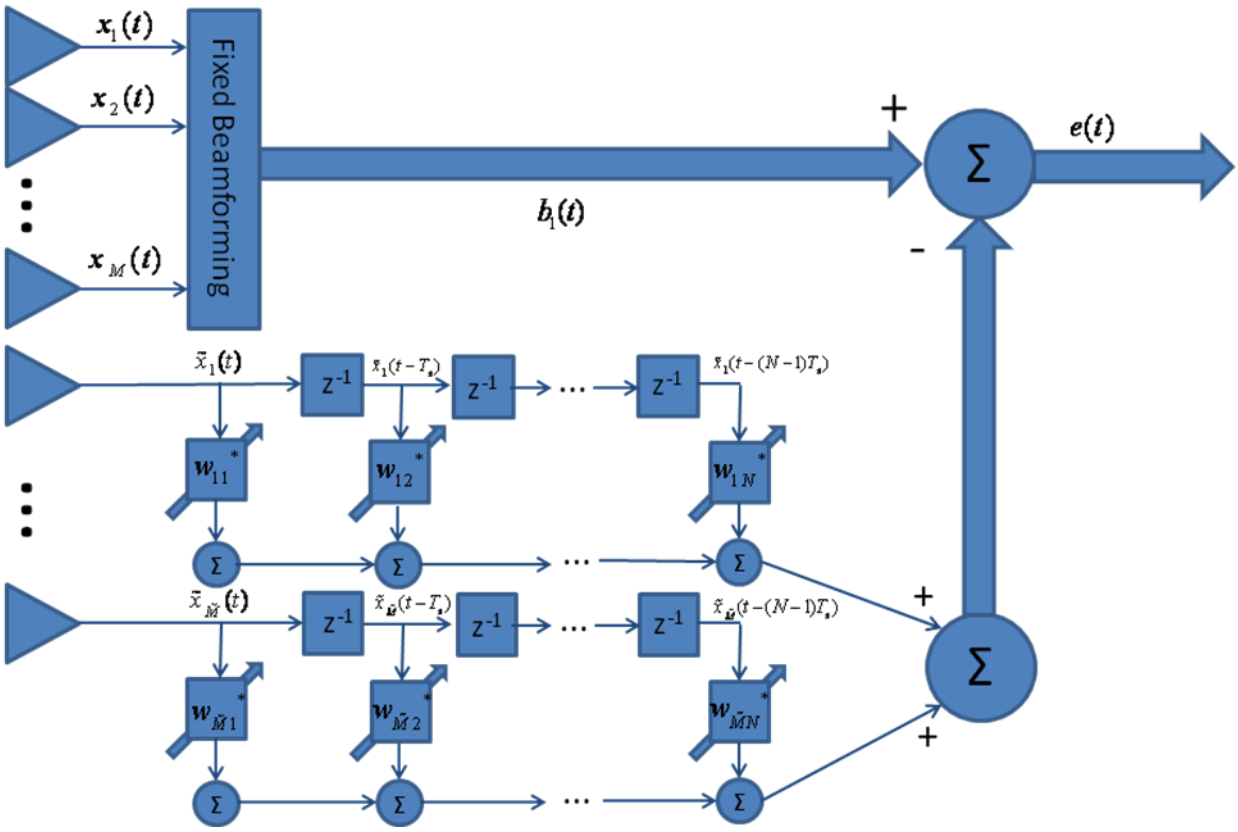

Figure 2-7 – Wideband side lobe canceller with time delay units. The weights are solved to minimize the error between the main beam, b(t), and the auxiliary channels using N time taps.

The cost function is almost identical to that of (2.26); however, the wideband error signal has an added component caused by the time difference between an auxiliary tap and the main beam.

$$J = E\left[e(t)e(t)^*\right]$$
$$= E\left[\left(b(t) - \sum_{n=1}^{N}\sum_{m=1}^{\tilde{M}} w_{mn}{}^* \tilde{x}_m(t-(n-1)T_s)\right)\left(b(t) - \sum_{n=1}^{N}\sum_{m=1}^{\tilde{M}} w_{mn}{}^* \tilde{x}_m(t-(n-1)T_s)\right)^*\right] \quad (2.33)$$

Equation (2.33) is the expression for the cost function of the wideband SLC and is dependent on the weights chosen. It is easier to work with (2.33) in vector-matrix notation and is shown below.

$$J(\mathbf{w}) = \sigma_b^2 - \mathbf{w}^H \mathbf{r}_{bx} - \mathbf{w}^T \mathbf{r}_{bx}^{\ *} + \mathbf{w}^H R_a \mathbf{w} \tag{2.34}$$

$$\mathbf{w} = \begin{bmatrix} w_{11} \\ w_{21} \\ \vdots \\ w_{\tilde{M}1} \\ w_{12} \\ \vdots \\ w_{\tilde{M}N} \end{bmatrix} \tag{2.35}$$

$$\mathbf{r}_{bx} = E\left\{ \begin{bmatrix} \tilde{\mathbf{x}}(t) \\ \tilde{\mathbf{x}}(t-T_s) \\ \vdots \\ \tilde{\mathbf{x}}(t-(N-1)T_s) \end{bmatrix} b(t)^* \right\} \tag{2.36}$$

$$R_a = E\left\{ \begin{bmatrix} \tilde{\mathbf{x}}(t) \\ \tilde{\mathbf{x}}(t-T_s) \\ \vdots \\ \tilde{\mathbf{x}}(t-(N-1)T_s) \end{bmatrix} \begin{bmatrix} \tilde{\mathbf{x}}(t) \\ \tilde{\mathbf{x}}(t-T_s) \\ \vdots \\ \tilde{\mathbf{x}}(t-(N-1)T_s) \end{bmatrix}^H \right\} \tag{2.37}$$

Once again, the cost function is minimized by taking the derivative of (2.34) with respect to w^*. Since the (2.34) is framed the same way as (2.26), the result is the same; therefore, if the vectors and matrices are structured properly, the weights required for the wideband SLC are:

$$\mathbf{w} = R_a^{\ -1} \mathbf{r}_{bx} \tag{2.38}$$

2.4.4 The Sub-banded Wideband Side Lobe Canceller

The last architecture that will be reviewed in this section is the sub-banded SLC. As one might guess, it is very similar to a sub-banded LCMV as far as how the wide-band nature of the problem is handled. Again, the wideband signal is filtered into narrowband components that are processed independently of one another. Figure 2-8 shows the architecture of this canceller.

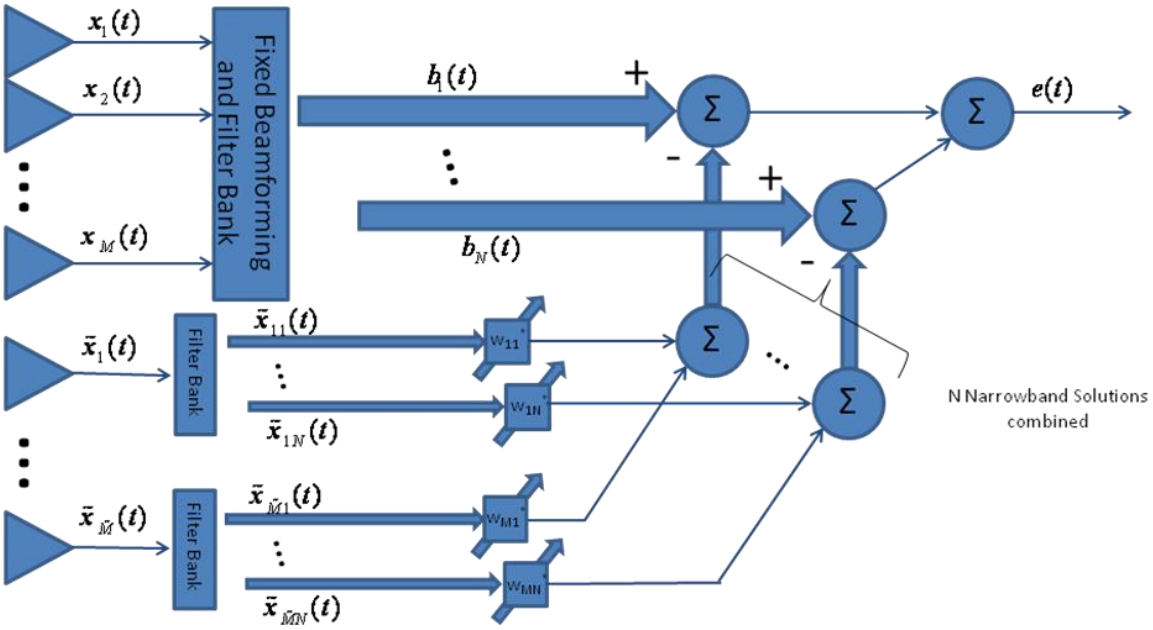

Figure 2-8 – The sub-banded wideband side lobe canceller. Each auxiliary channel is split into band-pass signals and processed to minimize the error between the auxiliaries and main beam.

Because the solution to SLC has already been solved for the narrowband problem in equation 2.27, there is no need to re-derive the solution. As long as the beam being processed has the same frequency band as the auxiliary channels, the solution can be written as:

$$\mathbf{w}_n = R_{a-n}{}^{-1}\mathbf{r}_{bx-n} \quad for\ n = 1, 2, ..., N \tag{2.39}$$

and the output of the canceller is:

$$y(t) = \sum_{n=1}^{N}\left[b_n(t) - \mathbf{w}_n{}^H \tilde{\mathbf{x}}_n(t)\right] \tag{2.40}$$

2.5 CONCLUSIONS

This chapter reviewed what is known about both fixed and adaptive beamforming. It covered both narrowband and wideband fixed beamforming. Then, it introduced LCMV and SLC while addressing both narrowband and wideband situations. There are two ways to address the wideband problem: with time delay units and with sub-bands, both of which were discussed. If the reader has interest in when the narrowband assumption is valid, he may refer to Appendix A. The next chapter will discuss the performance and computational burden of then algorithms.

CHAPTER 3

COMPUTATIONAL AND PERFORMANCE CONSIDERATIONS FOR ADAPTIVE ARRAY PROCESSING

Several techniques were introduced about array beamforming in the last chapter. It started with conventional beamforming then moved to adaptive processing to remove interference from beams; both narrowband and wideband architectures were covered. It was stated in the last section that LCMV is able to remove interference with constraints that preserve the signal of interest and that SLC experiences some degradation. It turns out that this degradation is often accepted because it is a worthwhile tradeoff for the computational savings achieved over LCMV. This chapter is going to demonstrate these two points. It will first explain the metrics used to characterize performance and how the architectures perform to them. These metrics are not prevalent in existing literature, but they are common in our field of work so we use them in this thesis. Next, a means for characterizing the computational burden is introduced and again the methods are mapped to the metric.

3.1 ADAPTIVE CANCELLATION PERFORMANCE METRICS

3.1.1 Interference Cancellation Ratio

The first metric used to determine the performance of an interference canceller is the Interference Cancellation Ratio (ICR). It is a measure of how much of the inteference was removed from the final signal y(t).

$$ICR = \frac{P_{JI} + P_{NI}}{P_{JO} + P_{NO}} \tag{3.1}$$

Equation (3.1) shows how the interference cancellation ratio is measured. In this equation P_{JI} is the power of the interference at the input to the canceller, P_{NI} is the power of the noise at the input, and P_{JO} and P_{NO} are the respective powers at the output of the canceller. Ideally, the interference cancellation would only be a measure of the interference powers without the noise powers included; however, this is not possible in practical measurements. Both the interference and the noise are going to be unknown signals so only their stochastic properties may be measured. Since only the interference is removed by the canceller in theory, it may be assumed that any reduction in output power is due to the removal of the interference.

3.1.2 Signal to Interference and Noise Ratio Improvement

The ICR is an excellent metric for determining how much of the external interference has been removed, but it is not the only important consideration. The case in which the canceller blocked any signal from passing through would produce an infinite ICR and appear to work very well. However, this is not desirable because the signal of interest is also blocked. Therefore, the Signal to Interference and Noise Ratio (SINR) Improvement is also considered and is measured in accordance with (3.2).

$$SINR\,\text{Improvement} = \frac{S_O / (J_O + N_O)}{S_I / (J_I + N_I)} = \frac{S_O}{S_I} ICR \tag{3.2}$$

This measurement is simply a measurement of the SINR before and after the canceller. The right has side of the equation shows this measurement simplifies to the ICR times the output divided by the input of the signal of interest. The right hand side is not what is measured, but it is good for showing that the SINR Improvement is a measure of the ICR with the consideration of how the signal of interest is distorted. It will be shown shortly that this is a very important metric, especially when using SLC which in fact distorts the signal of interest. The SINR Improvement is the main metric used in Chapter 5 because it encapsulates both ICR and signal distortion.

3.1.2 Signal to Interference and Noise Ratio Loss

The final metric that needs to be considered for interference is the SINR Loss which is shown in (3.3). This metric is needed to characterize how the canceller affects the signal of interest. A canceller may be able to completely remove an interfering signal and greatly improve the signal to noise ratio thus having an excellent ICR and SINR Improvement; however, it still may achieve the SINR that would be achieved if there were no interference present. As shown below, the SINR loss is measured by dividing the SINR when there is no interference by the SINR using a given canceller when interference is present. It should be noted that this is not measurable quantity in practical applications because one would not know what the SINR would be without an interference source when it is in fact present; however, this is a measureable quantity in simulations and test scenarios when one has control over the interference source.

$$SINR\ Loss = \frac{S_I / N_I}{S_O / (J_O + N_O)} \tag{3.3}$$

3.2 PERFORMANCE OF VARIOUS CANCELLERS AGAINST METRICS

The metrics just discussed are very useful for characterizing how well particular algorithms are suppressing interference while maintaining as much signal as possible. The ideal performance for each of these measures is to completely remove the interference and to completely preserve the signal for SINR Improvement. If one assumes the jamming power is much greater than the internal noise of the receiver, the ideal ICR can be estimated as the inverse of the interference to noise ratio. Since the SINR Improvement does not distort the signal of interest, it can also be estimated as the ICR when the output signal equals the input.

There are several factors that influence an interference canceller's ability to achieve this optimal performance. Most importantly is that the equations to solve for the adaptive weights in the previous chapter assumed true correlation matrices and vectors. In practice, these are not known and must be estimated. According to Brennan's rule, having about twice as many samples as there are degrees of freedom will cause an expected loss of three decibels compared to optimal performance [38]. Another loss is caused by the fact that narrowband signals contain more than a single frequency [31]. The optimal solution is designed for single frequency problems and thus will have losses associated with these extra frequencies. Similarly, the wideband problems of Section 2.4 assumed a fixed number of taps or sub-bands for a frequency range that contains infinite

frequencies. The design of these wideband approaches is going to affect how close to optimal performance a beamformer will get [31].

Although all of the losses mentioned are unavoidable in a practical system, it may be designed well enough so that they are negligible. However, there is one inherent loss in SLC that is unavoidable and is particular to its architecture. One may recall that the weights were solved to minimize the output of SLC when the signal of interest is not present and then is applied when the signal is present. The underlying assumption of this process is that the signal of interest and the interference are present in the main channel, and only the interference is present in the auxiliary channels. Then, the interference is removed when the adaptive weights are applied to the auxiliaries and subtracted from the main channel. This assumption turns out to never be true because the signal of interest actually happens to be present in the auxiliary channels. The consequence of this is that a portion of the signal of interest also gets removed from the main beam. The amount that gets subtracted is dependent on the gain of the main channel and the angles of the interferences. Therefore, there is a loss in the SINR Improvement and it may be significant enough that the signal power is reduced below the noise floor. It will be shown shortly that SLC comes with a great computational savings over LCMV, but this may be a costly compromise in certain situations.

The amount of signal loss caused by one channel can be calculated. Section 2.3.2 showed that the output of the beamformer is $y(t) = b(t) - \mathbf{w}^H \tilde{\mathbf{x}}(t)$. If one is considering only one aux channel, this may be simplified to $y(t) = b(t) - w^* \tilde{x}(t)$. Now, if the noise and interference contributions are ignored, the amount of the signal of interest may be solved for as follows:

$$s_{out}(t) = G_B s(t) - G_A s(t) w^* \tag{3.4}$$

where G_B is the gain of the main beam and G_A is the gain of the auxiliary channel, or one in this case. To solve for the adaptive weight, (2.27) can be solved for a single auxiliary channel:

$$w = \frac{E\left[G_B L_{SL} j(t)^* j(t) \right]}{E\left[j(t) j(t)^* \right]} = G_B L_{SL} \tag{3.5}$$

where L_{SL} is the loss caused by the side lobe of the array factor in (2.10). When (3.5) is substituted into (3.4), it is reduced to (3.6).

$$s_{out}(t) = G_B s(t)(1 - L_{SL}) \tag{3.6}$$

Equation (3.6) shows that the output of a SLC amplifies the signal of interest by the gain of the array much like a normal beamformer, but the auxiliary channel degrades the signal by a term dependent on the side lobe the interference falls into. The resulting SINR Improvement will be (1-SLL)*ICR. This result is for only one source of interference, but as more are added one can see how this may start to have a detrimental effect on the signal of interest.

3.3 COMPUTATIONAL COST

It has been shown that SLC has a degraded performance relative to LCMV. It will now be shown why such an approach is desirable. It turns out that SLC is much more computationally efficient.

When one is talking about computational cost, it is typically standard to talk in terms of Big O Notation [12]. This notation specifies how an algorithm's complexity

grows as the number of input arguments approach infinity. While this notation is interesting in its own right, this paper is not concerned with computations as their inputs approach infinity and is actually concerned with bounded real systems with finite inputs. For this reason, all algorithms are going to be characterized in terms of how many complex floating point operations are required, or FLOPs. The amount of FLOPs required for a particular algorithm are solved by first breaking the algorithm into its lowest level blocks, then using the text of Golub [19] to identify the amount of FLOPs needed for that particular low level operation.

3.3.1 The Linearly Constrained Minimum Variance Beamformer

The processing steps required to solve LCMV weights are shown in Figure 3-1. The first step is to take the data matrix, X, and form a covariance matrix estimate with it. X is formatted in the following structure:

$$X = \begin{bmatrix} x_1(t-(K-1)T_s & x_1(t-(K-2)T_s & \cdots & x_1(t-T_s) & x_1(t) \\ \vdots & \vdots & \ddots & \vdots & \vdots \\ x_M(t-(K-1)T_s & x_M(t-(K-2)T_s & \cdots & x_M(t-T_s) & x_M(t) \end{bmatrix}$$

where M and K are the number of elements and the number of samples respectively. The covariance matrix is estimated by normalizing the outer product of X by the number of samples as shown in (3.7).

$$\hat{R} = \tfrac{1}{K} XX^H \tag{3.7}$$

Since the steering vector is already known, (2.25) may now be solved. It is computationally inefficient to take the inverse of the covariance matrix estimate, so instead it is decomposed with the Cholesky factorization and then forward substitution is

used to solve for the weights. The Cholesky factorization may be used because a covariance matrix is always Hermitian and positive definite. Finally, the output of the beamformer is solved by applying the weights via matrix multiplication [19]. Table 3-1 shows the computational cost for each of these steps below.

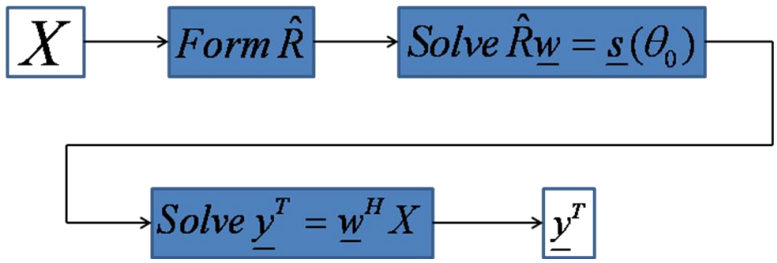

Figure 3-1 – Processing performed on data matrix, X, for LCMV.

Table 3-1: Computation Needed for Narrowband LCMV

$\hat{R} = XX^H$	$2M^2K - M^2$
$\hat{R} = \frac{1}{K}\hat{R}$	MK
Cholesky Factorization of $\hat{R}$	$\frac{1}{3}M^3 + \frac{1}{2}M^2 + \frac{1}{6}M$
Forward Substitution	M^2
$\underline{y}^T = \underline{w}^H X$	$2MK - K$
Total	$\frac{1}{3}M^3 + \frac{1}{2}M^2 + 2M^2K + 3MK + \frac{1}{6}M - K$

The steps for LCMV with TDUs is the same as those for the narrowband, except the data matrix is more complex because is also incorporates time delays. This is done as follows:

$$X = \begin{bmatrix} x_1(t-(K-M)T_s & \cdots & x_1(t-T_s) & x_1(t) \\ x_2(t-(K-M)T_s & \cdots & x_2(t-T_s) & x_2(t) \\ \vdots & \ddots & \vdots & \vdots \\ x_M(t-(K-M)T_s & \cdots & x_M(t-T_s) & x_M(t) \\ x_1(t-(K-M+1)T_s & \cdots & x_1(t-2T_s) & x_1(t-T_s) \\ x_2(t-(K-M+1)T_s & \cdots & x_2(t-2T_s) & x_2(t-T_s) \\ \vdots & \ddots & \vdots & \vdots \\ x_M(t-(K-M+1)T_s & \cdots & x_M(t-2T_s) & x_M(t-T_s) \\ \vdots & \ddots & \vdots & \vdots \\ x_1(t-(K-1)T_s & \cdots & x_1(t-NT_s) & x_1(t-(N-1)T_s) \\ x_2(t-(K-1)T_s & \cdots & x_2(t-NT_s) & x_2(t-(N-1)T_s) \\ \vdots & \ddots & \vdots & \vdots \\ x_M(t-(K-1)T_s & \cdots & x_M(t-NT_s) & x_M(t-(N-1)T_s) \end{bmatrix}$$

where N is the number of taps. Table 3-2 shows the computation needed for this larger problem.

Table 3-2: Computation Needed for Wideband LCMV with TDUs.

$\hat{R} = XX^H$	$2MNK - K$
$\hat{R} = \frac{1}{K}\hat{R}$	MNK
Cholesky Factorization of $\hat{R}$	$\frac{1}{3}(MN)^3 + \frac{1}{2}(MN)^2 + \frac{1}{6}(MN)$
Forward Substitution	$(MN)^2$
$\underline{y}^T = \underline{w}^H X$	$2(MN)^2 K - (MN)^2$
Total	$\frac{1}{3}(MN)^3 + \frac{1}{2}(MN)^2 + 2(MN)^2 K + 3(MN)K + \frac{1}{6}(MN) - K$

The processing required for a wideband LCMV with sub-bands is the same as that of the narrowband problem, except it needs to be done on all of the sub-bands. This causes an N time increase in FLOPs over narrowband process; however, it is worth mentioning that these sub-bands are independent of one another so they may be done in

parallel. This is a very important consideration if speedy computation is necessary and a parallel computing architecture is available. The sub-banded wideband beamformer has the additional computational step of adding the sub-bands together once their adaptive weights are applied. This is shown below in Table 3-3.

Table 3-3: Computation Needed for Wideband LCMV with Sub-Bands.

$\hat{R}_n = X_n X_n^H$	$2NM^2K - NM^2$
$\hat{R}_n = \frac{1}{K}\hat{R}_n$	NMK
$Cholesky\ Factorization\ of\ \hat{R}_n$	$\frac{1}{3}NM^3 + \frac{1}{2}NM^2 + \frac{1}{6}NM$
$Forward\ Substitution$	NM^2
$\underline{y}_n^T = \underline{w}_n^H X_n$	$2NMK - NK$
$\underline{y}^T = \sum_{n=1}^{N} \underline{y}_n^T$	$K(N-1)$
$Total$	$N(\frac{1}{3}M^3+\frac{1}{2}M^2+2M^2K+3MK+\frac{1}{6}M-K)+K(N-1)$

3.3.2 The Side lobe Canceller

The computational steps required for a side lobe canceller are shown in Figure 3-2. The auxiliary data matrix, $\tilde{X}$, will need to be formed again and is the same as LCMV. However, an additional auxiliary data matrix also needs to be formed to represent the information from the auxiliary channels. The auxiliary channels may actually be elements from the full array, but the assumption is that $M >> \tilde{M}$ where the tilde symbol denotes an auxiliary channel. The structure of the auxiliary data matrix is shown below.

$$\tilde{X} = \begin{bmatrix} \tilde{x}_1(t-(K-1)T_s & \tilde{x}_1(t-(K-2)T_s & \cdots & \tilde{x}_1(t-T_s) & \tilde{x}_1(t) \\ \vdots & \vdots & \ddots & \vdots & \vdots \\ \tilde{x}_{\tilde{M}}(t-(K-1)T_s & \tilde{x}_{\tilde{M}}(t-(K-2)T_s & \cdots & \tilde{x}_{\tilde{M}}(t-T_s) & \tilde{x}_{\tilde{M}}(t) \end{bmatrix}$$

The covariance matrix is formed in the same way as it was for LCMV, except the auxiliary data matrix is used instead. The cross covariance vector, $\mathbf{r}_{bx}$, is formed as follows:

$$\mathbf{r}_{bx} = \frac{1}{K}\tilde{X}\begin{bmatrix} b^*(t-(K-1)T_s) \\ \vdots \\ b^*(t-T_s) \\ b^*(t) \end{bmatrix} \tag{3.8}$$

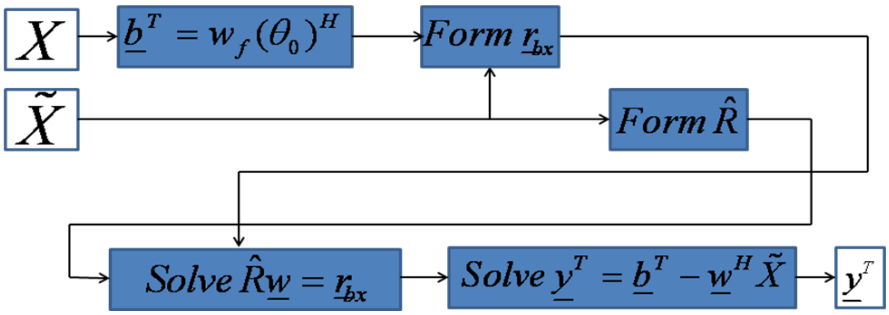

Figure 3-2 – Computational steps for SLC

The computational cost required for each step is shown in Table 3-4.

Table 3-4: Computation needed for narrowband side lobe canceller

$\underline{b}^T = \underline{w}_f^H X$	$2MK - K$
$\hat{R} = \tilde{X}\tilde{X}^H$	$2\tilde{M}^2 K - \tilde{M}^2$
$\hat{R} = \frac{1}{K}\hat{R}$	$\tilde{M}K$
$\underline{\hat{r}} = X\underline{b}^*$	$2\tilde{M}K - \tilde{M}$
$\underline{\hat{r}} = \frac{1}{K}\underline{\hat{r}}$	K
Cholesky Factorizationof $\hat{R}$	$\frac{1}{3}\tilde{M}^3 + \frac{1}{2}\tilde{M}^2 + \frac{1}{6}\tilde{M}$
Forward Substitution	$\tilde{M}^2$
$\underline{y}^T = \underline{b}^T - \underline{w}^H \tilde{X}$	$2\tilde{M}K$
Total	$\frac{1}{3}\tilde{M}^3 + \frac{1}{2}\tilde{M}^2 + 2\tilde{M}^2 K + 5\tilde{M}K - \frac{5}{6}\tilde{M} + 2MK$

In order to perform this processing with time delay units, additional computation is needed as is shown in Table 3-5. The time delay units are represented in the data matrix are shown below while the covariance vector is still formed with (3.8).

$$\tilde{X} = \begin{bmatrix} \tilde{x}_1(t-(K-M)T_s & \cdots & \tilde{x}_1(t-T_s) & \tilde{x}_1(t) \\ \tilde{x}_2(t-(K-M)T_s & \cdots & \tilde{x}_2(t-T_s) & \tilde{x}_2(t) \\ \vdots & \ddots & \vdots & \vdots \\ \tilde{x}_M(t-(K-M)T_s & \cdots & \tilde{x}_M(t-T_s) & \tilde{x}_M(t) \\ \tilde{x}_1(t-(K-M+1)T_s & \cdots & \tilde{x}_1(t-2T_s) & \tilde{x}_1(t-T_s) \\ \tilde{x}_2(t-(K-M+1)T_s & \cdots & \tilde{x}_2(t-2T_s) & \tilde{x}_2(t-T_s) \\ \vdots & \ddots & \vdots & \vdots \\ \tilde{x}_M(t-(K-M+1)T_s & \cdots & \tilde{x}_M(t-2T_s) & \tilde{x}_M(t-T_s) \\ \vdots & \ddots & \vdots & \vdots \\ \tilde{x}_1(t-(K-1)T_s & \cdots & \tilde{x}_1(t-NT_s) & \tilde{x}_1(t-(N-1)T_s) \\ \tilde{x}_2(t-(K-1)T_s & \cdots & \tilde{x}_2(t-NT_s) & \tilde{x}_2(t-(N-1)T_s) \\ \vdots & \ddots & \vdots & \vdots \\ \tilde{x}_M(t-(K-1)T_s & \cdots & \tilde{x}_M(t-NT_s) & \tilde{x}_M(t-(N-1)T_s) \end{bmatrix}$$

Table 3-5: Computation Needed for Side Lobe Cancellation with Time Delay Units

$\underline{b}^T = \underline{w}_f^H X$	$2MK - K$
$\hat{R} = \tilde{X}\tilde{X}^H$	$2(\tilde{M}N)^2 K - (\tilde{M}N)^2$
$\hat{R} = \frac{1}{K}\hat{R}$	$\tilde{M}NK$
$\underline{\hat{r}} = X\underline{b}^*$	$2\tilde{M}NK - \tilde{M}N$
$\underline{\hat{r}} = \frac{1}{K}\underline{\hat{r}}$	K
Cholesky Factorization of $\hat{R}$	$\frac{1}{3}(\bar{M}N)^3 + \frac{1}{2}(\bar{M}N)^2 + \frac{1}{6}\bar{M}N$
Forward Substitution	$(\tilde{M}N)^2$
$\underline{y}^T = \underline{b}^T - \underline{w}^H \tilde{X}$	$2\tilde{M}NK$
Total	$\frac{1}{3}(\bar{M}N)^3 + \frac{1}{2}(\bar{M}N)^2 + 2(\bar{M}N)^2 K + 5\bar{M}NK - \frac{5}{6}\bar{M}N + 2MK$

Finally, everything that was true for a sub-banded LCMV are also true for SLC. The wideband main beam and auxiliary channels may be broken up into narrowband components which may be processed in parallel. Table 3-6 shows the computation required for the sub-banded SLC.

Table 3-6 – Computation Needed for Sub-Banded Side Lobe Cancellation

$\underline{b}_n^T = \underline{w}_{fn}^H X_n$	$2MNK - NK$
$\hat{R}_n = \tilde{X}_n \tilde{X}_n^H$	$2N\tilde{M}^2K - N\tilde{M}^2$
$\hat{R}_n = \frac{1}{K}\hat{R}_n$	$\tilde{M}NK$
$\underline{\hat{r}}_n = X_n \underline{b}_n^*$	$2\tilde{M}NK - \tilde{M}N$
$\underline{\hat{r}}_n = \frac{1}{K}\underline{\hat{r}}_n$	K
Cholesky Factorization of $\hat{R}_n$	$\frac{1}{3}N\bar{M}^3 + \frac{1}{2}N\bar{M}^2 + \frac{1}{6}\bar{M}N$
Forward Substitution	$N\tilde{M}^2$
$\underline{y}_n^T = \underline{b}_n^T - \underline{w}_n^H \tilde{X}_n$	$2\tilde{M}NK$
$\underline{y}^T = \sum_{n=1}^{N} \underline{y}_n^T$	$K(N-1)$
Total	$N(\frac{1}{3}\bar{M}^3 + \frac{1}{2}\bar{M}^2 + 2\bar{M}^2K + 5\bar{M}K - \frac{5}{6}\bar{M} + 2MK) + K(N-1)$

3.3.3 Computational Comparison of Various Interferece Cancellation Techniques

Tables 3-1 through 3-6 give the computational costs for various interference cancelation algorithms. We now do a side by side comparison of the algorithms. Consider a radar with an unambiguous range of 100 kilometers. It would require a pulse repetition frequency of $\left(\frac{2*100km}{3e8m/s}\right)^{-1} = 1.5kHz$. An array operating at S-band with 100 elements in one dimension can still satisfy the narrowband assumption with a 2.5 MHz signal. When this pulse repetition interval is sampled at this rate, 1667 samples are needed. If the bandwidth is increased by a factor of ten, then the sampling rate for the TDU approach needs to go up by a factor of ten and each channel needs to have 10 taps.

For the sub-banding approach the sampling rate remains the same, but ten sub-bands will be needed. Assume that the side lobe canceller has ten auxiliary which can handle ten sources of interferences. Figure 3-3 shows how the various methods compare computationally versus the number of elements there are in the main array. The number of elements range from two for a two element linear array to 10,000 for a 100 x 100 element planar array.

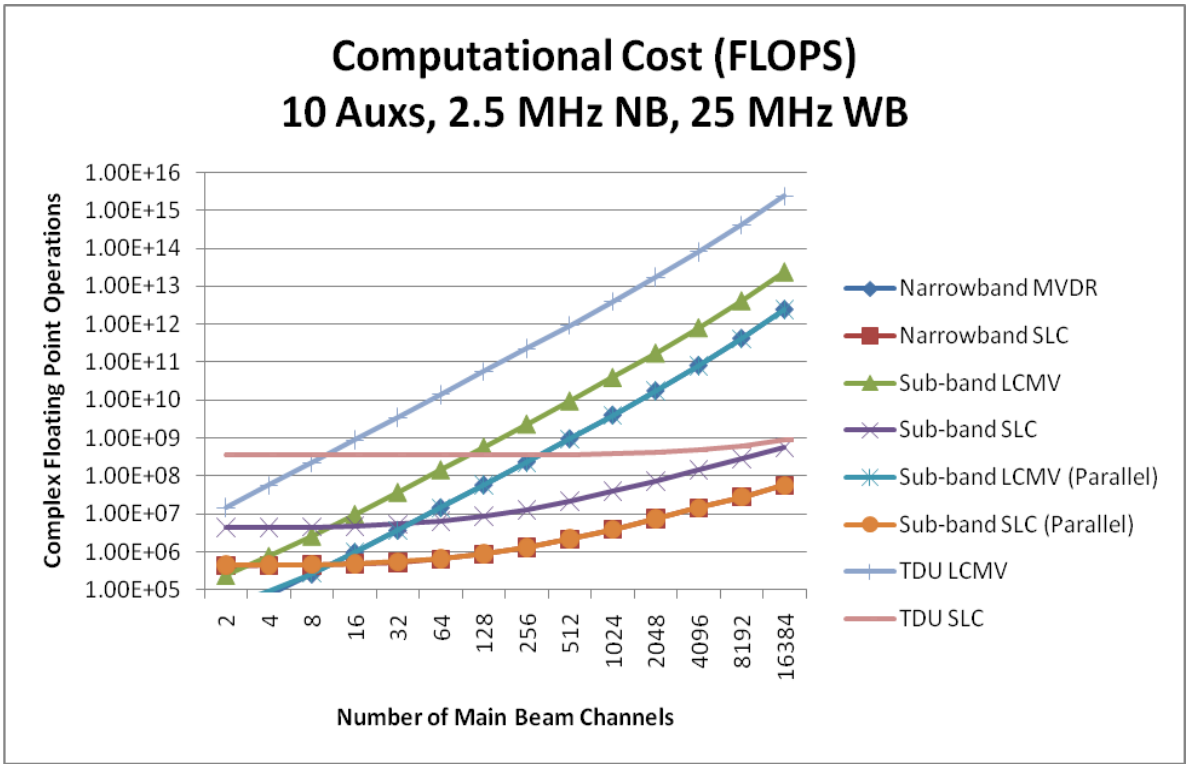

Figure 3-3 – Computational cost in terms of FLOPs for various methods of interference cancellation.

One can see that when there are more main beam elements than there are auxiliary channels, LCMV is always the most expensive solution. Additionally, once the signal becomes a wideband signal, the TDU approach is much more expensive than the sub-

banding approach. In fact, if the sub-banding is done in parallel the computation time is comparable to that of a narrowband signal. An interesting thing to note about SLC is that its growth accelerates for larger main arrays. This is because the cost of (2.40) becomes more dependent on the size of the main beam than the auxiliary processing.

3.4 CONCLUSIONS

This chapter characterized the existing methods of interference cancellation. It first provided metrics that help to show how well a certain algorithm is performing and a means to compare different ones. It then showed how much SLC will distort the signal of interest, and thus degrade performance, under ideal circumstances. Once we conveyed the undesirable aspects of SLC, we showed why it was better in terms of computational cost. We characterized how many FLOPs LCMV and SLC used for both the narrowband and wideband cases. Because the number of auxiliary channels is typically much smaller than the number of elements in the array, SLC is much less costly. We finished the chapter with an example of using generic parameters typical for a pulse-doppler radar. When the number of elements where increased, we saw that LCMV costs grew at a much faster rate than those of SLC.

CHAPTER 4

STEERED AUXILIARY BEAM CANCELLATION

In this chapter we introduce SABC, our algorithm to improve the performance of SLC without a large increase in computational cost which is the main contribution of this thesis. We start by explaining how the algorithm works then characterize it in terms of performance and cost, much like how we did for SLC. We then compare its performance to SLC and the cost to SLC and LCMV.

4.1 THE STEERED AUXILIARY BEAM CANCELLER

Up until this point, only the commonly used interference cancellation algorithms have been discussed. Now we introduce a new method that improves some losses of SLC discussed in Chapter 3 without being burdened by the computational cost of LCMV.

One may recall from (3.3) that the signal of interest experienced a loss because a part of this signal was present in the auxiliary channel. The amount of signal is actually proportional to the gain of the auxiliary channel in the direction of the signal of interest. For simplicity, the auxiliary channel was assumed to be isotropic. This caused a higher distortion on the signal of interest when the interference appeared in a higher side lobe.

SABC uses SLC architecture, but a formed beam from the main array is used instead of an isotropic auxiliary channel. The result of this is a smaller correlation between the auxiliary channel and the main channel. This is shown graphically in figure

4-1. One can see that when an auxiliary channel is adapted to the proper level, there is a high amount of the signal of interest's energy that gets removed. However, much less signal of interest is lost if another beam is formed on the interference. This is because the signal of interest now falls in the side lobe of the auxiliary beam.

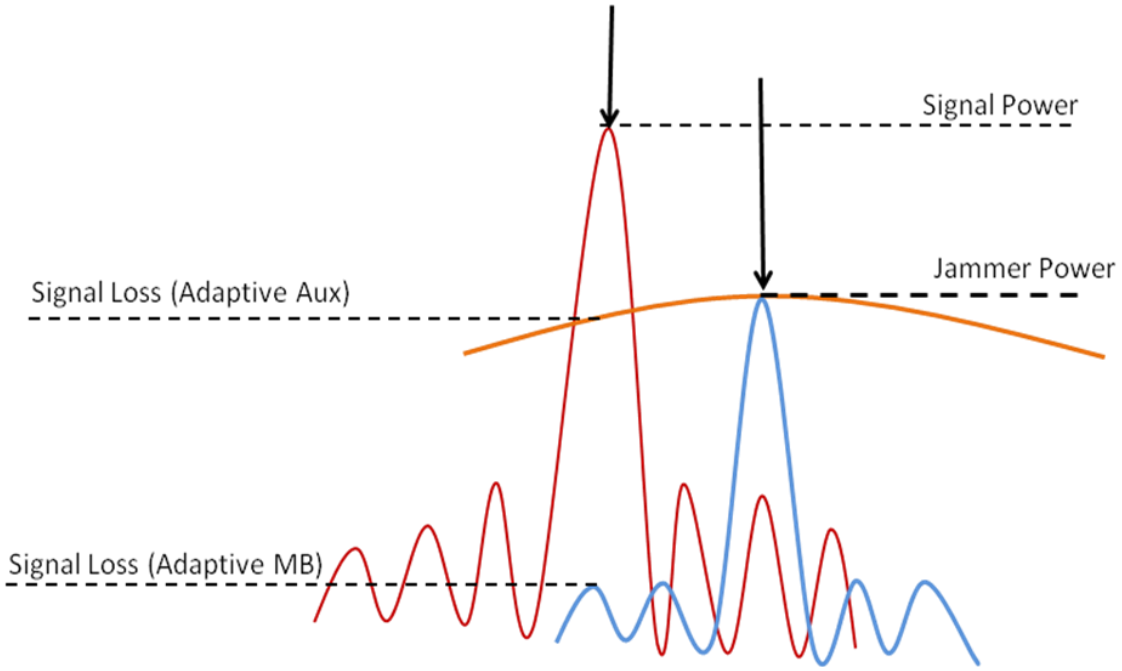

Figure 4-1 – A graphical representation of SLC and SABC. In this figure, the main channel is red, the auxiliary channel is orange, and the steered auxiliary beam is blue.

The implication of this technique is that the angle of the interference must be known so that a beam may be steered towards it. This may seem like an unfeasible problem, but there are existing array processing methods such as MUSIC and ESPRIT that can estimate the angle of arrival of several simultaneous signals using a digital array. For computational reasons, ESPRIT is used in this paper and is further discussed in Appendix B. One reason ESPRIT is computationally efficient is that one only needs to

process as many elements as there are sources of interference. This means that if one has a 100 element array, but there are less than 10 sources of interference, then only 10 elements need be processed by ESPRIT.

4.2 PERFORMANCE OF SABC

4.2.1 Ideal Performance of SABC

Much like (3.3) through (3.5), SABC may be characterized in terms of losses in the signal of interest. The output of SABC is shown below where G_B is the gain of a beam and L_{SL} is the loss of the side lobe in which the Interference appears relative to the boresight gain.

$$s_{out}(t) = G_B s(t) - G_B L_{SL} s(t) w^* \tag{4.1}$$

The weight used above is also shown in (4.2).

$$w = \frac{E\left[G_B L_{SL} j(t)^* G_B j(t)\right]}{E\left[G_B j(t)^* G_B j(t)\right]} = L_{SL} \tag{4.2}$$

If (4.2) is substituted into (4.1), the final output of SABC is obtained.

$$s_{out}(t) = G_B s(t)(1 - {L_{SL}}^2) \tag{4.3}$$

To determine the improvement gained over the standard SLC, one may divide (4.3) by (3.5).

$$SABC\,Gain = \frac{G_B s(t)(1 - {L_{SL}}^2)}{G_B s(t)(1 - L_{SL})} = \frac{(1 - {L_{SL}}^2)}{(1 - L_{SL})} \tag{4.4}$$

The gain in (4.4) is dependent on the angle of arrival of the interference, the angle of arrival of the signal of interest, and the number of elements in the array. Figure 4-2 shows the gain of SABC over SLC for a linear array with a range of elements. This figure assumes the signal of interest is at zero degrees and that only one source of interference is present.

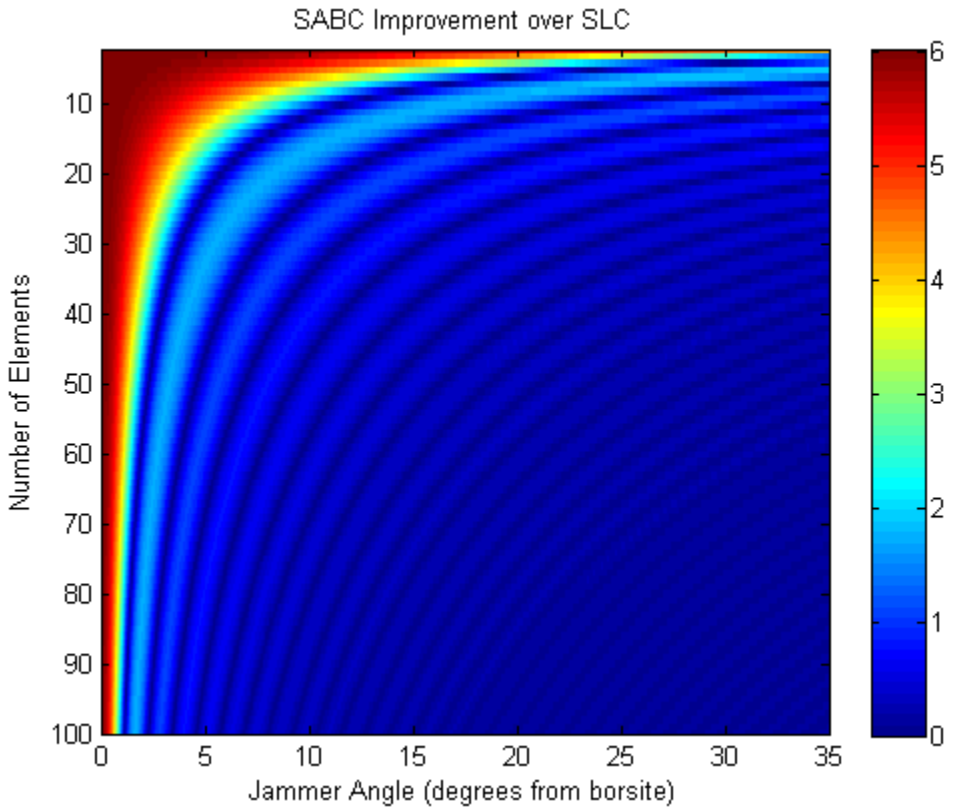

Figure 4-2 – The gain of SABC over SLC, in decibels, as the source of interference is moved away from the signal of interest.

Analysis of Figure 4-2 can shed some insights into the benefits of SABC. First of all, the gain of SABC is never less than zero meaning it always performs at least as well as SLC. Additionally, there are several areas of the figure where SABC shows a gain of

about 2 dB, particularly in the peaks of the first two side lobes, which is a significant increase. However the greatest gain occurs when the interference is located in the main beam where an increase of 4 to 6 dB is experienced. This should be of no surprise since SLC is designed for side lobe interference as its name suggests, but this does show that SABC is capable of dealing with interference in the main beam of the array. We will show in chapter five that SABC also causes distortion on the signal of interest with main beam interference; however, it turns out that LCMV encounters this problem too and SABC performs as well in these situations.

4.2.2 Performance of SABC in the Presence of Noise

Equation (4.4) was derived assuming that the weights were solved such that the interference source was perfectly removed from the main beam. From this it was shown that SABC performs better than SLC because it distorts the signal less. However, the correlation matrices must be known in order to compute the weights that perfectly cancel the interference. These will never be known and must be estimated in the presence of noise. For this reason SABC presents another gain over the performance of SLC that turns out to be much more substantial than the ideal gain.

Equation (3.4) only considers what happens to the signal of interest and (3.5) did not model the noise in the channels. Below, these equations are re-written for SLC canceller to accommodate these considerations.

$$y(t) = b(t) - w^{*}\tilde{x}_1(t)$$

$$y(t) = \left(G_B A_s s(t) + G_B L_{SL} A_j j(t) + \sum_{i=1}^{G_B} A_n n_i(t) e^{j2\pi \frac{d}{c} \sin\theta_s (i-1)} \right) - w^* \left(A_s s(t) + A_j j(t) + A_n n_{\tilde{1}}(t) \right) \tag{4.5}$$

In this equation, G_B is the gain of the main beam and is equal to the number of elements, M, L_{SL} is the loss of the side lobe the interference happens to fall in, and $n_{\tilde{1}}(t)$ is the noise in the auxiliary channel. If one assumes there is a training region where the signal is not present, the solution for the weights is:

$$w = \frac{E\left[\left(ML_{SL} A_j j(t) + \sum_{i=1}^{M} A_n n_i(t) e^{j2\pi \frac{d}{c} \sin\theta_s (i-1)} \right)^* \left(A_j j(t) + A_n n_{\tilde{1}}(t) \right) \right]}{E\left[\left(A_j j(t) + A_n n_{\tilde{1}}(t) \right) \left(A_j j(t) + A_n n_{\tilde{1}}(t) \right)^* \right]}$$

$$= \frac{ML_{SL} A_j^2 E\left[j(t) j(t)^* \right] + A_n^2 E\left[n_{\tilde{1}}(t) n_{\tilde{1}}(t)^* \right]}{A_j^2 E\left[j(t) j(t)^* \right] + A_n^2 E\left[n_{\tilde{1}}(t) n_{\tilde{1}}(t)^* \right]} \neq ML_{SL} \tag{4.6}$$

It is immediately obvious that the weight estimate becomes corrupted in the presence of noise. SABC is not immune to this phenomenon, but the impact is far less severe as shown below. Equation 4.5 can be re-written for SABC as follows:

$$y(t) = \left(MA_s s(t) + ML_{SL} A_j j(t) + \sum_{i=1}^{M} A_n n_i(t) e^{j2\pi \frac{d}{c} \sin\theta_s (i-1)} \right) - w^* \left(ML_{SL} A_s s(t) + MA_j j(t) + \sum_{i=1}^{M} A_n n_i(t) e^{j2\pi \frac{d}{c} \sin\theta_j (i-1)} \right) \tag{4.7}$$

The equation to solve for the weights for the steered aux beam is:

$$w = \frac{E\left[\left(ML_{SL}A_j\,j(t) + \sum_{i=1}^{M} A_n n_i(t) e^{j2\pi\frac{d}{c}\sin\theta_s(i-1)}\right)^*\left(MA_j\,j(t) + \sum_{i=1}^{M} A_n n_i(t) e^{j2\pi\frac{d}{c}\sin\theta_j(i-1)}\right)\right]}{E\left[\left(MA_j\,j(t) + \sum_{i=1}^{M} A_n n_i(t) e^{j2\pi\frac{d}{c}\sin\theta_j(i-1)}\right)\left(MA_j\,j(t) + \sum_{i=1}^{M} A_n n_i(t) e^{j2\pi\frac{d}{c}\sin\theta_j(i-1)}\right)^*\right]}$$

$$= \frac{L_{SL}M^2A_J{}^2E\left[\,j(t)\,j(t)^*\right] + \sum_{i=1}^{M} E\left[A_n{}^2 n_i(t)n_i(t)^*\right]}{M^2A_J{}^2E\left[\,j(t)\,j(t)^*\right] + \sum_{i=1}^{M} E\left[A_n{}^2 n_i(t)n_i(t)^*\right]} \simeq L_{SL} \qquad (4.8)$$

Upon comparison of (4.6) and (4.8), one can see that both are corrupted by unwanted noise; however, the contribution of interference grows on the order of M squared whereas the noise only grows on the order of M in (4.6). This means that the larger M is for the weight estimation, the closer it is to the ideal weight of (4.2). Equation (4.6) does not enjoy any such improvement and the interference and noise contribute equally to the result.

The gains in the presence of noise should not be overlooked because they cause the ICR of SABC to be significantly higher than SLC. There is no elegant way to characterize this gain as there was with (4.4), but it will be demonstrated in the next section how much better SABC performs via simulations.

4.3 WIDEBAND SABC

Unlike LCMV and SLC, SABC only has one method to solve the wideband problem which is by sub-banding the beams. There are two reasons why the time-delay

unit approach will not work for SABC. First of all, the method used to determine the interference angles, ESPRIT, only works for narrowband signals; therefore, it is convenient to do this step on sub-banded data. This shortcoming may be overcome if other wideband angle of arrival estimators are found and happen to be computationally efficient. The second problem with the TDU approach is that beamforming on the interference sources de-correlates them from the interference in the main beam. SLC only works because the interference in the auxiliary channels are correlated and may be weighted and subtracted out; thus, the TDU SABC approach will not work because this necessity is violated.

4.4 COMPUTATIONAL COST OF SABC

The computational cost of SABC is similar to that of SLC because the techniques are so similar. The only difference between the two is the step used in SABC to for the angles of the interference sources and forming beams on them. This is shown below in Figure 4-3.

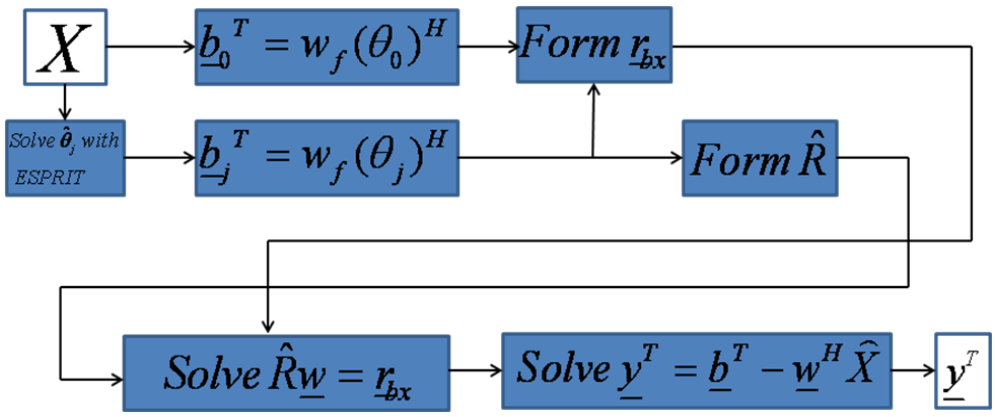

Figure 4-3 – The processing steps performed by SABC. One will notice that it is very similar to SLC, with the additional step of solving for the interference angles and steering beams towards there.

One can see that the processing is very similar to that solved in Chapter 3 for SLC. For this reason, Tables 4-1 and 4-2 do not repeat the information of SLC. These two tables do include extra variables not mentioned in Chapter 3. These variables are J and $\widehat{M}$ which represent the number of interference sources and the number of elements used in the ESPRIT algorithm. To ensure the comparisons in this thesis are unbiased, the remainder of this paper assumes that $\widehat{M}$ is equal to the number of auxiliary channels of an SLC.

Table 4-1: Computational cost of narrowband SABC

ESPRIT on $\widehat{X}$ for θ_j	$12\widehat{M}^3 - \widehat{M}^2 + 3\widehat{M}K + 4\widehat{M}^2 J + \frac{8}{3}J^3 + 11J^2 + 3J - \widehat{M}J$
$\underline{b}_i^T = \underline{w}_{fi}^H X \quad$ ***for i*** $= 1:(J+1)$	$(J+1)(2MK - K)$
SLC with mainbeam and aux beams	$\frac{1}{3}J^3 + \frac{1}{2}J^2 + 2J^2K + 5JK + K - \frac{5}{6}J$
Total	$12\widehat{M}^3 + \frac{1}{3}J^3 + 2J^2K + \frac{1}{2}J^2 - \widehat{M}^2 + 5JK + 3\widehat{M}K + 4\widehat{M}^2 J + \frac{8}{3}J^3 \ldots$ $+11J^2 + 3J - \widehat{M}J + K - \frac{5}{6}J + 2JMK - JK + 2MK - K$

Table 4-2 Computational cost of wideband SABC

$ESPRIT\ on\ \widehat{X}\ for\ \theta_j$	$N(12\widehat{M}^3-\widehat{M}^2+3\widehat{M}K+4\widehat{M}^2J+\frac{8}{3}J^3+11J^2+3J-\widehat{M}J)$
$\underline{b}_i^T=\underline{w}_{fi}^H X \quad for\ i=1:(J+1)$	$N(J+1)(2MK-K)$
$SLC\ with\ main\ beam\ and\ aux\ beams$	$N(\frac{1}{3}J^3+\frac{1}{2}J^2+2J^2K+5JK+K-\frac{5}{6}J)+K(N-1)$
$Total$	$N(12\widehat{M}^3+\frac{1}{3}J^3+2J^2K+\frac{1}{2}J^2-\widehat{M}^2+5JK+3\widehat{M}K+4\widehat{M}^2J+\frac{8}{3}J^3\ldots$ $+11J^2+3J-\widehat{M}J+K-\frac{5}{6}J+2JMK-JK+2MK-K)+K(N-1)$

The computational costs of SABC may be compared to those of LCMV and SLC as shown in Figure 4-4. In this figure only the wideband case is considered since it is the most demanding computationally. This figure shows that for the case under consideration, SABC is always more efficient than TDU LCMV and sub-band LCMV for larger arrays. Additionally, it is more efficient than TDU SLC for the range being considered, but it may grow more complex for larger arrays. However, an array with more than 2^{14} elements would be very computationally expensive regardless. The only method which is always more efficient than SABC is the sub-banded SLC; however, it has been shown that SABC provides better performance in terms of signal distortion and this happens to be the trade-off that one must accept for SABC.

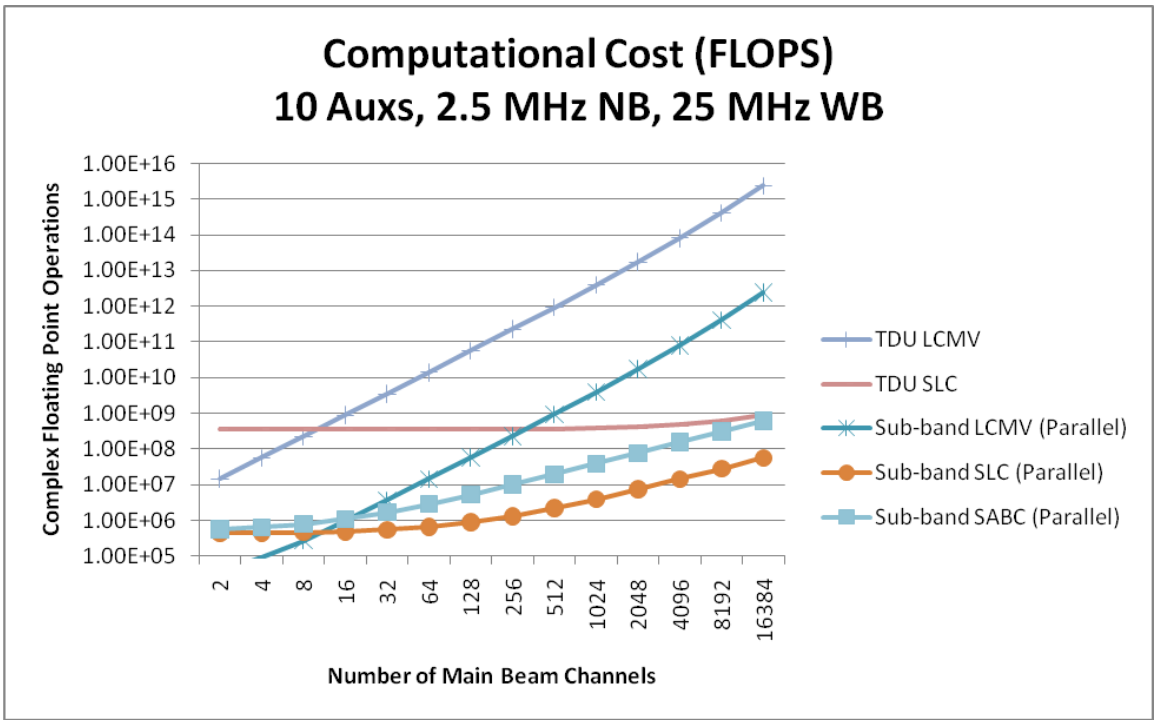

Figure 4-4 – Computational cost in terms of FLOPs for various methods of interference cancellation.

4.5 CONCLUSIONS

In this chapter we introduced a new algorithm for interference cancellation, SABC. The method uses an SLC architecture, but uses beams from the main array instead of extra elements for the auxiliary channels. ESPRIT is used to solve for the angle of the source of interference. We showed that not only does SABC distort the signal of interest less than SLC, but it also solves better estimates of the weights in the presence of noise. We will show in the next chapter how this allows for a significant performance increase. We also showed SABC is much more reasonable computationally than LCMV. In the next chapter we will validate these analytical solutions with simulations.

CHAPTER 5

SIMULATIONS OF THE SIDE LOBE CANCELLER AND STEERED AUXILIARY BEAM CANCELLER

In this section show that the claims made in previous sections hold up when implemented in Matlab simulations. The main purpose of this section is to show that SABC always performs at least as well as SLC, but performs much better in most cases. The computational costs of these algorithms will not be addressed in this section since it was already addressed in previous sections; instead, the two methods will be compared using the metrics described in the beginning of Chapter 3. The case will first be made for the narrowband case and then extended to wideband. Finally, a discussion of breakdown points will be given.

All simulations for this paper will be implemented in the FRAME, a radar signal processing modeling tool co-developed by the author at the Johns Hopkins Applied Physics Lab. It was developed to be able to rapidly model the signal processing environment for digital phased array radars. It has the ability to simulate the propagation effects of the radar, interference sources, and the noise characteristics internal to the radar. The philosophy of the model is that anybody who understands the inputs and outputs of the model should be able to write customized signal processing algorithms

without having to worry about simulating the environment which is what we did for this chapter.

5.1 SIMULATION OF A NARROWBAND LINEAR ARRAY

The first simulation is of a 51 element linear array with its array factor shown below in Figure 5-1. The elements are spaced half of a wavelength apart for a 3.0 GHz carrier. One can see from the figure that the pattern has a 3 dB beamwidth of about 3 degrees and a first null beamwidth of about 4.5 degrees.

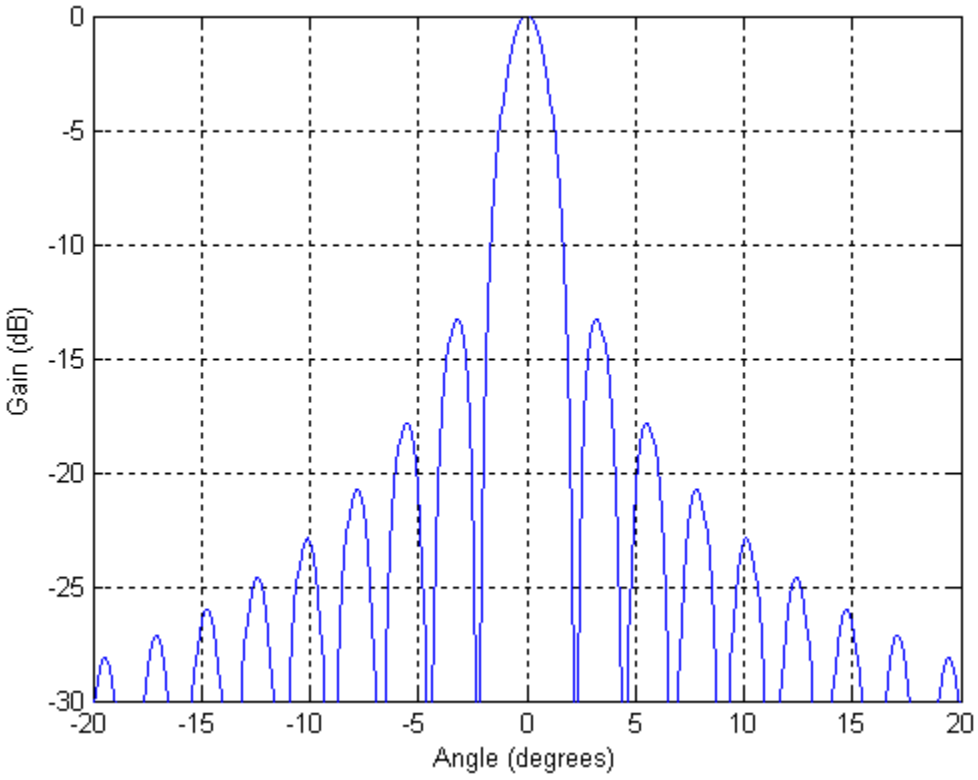

Figure 5-1 – The array factor of the antenna used in simulation. The antenna is a 51 element uniform linear array with a beamwidth of 3 degrees.

The waveform used is a Linear Frequency Modulation (LFM) pulse with a bandwidth of 2.5 MHz centered on the carrier frequency. Figure 5-2 shows signal received by the array after beamforming on the signal of interest and coherent integration via Doppler processing.

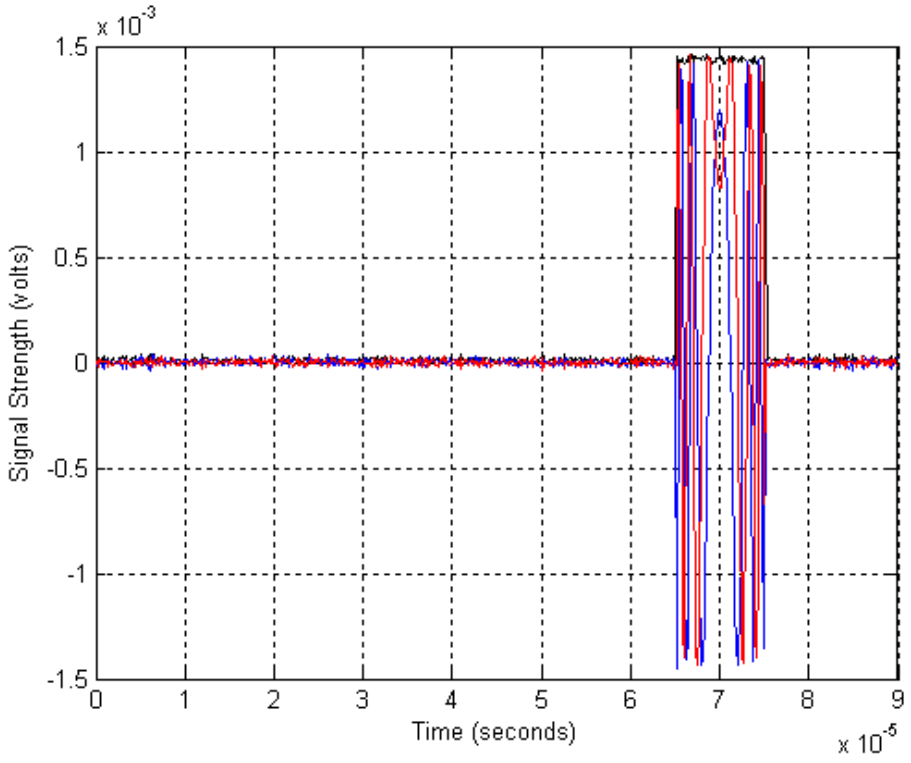

Figure 5-2 – Signal received by the array in the presence of noise without external interference. The real part of the signal is blue, the imaginary part is red, and the magnitude of the signal is black.

One can see that this signal was received in the presence of thermal noise; however, the signal of interest greatly overpowers it.

5.1.1 Addition of a Source of Interference in Antenna Side-Lobe

The next step of the simulation is to add a single interference source in the far field. The antenna and auxiliary gain patterns play a vital role in SLC and SABC, so it is essential to note the placement of any interference source when comparing these algorithms. For this reason, the angle of the interference source is swept parametrically from near the antenna boresight to 40 degrees where the side lobe level of the antenna is low. The interference signal is strong enough that it completely masks the signal of interest. Figure 5-3 shows what the signal now looks like with interference for all range cells of the receive window when the interference is 40 degrees off boresight.

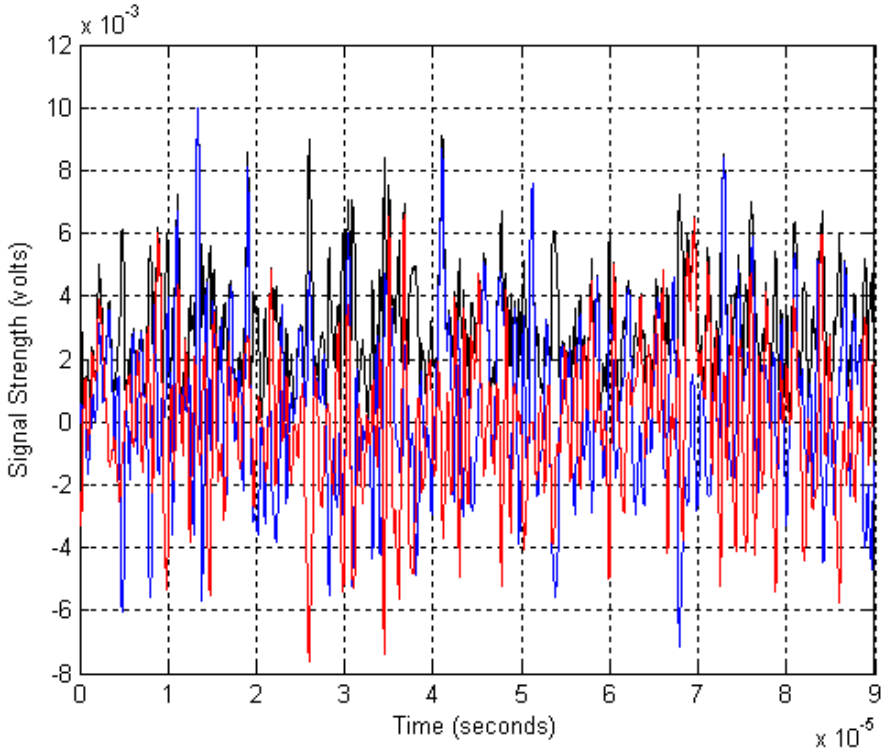

Figure 5-3 – Signal Received by array once corrupted by interference. The real part of the signal is blue, the imaginary part is red, and the magnitude of the signal is black.

Below in Figures 5-4 and 5-5, the signal is shown for an interference source at 40 degrees off boresight when SLC and SABC are used respectively to compare to Figure 5-3. It is clear that the loss in signal to noise ratio caused by the interference source is greatly mitigated by both SLC and SABC. If one looks closely at the interference residues and noise during the first 40 μs, one can see that SABC performs better than SLC, but is still not as good as the case when no interference is present. It is difficult to show how the interference levels differ on a linear scale, so Figure 5-7 shows the magnitudes of these different signals in decibels. Again, one can see the decrease in interference power as one steps from no cancellation, to SLC, to SABC, and finally to a signal with no interference present. Lastly, one should note that the signal to interference and noise ratios of SLC, SABC, and no interference case are 22.3 dB, 26.5 dB, and 27.6 dB respectively.

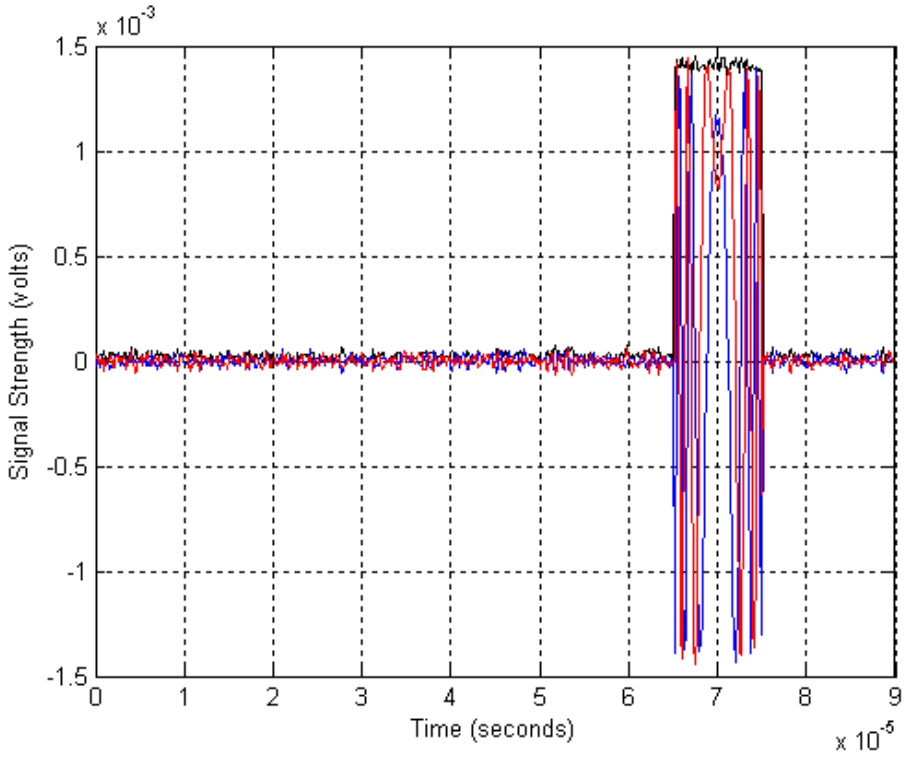

Figure 5-4 – Signal and interference after SLC processing. The real part of the signal is blue, the imaginary part is red, and the magnitude of the signal is black.

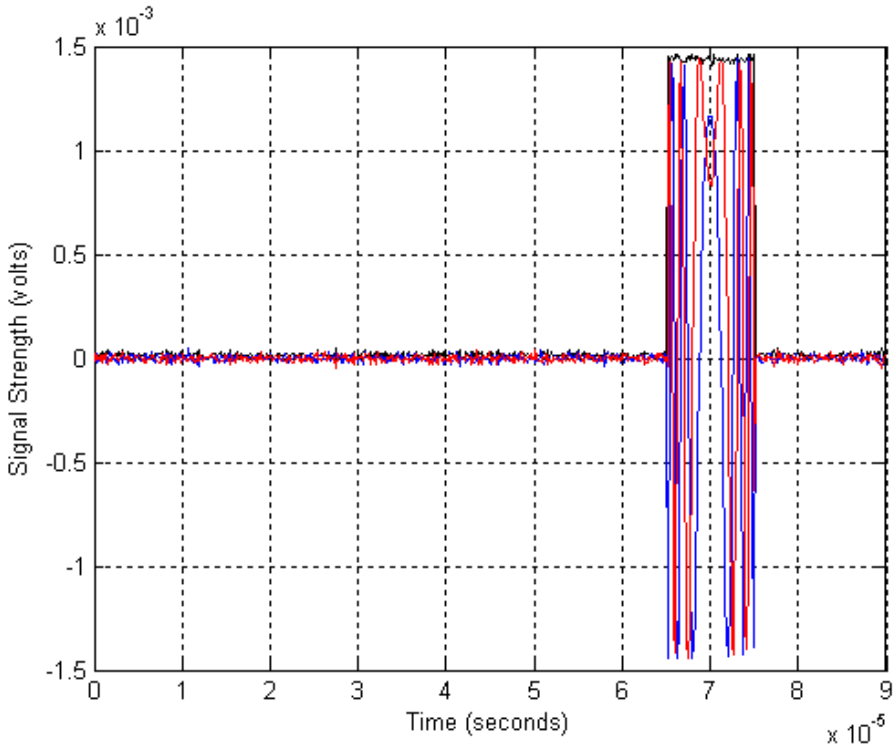

Figure 5-5 – Signal and interference after SABC processing. The real part of the signal is blue, the imaginary part is red, and the magnitude of the signal is black.

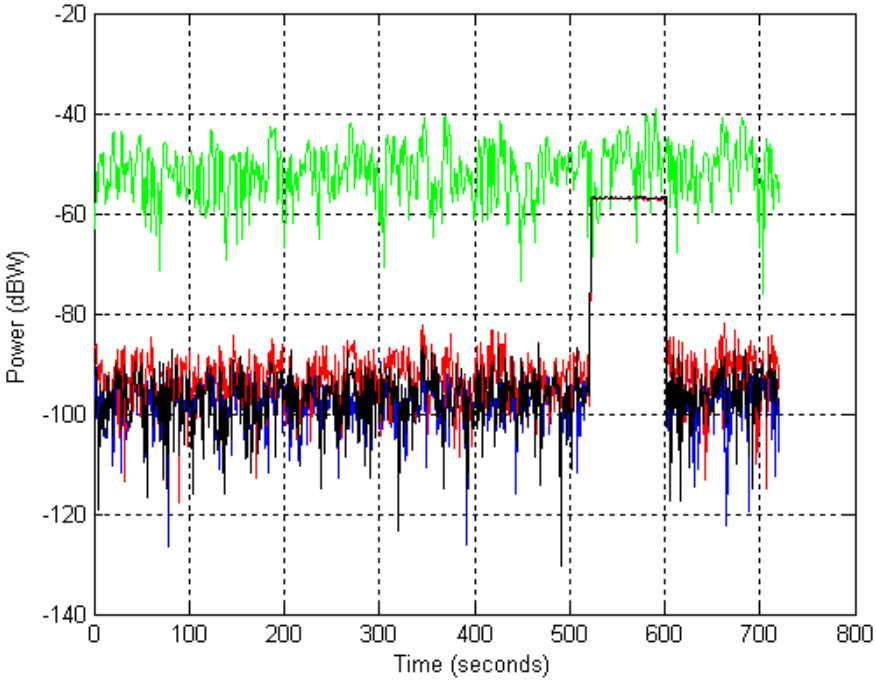

Figure 5-6 – Signal power received with no interference (blue), with interference (green), with interference and SLC Processing (red), and with interference and SABC processing (black).

5.1.2 How the Interference Angle Influences Interference Cancellation

How SLC and SABC perform relative to one another is dependent on the angle which the interference is located relative to the signal of interest. The last section showed results for a constant angle of 40 degrees off boresight; however, next the cancellers will be tested as the interference is moved parametrically through various angles.

In this simulation, the signal of interest has a power of -67.7 dBW and the interference has a signal power that is dependent on its angle. Figure 5-7 shows the power level for the interference as the interference source is moved away from boresight.

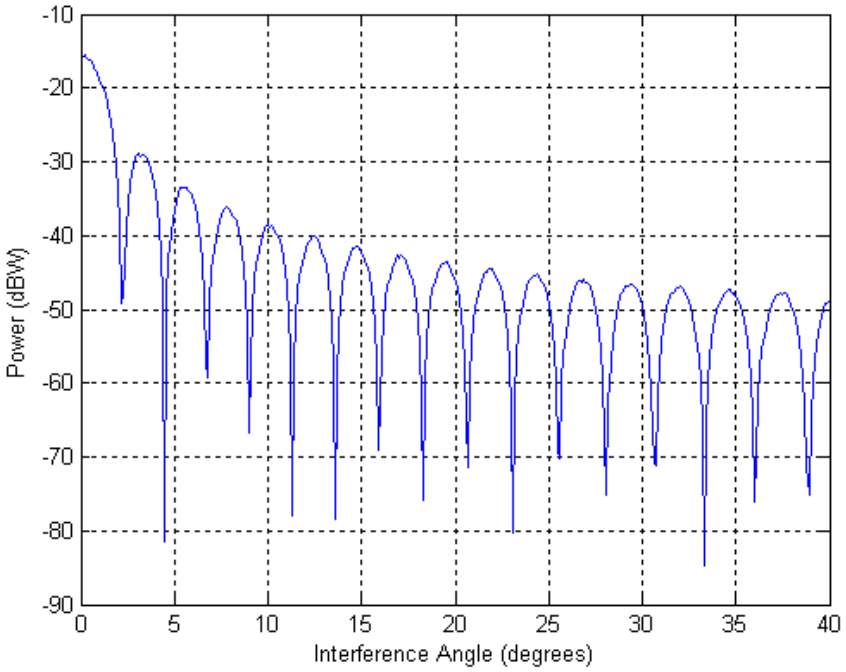

Figure 5-7 – Power of interference received by array as the interference is swept across a range of angles. One can see how the signal level of the interference is correlated with the antenna pattern.

It is immediately obvious that the power of the interference source in the receiver is directly correlated with the antenna pattern of the array. One should take note how much stronger the interference power is when it is inside the main lobe of the antenna pattern. It will be shown shortly that this poses a major problem for SLC.

The next figure shows the SINR of the original signal uncorrupted by interference on the same plot as SLC and SABC as well as LCMV with interference present. One can see from the plot that LCMV comes very close to achieving the SINR of the original signal when the interference is in the side lobes; it is of course plagued by the computational complexity mentioned in previous sections. For this same interval of interference angles SLC has performed about 5 dB below that of LCMV and SABC has a

performance that oscillates between the two. Once the interference source enters the main lobe of the antenna pattern, the performance of all algorithms degrades, including LCMV. However, SABC performs much better that SLC during this interval and as well as LCMV. This turns out to be a very important discovery about SABC. It was developed as a method to improve performance over SLC in the side lobes, but it turns out that it performs as well as LCMV in the main lobe. This is a very practical discovery because LCMV is the best performance one can hope for in the main lobe.

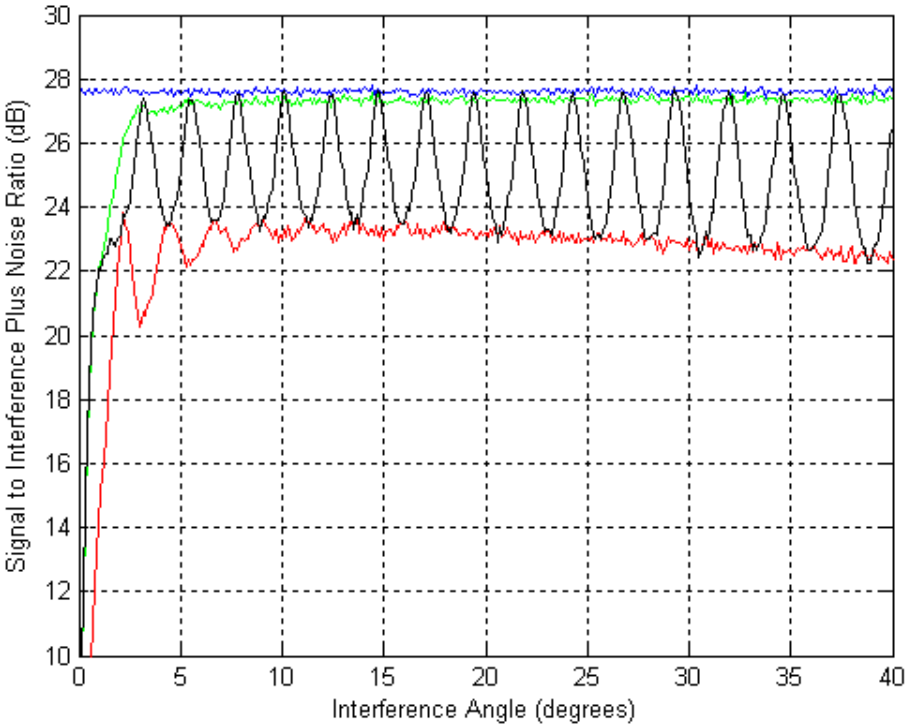

Figure 5-8 – Signal to interference plus noise levels when no interference is present (blue), for LCMV (green), for SLC (red), and for SABC (black).

It is important to understand what is happening to the signal of interest and the interference when SLC and SABC are used if one wants to understand why SABC is

better. It was stated previously that SABC should perform better for two reasons: because it distorts the signal of interest less and it is better able to calculate the weights in the presence of noise with limited training samples. Figures 5-9 and 5-10 show the latter plays a much bigger role in the performance improvement. Figure 5-9 is a plot of the signal power after the canceller. SLC has a variation on this power while SABC has one that is constant in the side lobes; however, this effect accounts for less than a decibel. Figure 5-10 shows the amount of interference residue present after the canceller. SLC always has at least 4 dB of extra residue over the case with no interference whereas SABC oscillates between 0 to 4 dB of extra residue. It turns out that SABC performs best when the interference is in the peak of a side lobe. This reinforces the idea stated in section 4.2.2 that the extra gain of the beam allows for the algorithms to solve for a more accurate weight that is able to subtract out the interference.

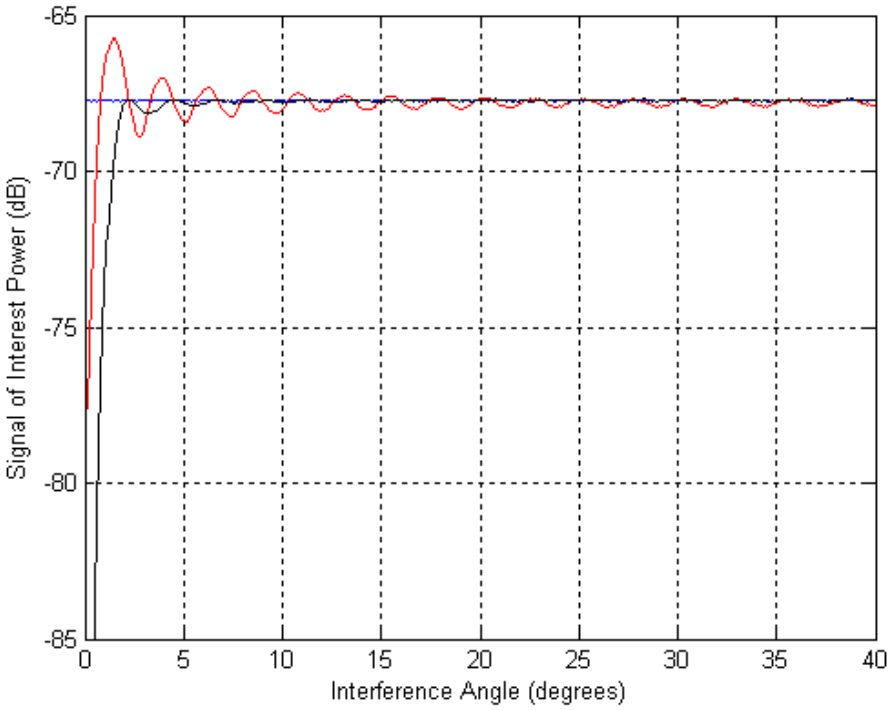

Figure 5-9 – Power of the signal of interest with no interference present (blue), after SLC (red), and after SABC (black).

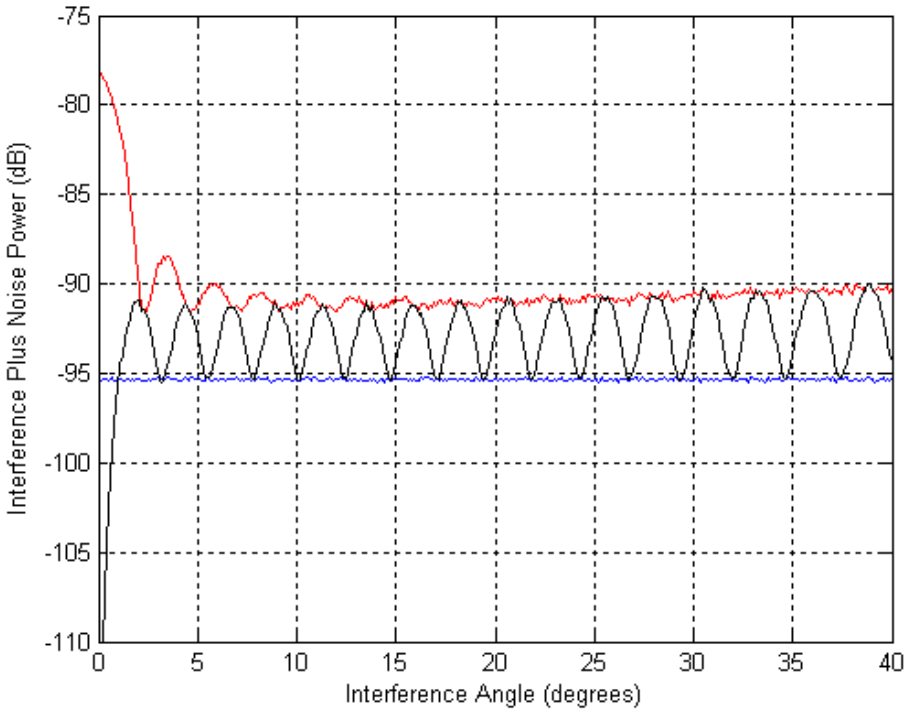

Figure 5-10 – Power of the interference plus noise with no interference present (blue), after SLC (red), and after SABC (black).

5.1.3 How Extra Auxiliaries Impact Interference Cancellation

Up until this point, all simulations of SLC have had a single auxiliary channel to deal with one source of interference. It was shown SLC provided a reasonable gain in performance under this condition; however, this configuration is only useful when the operator knows only one interfering signal is present; this is not a reasonable assumption.

It is well known that SLC needs as many auxiliary channels as there are interference sources. The array is usually designed to have as many auxiliary channels as the system is suspected to need in operation which means there may be unused auxiliary channels. This presents a problem because extra auxiliary channels will cancel out the

signal of interest if it is present in the training data and there is no interference for the auxiliary to cancel. This problem may be avoided by training on a region free of the signal such as a Doppler processed region; however, there is another problem that is much harder to deal with for a multi-auxiliary system.

If there are more auxiliary channels than interference sources, the signal received by the auxiliary channels become highly correlated. This is demonstrated below in Figures 5-11 and 5-12. In both of these figures the blue and red plots are the auto-correlation of auxiliaries one and two respectively while the black is the cross-correlation between the cannels. The first is for when only one source of interference is present while 5-12 is for when there are two sources of interference. One can see that when there are more auxiliaries than interferers, and thus extra degrees of freedom, the auxiliaries are as correlated to each other as they are to themselves. However, when there are not any extra degrees of freedom then the auxiliaries are not as correlated. The problem that arises when the auxiliaries are too correlated is that the covariance matrix in (2.27) becomes close to singular and the resulting weights are unstable. The ways to avoid this problem are to ensure that there are not more auxiliaries than interference sources, or to decompose the covariance matrix.

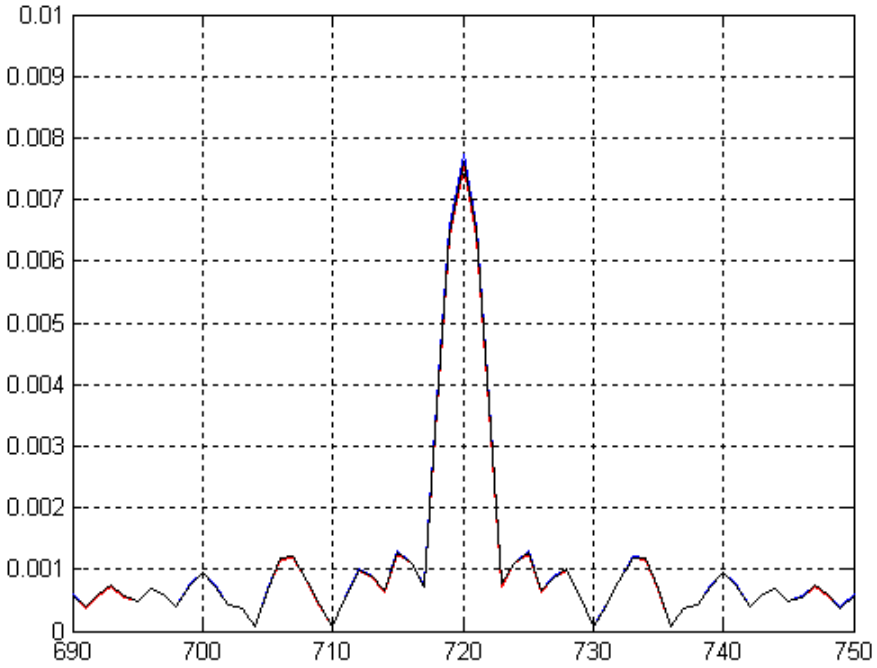

Figure 5-11 – The auto-correlation of auxiliary channels one (blue), two (red), and their cross-correlations (black) with only one source of interference. One can see that the cross-correlation is as high as the auto-correlations meaning the auxiliaries are very correlated.

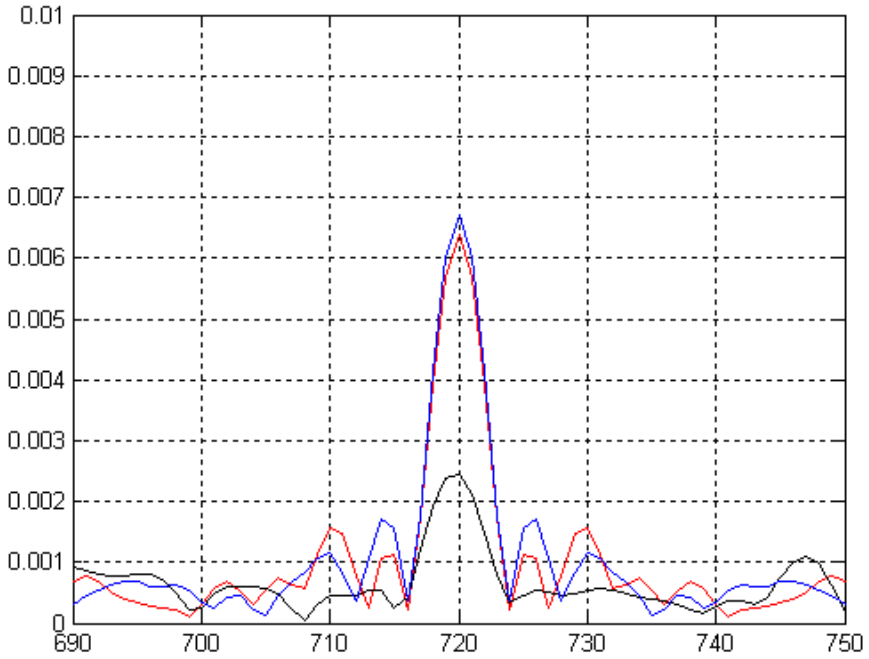

Figure 5-12 – The auto-correlation of auxiliary channels one (blue), two (red), and their cross-correlations (black) with two sources of interference. One can see that the cross-correlation is not as high as the auto-correlations, but is still quite high.

It turns out that this is not a problem for SABC because it independently solves for the amount of interference sources and their directions using ESPRIT; therefore, it never has extra auxiliary beams. In addition, because SABC forms high gain beams on the interference sources, they are much less correlated than the low gain auxiliary channels as shown below in Figure 5-13.

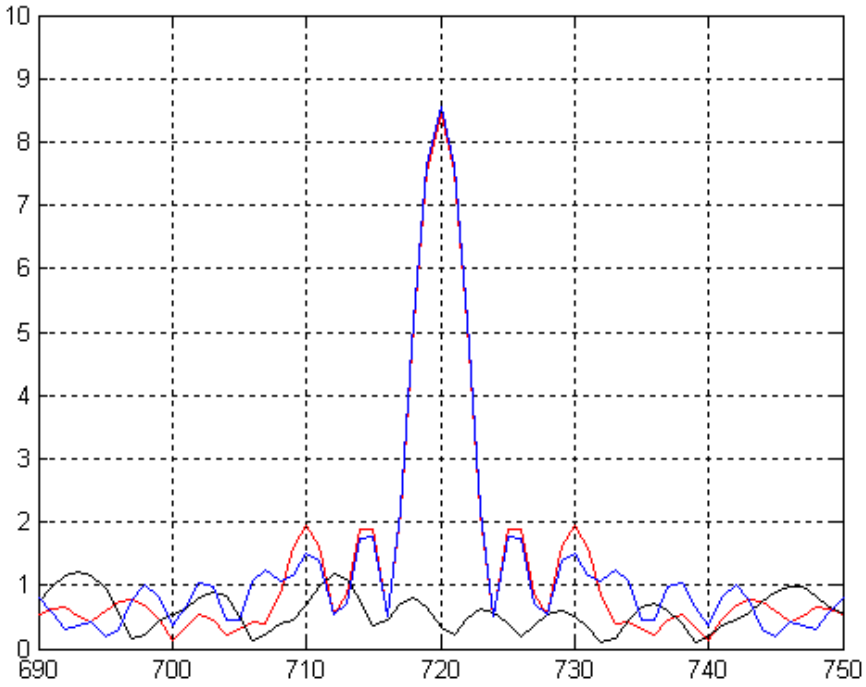

Figure 5-13 – The auto-correlation of SABC auxiliary channels one (blue), two (red), and their cross-correlations (black) with two sources of interference. One can see that the cross-correlation is not very low relative to that of SLC auxiliary channels.

5.1.4 Performance in the Presence of Multiple Interference Sources

The last section discussed one of the major problems associated with SLC in that the performance is impacted when more auxiliary channels are available than the amount of interference sources present. This section examines the performance of SABC and SLC under the assumption that there are as many auxiliary channels as there are interference sources. Two scenarios with two conditions each will be examined in this section. The two scenarios are when there are two and six interference sources respectively, and the conditions are whether or not the interference overpowers the signal of interest.

The first situation is for when there are only two interference sources and the signal of interest is stronger than the interference in the main beam. At first, one source of interference is kept at a constant angle of -40 degrees while the other is swept from 30 to 40 degrees.

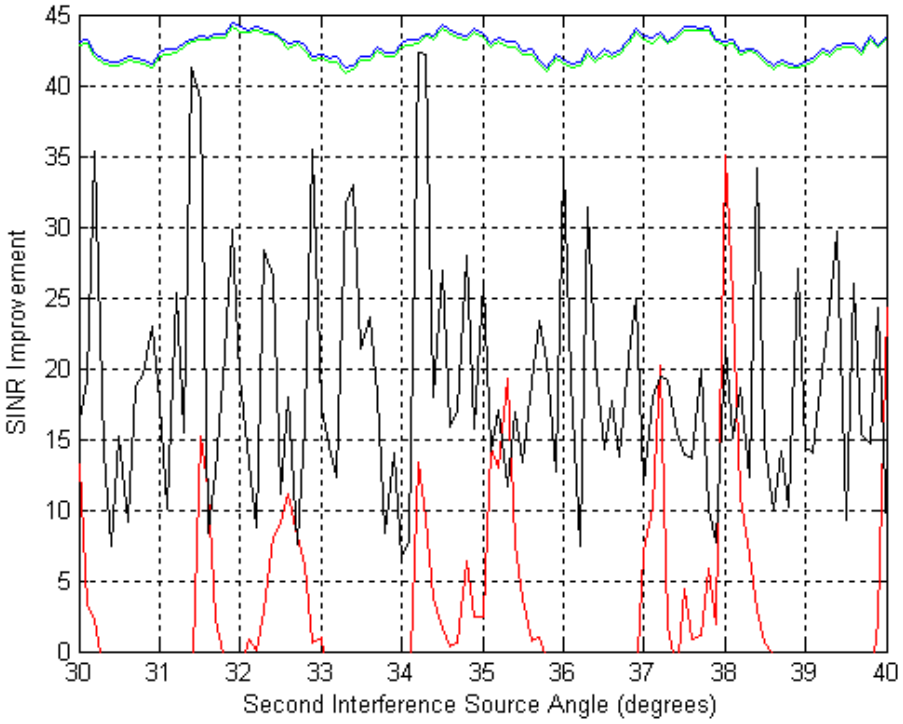

Figure 5-14 – SINR Improvement for the ideal case (blue), LCMV (green), SABC (black), and SLC (red) when the signal is stronger than the interference.

One can see from the figure that LCMV has the best performance when there is more than one source of interference since it is always within half a decibel of the ideal case. SABC always provides a gain in performance of at least 10 dB while SLC struggles to provide an increase in performance. With careful inspection, the areas where SLC is

providing a performance gain is when the second interference source is in the peak of a side lobe. This is consistent with what was covered last section because there is essentially only one source of interference in the regions where the second interference source is weak, thus breaking SLC.

With the exception of the pattern of SLC just mentioned, the performance of SLC and SABC does not follow a smooth curve as it did with a single source of interference. Although it has not been verified, we feel this is most likely because the sources of interference themselves are random signals and how their signals add in the array affects the its performance. Ideally, they would be completely uncorrelated; however, they will be correlated because of the fact that they are band limited and thus colored. Figures 5-15 and 5-16 show how the performance varies across trials for two different but fixed interference scenarios. One can see how the performance varies from trial to trial which may be due to the coloring of the interference. It is important to note that while the performance of SABC is stochastic, it provides a major performance gain in both cases. However, SLC only provides a guaranteed gain in the second scenario when the interference configuration seems to allow for favorable performance from SLC.

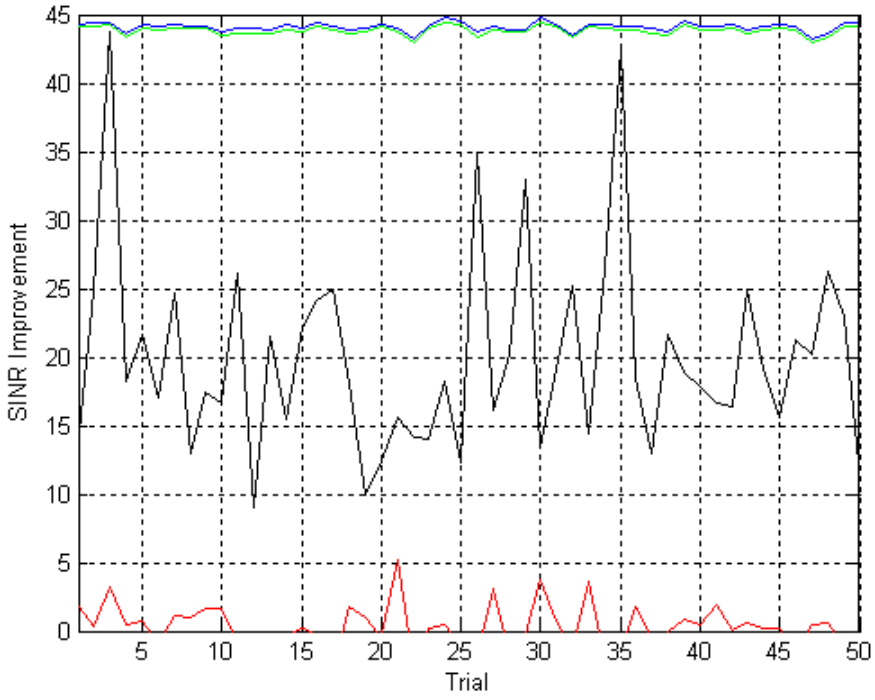

Figure 5-15 – SINR Improvement for the ideal case (blue), LCMV (green), SABC (black), and SLC (red) for interference at -40 and 32 degrees.

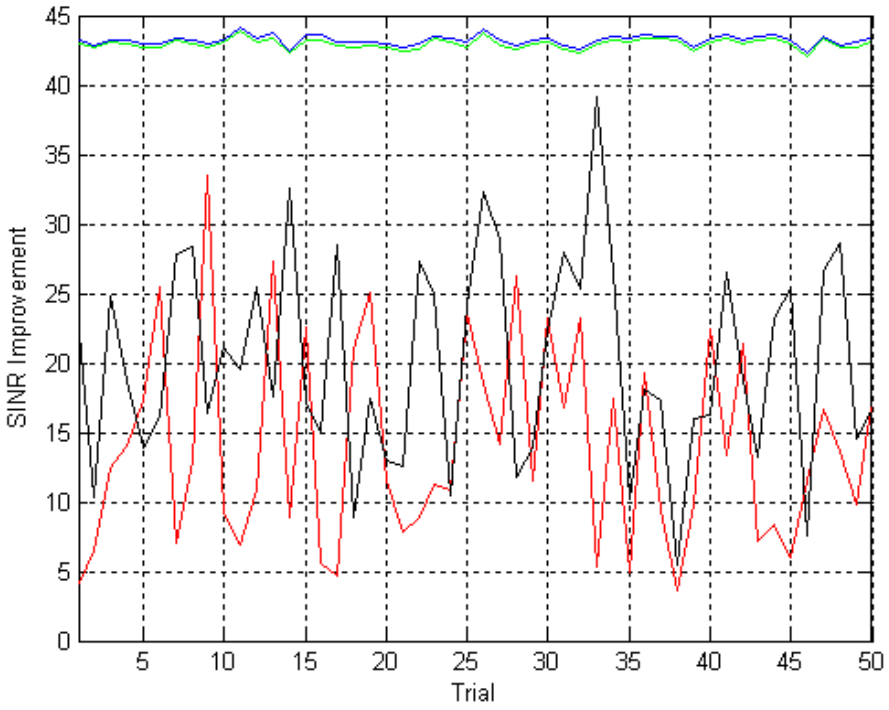

Figure 5-16 – SINR Improvement for the ideal case (blue), LCMV (green), SABC (black), and SLC (red) for interference at -40 and 38 degrees.

The next case to consider is how the cancellers work in the presence of two interference sources whose power in the array is greater than that of the signal of interest which is what is shown in Figure 5-17. In this scenario, one interferer is positioned at -40 degrees and the other is scanned from 30 to 40 degrees. Also, the interference overpowers the signal of interest because of a decrease in the signal of interest, not an increase in the interference power.

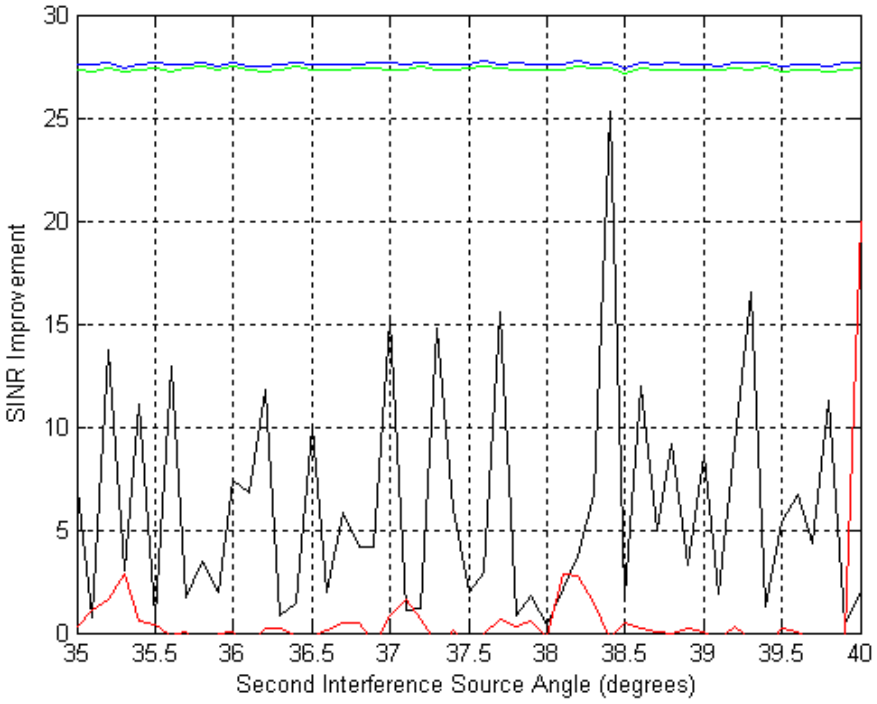

Figure 5-17 – SINR Improvement for the ideal case (blue), LCMV (green), SABC (black), and SLC (red) when the signal is weaker than the interference.

It is evident from this figure that SLC and SABC are not performing as well as when the signal of interest was stronger than the interference. Part of this may be due to the trivial fact that less performance gain is available since the signal to noise ratio is lower; however, there is a more severe loss occurring also. Since the signal of interest is much smaller than the interference, the canceller is much more sensitive to the calculated weights. If there are any errors in the weights caused by the limited training data or correlation between the auxiliaries, then the signal will be severely distorted. This phenomenon manifests itself much more in SLC than it does SABC as is evident by the figure. SABC is still able to achieve reasonable performance gain because of the high gain on the interference sources. Once again, SABC performs better than SLC.

The final case that will be tested for the narrowband simulations is how the cancellers perform in the presence of more than two sources of interference, or six in this case. In this experiment, only two auxiliaries are used for SLC because it does not work when six are used. This is again due to the fact that the auxiliaries are too correlated and cause an unstable weight calculation.

Figure 5-18 shows the performance of the various cancellers for one hundred Monte Carlo trials of an interference scenario. In each trial the six interferers are randomly placed between -80 and 80 degrees dictated by a uniform random variable. Any trials with an interferer between -2 and 2 degrees are thrown out so that main lobe interference is not a possibility. The signal of interest has enough power that it overpowers the interference most of the time. There are a few trials when the interference is stronger due to several sources being in side lobe peaks.

It is evident that SABC and SLC do not perform as well as LCMV; however, SABC outperforms SLC. It is always performing at least as well as SLC, but in most cases is performing much better being several decibels better. In many instances SLC does not even provide a performance increase; however, SABC almost always does even though it may only be less than a decibel.

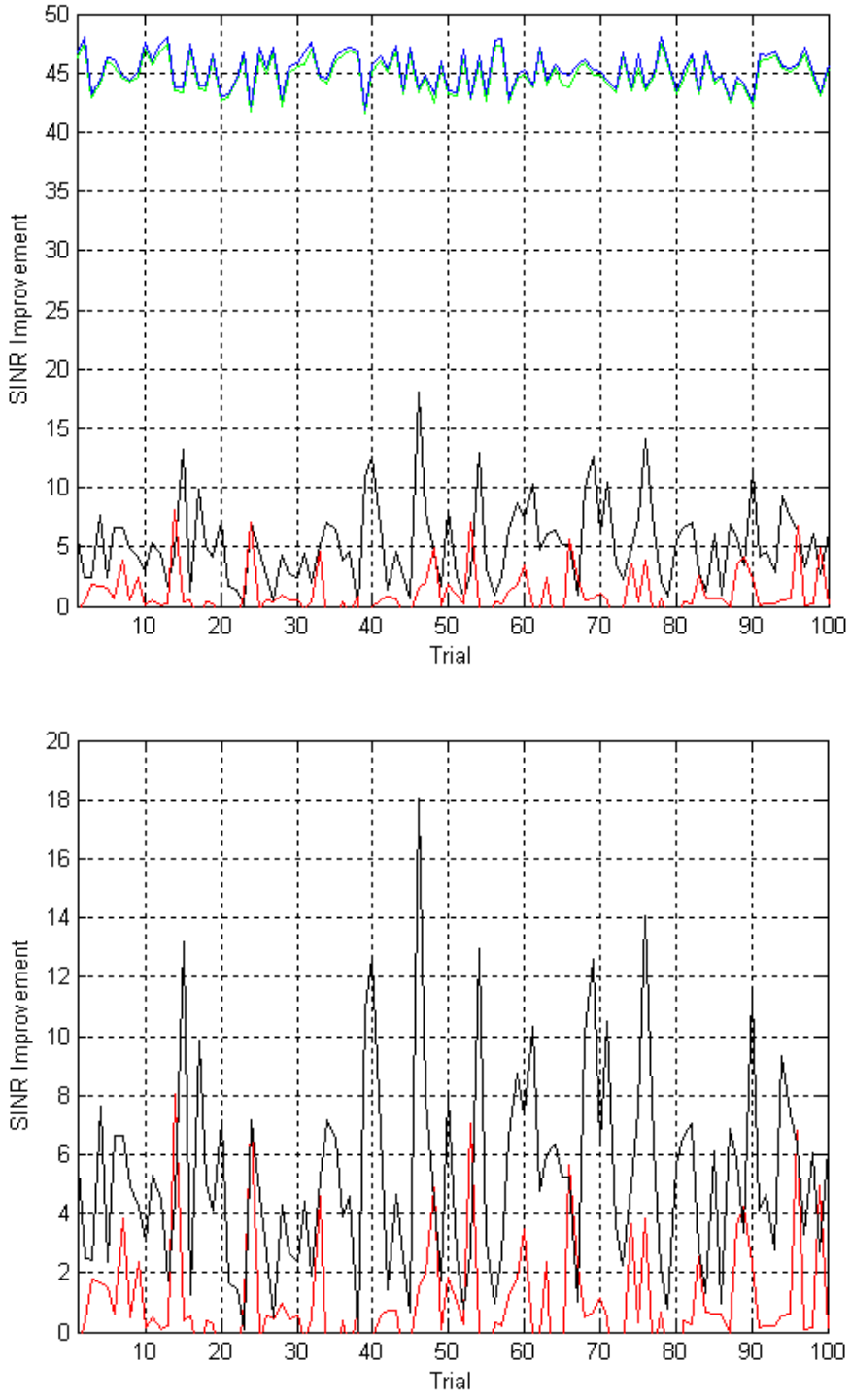

Figure 5-18 – SINR Improvement for the ideal case (blue), LCMV (green), SABC (black), and SLC (red) with six randomly placed sources of interference. Both plots show the same information; however, the bottom is zoomed in on SABC and SLC.

Both SABC and SLC break when the signal is weak relative to the six sources of interference. This is most likely because of the reason mentioned in section 5.1.3 where the canceller performance is sensitive to weight calculations due to the weak signal and any error in the weights will cause a drastic error in the signal of interest.

5.2 SIMULATION OF A WIDEBAND LINEAR ARRAY

The previous section showed the results for several interference configurations with a narrowband linear array. This section extends the same concept to an array where the narrowband assumption may no longer be used. To account for the wideband nature of the signal and interference, sub-banding is used. For this simulation, both the signal of interest and the interference have a bandwidth of 120 MHz with a center frequency of 3 GHz.

5.2.1 Choice of the Number of Sub-bands

When doing a wideband problem, the selection of the number of sub-bands to use is a very important consideration. Figure 5-19 graphically shows the justification for choosing 10 sub-bands in this problem. This figure shows the envelope of the signal of interest. Since this is a LFM pulse, the edges of the pulse contain the highest and lowest frequency components. One can see that the most extreme frequencies contain about half the power of the center frequency for the case with one sub-band, or simply a narrowband array. The loss is no longer present when using five sub-bands; however, there is some ripple in the envelope of the signal. There is also no loss when ten sub-bands are used with the added benefit of a flat envelope as desired. For this reason, the wideband

simulations will all be using ten sub-bands. Most of the things that were learned about SLC and SABC in the narrowband case still apply to the wideband situation, but there are some new effects that will be shown that are unique to the wideband case.

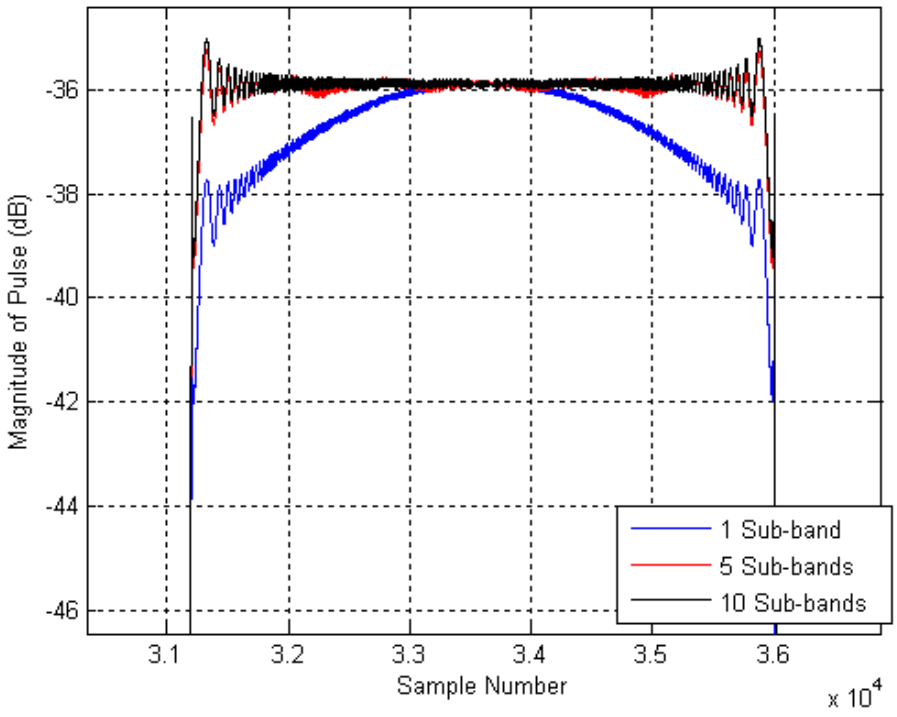

Figure 5-19 – Signal distortion caused by using only one sub-band (blue), five sub-bands (red), and ten sub-bands (black). Notice how the pulse envelope has the flattest response when ten sub-bands are used.

5.2.2 SLC and SABC Performance with One Source of Interference

The first simulation for the wideband array is to sweep an interference source from the boresight of the antenna and parametrically sweep it through the side-lobes. Figures 5-20 and 5-21 show the results of this simulation. One can see that both SABC and SLC provide an improvement most of the time. The only times they do not provide

an improvement is when the SINR is already high since the interference source is in a null of the antenna. One can also see that SABC still outperforms SLC; however, the improvement is not nearly as dramatic and does not reach the performance of the ideal canceller as it does in the narrowband case. The one area where it still provides the greatest gain is in the main beam of the antenna where it is able to provide a consistent five decibels of SINR unlike SLC.

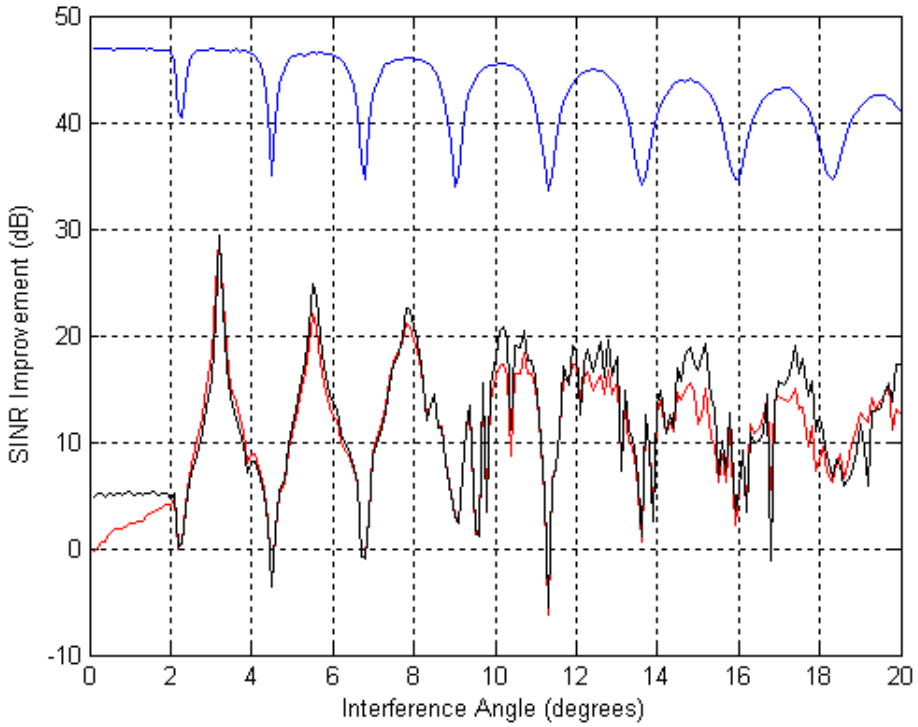

Figure 5-20 – SINR Improvement for the ideal case (blue), SLC (red), and SABC (black) when one source of interference is present.

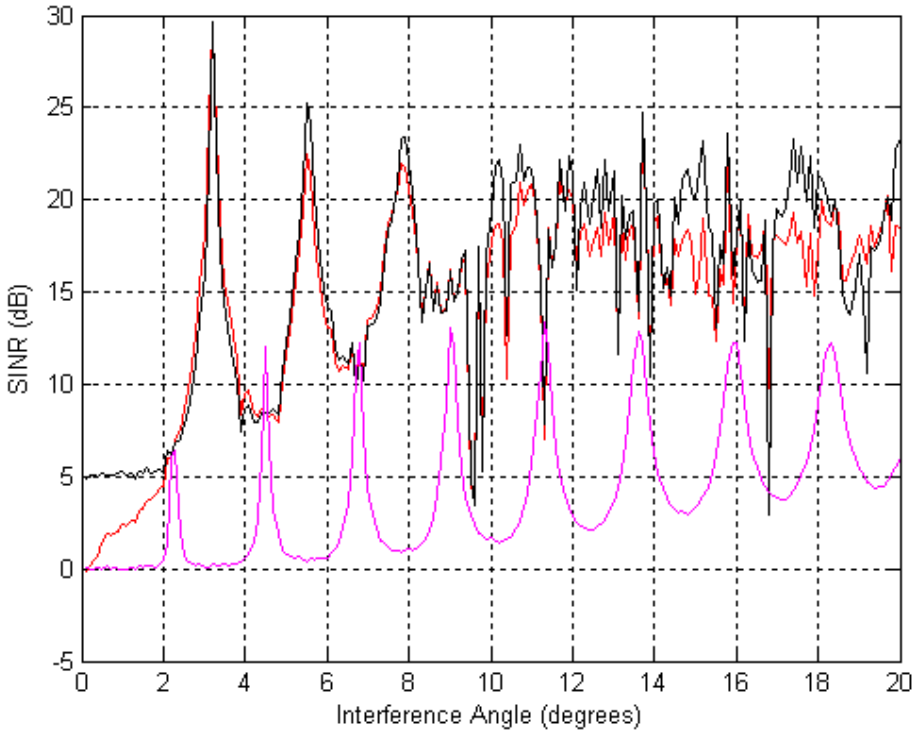

Figure 5-21 – Signal to noise ratio without any interference cancelation (magenta), with SLC (red), and with SABC (black).

5.2.3 SLC and SABC Performance with Multiple Sources of Interference

The next simulation is to include multiple sources of interference as was done with the narrowband problem. Figures 5-22 and 5-23 show how SLC and SABC perform when there is an interference source located 40 degrees off boresight, and a second is swept from 20 to 25 degrees.

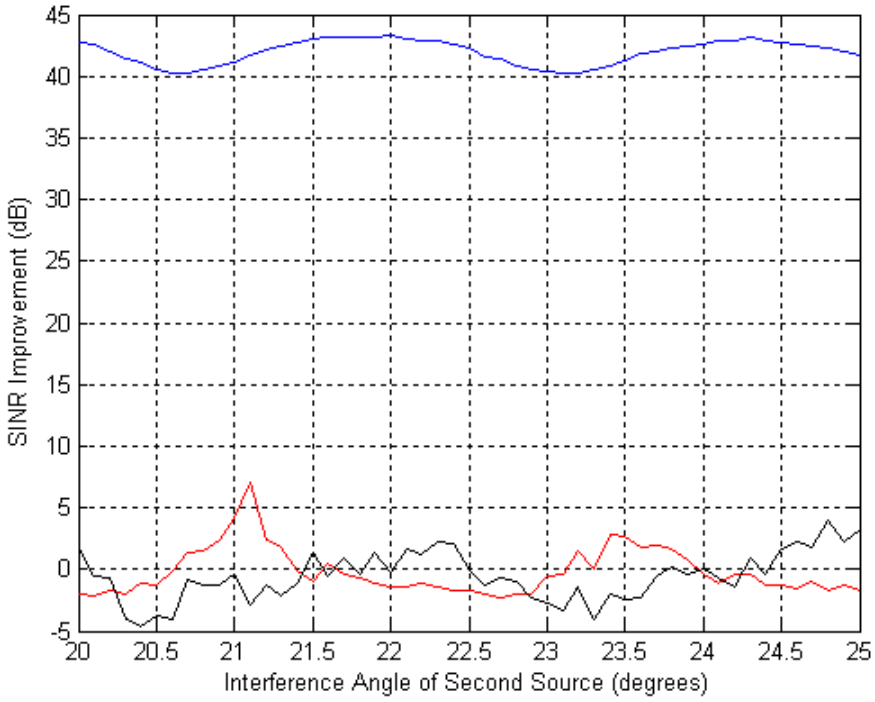

Figure 5-22 – SINR Improvement for the ideal case (blue), SLC (red), and SABC (black) when two sources of interference are present.

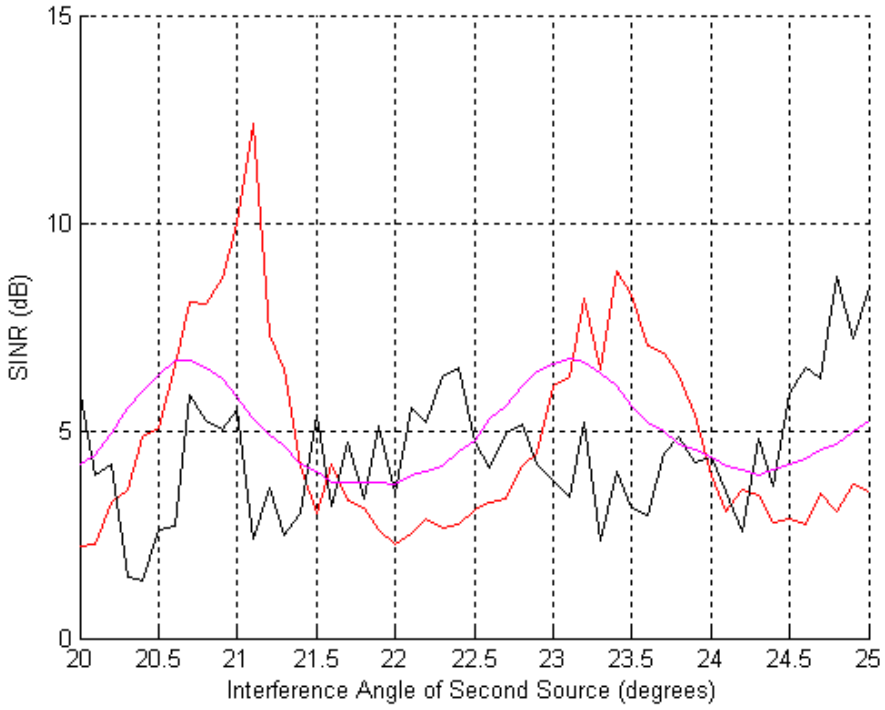

Figure 5-23 - SINR with no interference cancellation (magenta), SLC (red), and SABC (black) when two sources of interference are present.

In this scenario both cancellers don't seem to provide too much of an increase in SINR. Both cancellers either provide a modest improvement in SINR or a minor degradation. The degradation is never so much that it eliminates the signal to below the interference for either SLC or SABC. An interesting thing to note from Figure 5-23 is that there is an oscillating pattern of when SABC and SLC provide a gain or loss and that one is improving performance while the other is degrading it. It turns out SLC works better when the interference power is weakest and SABC when it is strongest. For this reason, the trial of two interference sources is repeated with one interference source much closer to the boresight of the array. This trial helps to show how SABC performs better for higher levels of interference and its results are shown in Figures 5-24 through 5-26.

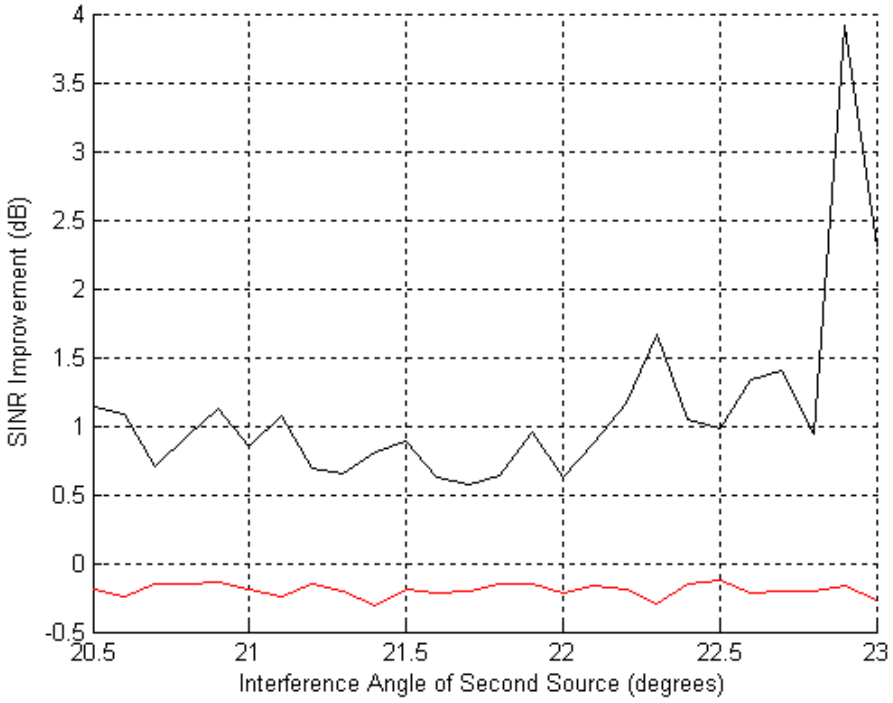

Figure 5-24 – SINR Improvement for SLC (red) and SABC (black) when one interference source is located 10 degrees off boresight and the other is swept from 20.5 to 23 degrees.

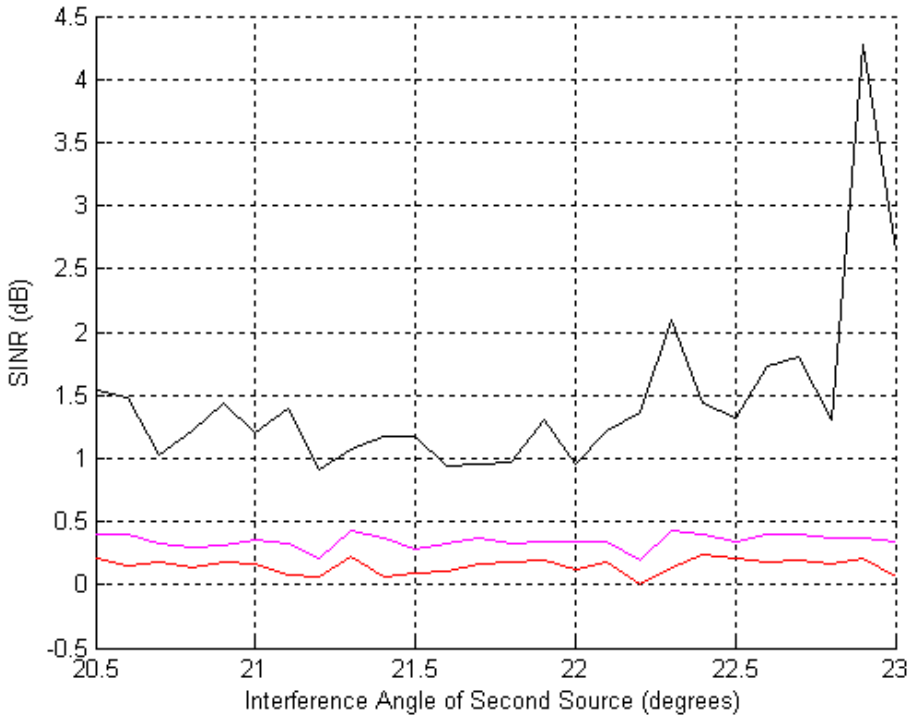

Figure 5-25 - SINR for the corrupted signal (magenta), SLC (red) and SABC (black) when one interference source is located 10 degrees off boresight and the other is swept from 20.5 to 23 degrees.

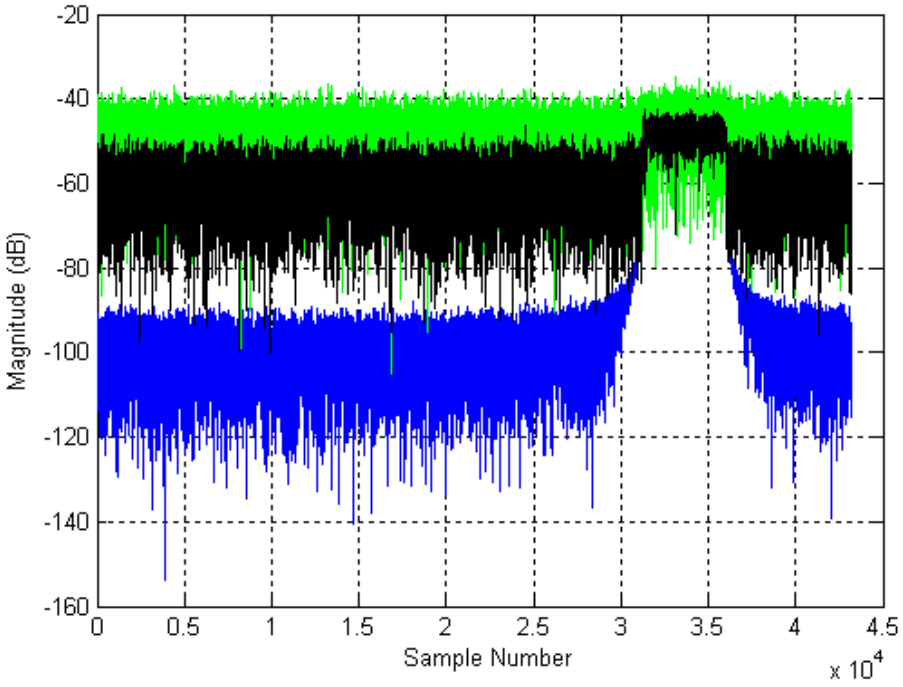

Figure 5-26 – Magnitude vs. time of the signal of interest without interference (blue), with interference (green), and with SABC correction applied (black).

Now that the first interference source is located much closer to the boresight of the array, SABC provides a more significant improvement and SLC is in fact degrading the performance. SABC may not be reaching the ideal performance of about 45 dB, but it is better than not having a canceller.

The final simulation is to test the performance of SABC and SLC in the presence of several sources of interference. In this experiment the six interference sources are placed randomly between 2 and 80 degrees with a uniform distribution for 50 trials. Figure 5-27 shows the results of this experiment. How the two cancellers perform is stochastic in nature, but it is important to gather that SABC is performing better than SLC. SABC provides a performance increase more than 50% of the time while SLC

degrades the performance more than 50% of the time. Additionally, SABC provides a better SINR improvement on a trial by trial basis. Based on information from previous experiments, it may be inferred that SABC performs better when the interference sources are strong.

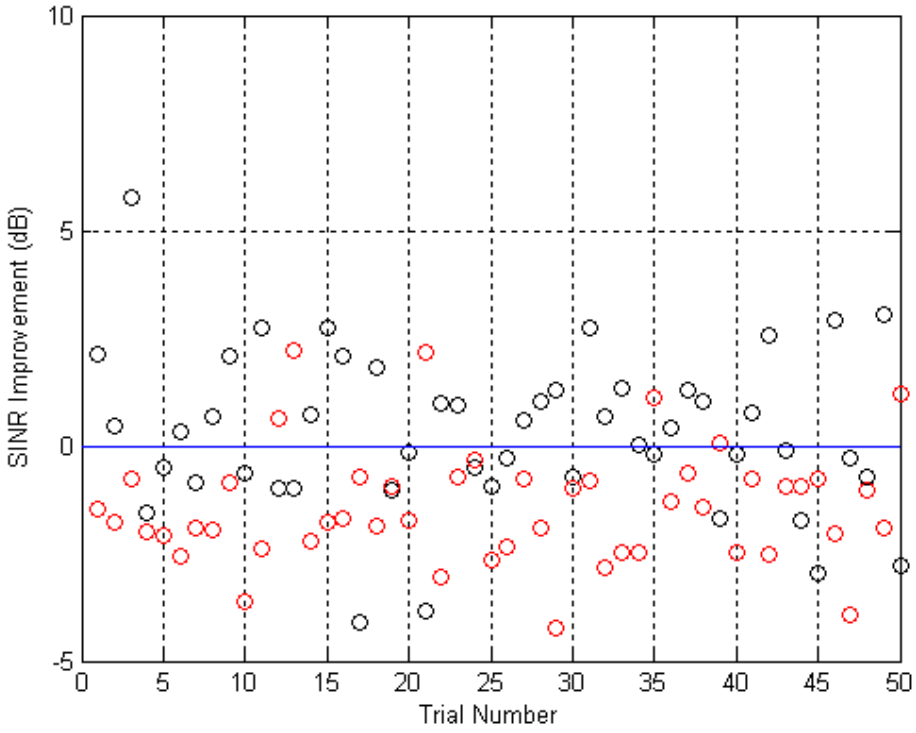

Figure 5-27 – SINR Improvement for SLC (red) and SABC (black) for 50 trials of six randomly placed interference sources.

5.3 CONCLUSIONS

In this chapter we performed several simulations of both SLC and SABC and compared them to LCMV and ideal case. Through these simulations we learned a lot about both SLC and SABC; when they work well and when they don't. SLC never

performs as well as LCMV, but SABC sometimes does. In situations where several sources of interference are present, the performance of SLC and SABC are somewhat random; however, SABC performs better on the average. Overall, these simulations showed SABC met the criteria that it was designed for. That is, one is better off using SABC than SLC in terms of performance without the computational burden of LCMV.

CHAPTER 6

CONCLUSIONS

This thesis has covered several topics in array signal processing. It started by explaining how to use time delays to focus a beam towards a certain direction to increase the strength of a desired signal; this was done for both narrowband and wideband signals. It then continued to explain how this may be done in the presence of interference with the goal of maintaining the strength of the signal of interest while minimizing the strength of the interference. The two methodologies to do this were LCMV and SLC. It was shown that both are capable of completely removing the interference under ideal circumstances; however, SLC has the problem of distorting the signal of interest. The reason this degradation has been tolerated to date is that SLC is a much simpler solution to calculate computationally.

We then introduced a new method, SABC, which is now possible because of digital arrays where every element is sampled. Since the information from all channels is saved instead of being combined into one channel, much more information is available about the interference and more operations may be performed on the data. SABC works by forming a beam on the signal of interest and the sources of interference and then using these channels as inputs to a side-lobe cancelling architecture. ESPRIT was used to solve for the locations of the interference sources.

We showed that SABC is much cheaper than LCMV in a computational sense and operates on a scale much closer to SLC. It was shown mathematically why SABC

performs better than SLC and verified with simulations. The simulations showed that for a narrowband signal SABC performs as well as LCMV in the main beam where SLC has poor performance. It also showed that with one source of interference, SABC performance is bounded by LCMV and SLC for its highest and lowest performance levels. SABC was designed as a means to reduce the amount of signal distortion, but it turned out it gained most of its performance gain over SLC because it was able achieve higher levels of ICR. This happed because the extra gain on the interference in SABC provided better training data to calculate the weights.

As more sources of interference were added, the performance of SABC became less predictable and no longer operated as well as LCMV but still performed better than SLC. The reason for this was SABC was more capable of calculating weights due to a higher gain on the interference and the auxiliary channels being less correlated.

The same simulations were performed on wideband signals with similar results. LCMV was not computed for these problems because they added too much time to simulations that already took several hours, but it is assumed that it still outperformed SABC in the wideband case. A parametric scan of the interference angle showed that SABC was still performing better than SLC for all angles and was much better in the main beam of the array. As more interference sources were added, the performance of SABC and SLC degraded and became difficult to predict, but the ensemble of trials showed that SABC tended to perform better than SLC.

These simulations showed that SABC does not outperform LCMV, but matches its performance under certain circumstances and is much more efficient computationally. In fact, its computational cost is much closer to that of SLC, which it outperforms.

SABC is able to outperform SLC because it distorts the signal of interest less, is more capable of training on the interference in the presence of noise, has auxiliary channels that are much less correlated, and automatically calculates the number of interference sources so that it does not have un-used auxiliary channels. Another benefit not mentioned in this paper is that SABC is able to provide the location of the interference so that the operator may take action to turn off the interference. This is something that neither SLC nor LCMV does.

There is one case neither SLC, SABC, nor LCMV is able to handle, which is when the interference is arriving from the same angle of arrival as the desired signal. In this case, the interference is removed but so is the signal of interest. We plan to explore methods in the future to overcome this problem.

In our future work, we also plan to re-run our simulations with arrays more relevant in real world situations. Our simulations had element spacing of half a wavelength and did not use a taper. We decided not to use a taper because we were not using clutter in our model; however, a real phased array will need a taper. Our next simulations will be on a phased array with elements spaced 0.6 wavelengths apart and with a taper that will suppress the first side-lobe to -25 dB.

Another area of future work on this subject will be to further investigate how to implement these algorithms in hardware. A digital array needs to have a receiver and an analog-to-digital converter for every element. Ideally, these receivers would be perfectly equalized; however, in real hardware they will be mismatched across their pass-bands and introduce errors between the channels that cannot be removed by the adaptive algorithms because they are uncorrelated. These effects need to be studied so that we

understand how well the receivers need to be matched to obtain given levels of interference cancellation.

Another area of future work concerns the processing of these algorithms. This thesis went through great lengths to emphasis the importance of computational complexity of these algorithms and it made the case for simplicity. While it was demonstrated that SABC was more computationally efficient than LCMV, it only implemented the algorithms in Matlab simulations. The next important step is to implement these algorithms in hardware capable of operating in real time. Among other things, this is going to require handling of time requirements and dealing with the parallel nature of the problem. We plan to study how to process digital array data with these algorithms in real time using various technologies to include general purpose processors, graphical processing units, and field programmable gate arrays.

Finally, we hope to try these algorithms on real data recorded from field trials. There are many artifacts that are not captured by simulations such as multipath, third-order modulations, and other hardware effects. Although simulations are useful, the data from field trial will help give us much more confidence in our algorithms.

REFERENCES

[1] Ahmed, K.M.; Evans, R.J.; , "Broadband adaptive array processing," *Communications, Radar and Signal Processing, IEE Proceedings F* , vol.130, no.5, pp.433-440, August 1983

[2] Adaptive Array Radar Processing (22-25 April, 2008), Georgia Institute of Technology, Defense Technology Short Course, "Theory of Adaptive Algorithms," D.D. Aalfs

[3] Applebaum, S.; Chapman, D.; , "Adaptive arrays with main beam constraints," *Antennas and Propagation, IEEE Transactions on* , vol.24, no.5, pp. 650- 662, Sep 1976

[4] Baowei Su; Yongliang Wang; Liangzhu Zhou; , "A mainlobe interference cancelling method," *Microwave, Antenna, Propagation and EMC Technologies for Wireless Communications, 2005. MAPE 2005. IEEE International Symposium on* , vol.1, no., pp.23-26 Vol. 1, 8-12 Aug. 2005

[5] Breed, B.R.; Strauss, J.; , "A short proof of the equivalence of LCMV and GSC beamforming," *Signal Processing Letters, IEEE* , vol.9, no.6, pp.168-169, Jun 2002

[6] Brookner, E.; Howell, J.M.; , "Adaptive-adaptive array processing," *Proceedings of the IEEE* , vol.74, no.4, pp. 602- 604, April 1986

[7] Brookner, E.; , "Phased-array and radar astounding breakthroughs — an update," *Radar Conference, 2008. RADAR '08. IEEE* , vol., no., pp.1-6, 26-30 May 2008

[8] Byun, Bok Sub, Gangi, Anthony F., "A Constraint-Elimination Technique for Linearly Constrained Array Processing", *Geoscience and Remote Sensing, IEEE Transactions on*, On page(s): 8 - 15, Volume: GE-19 Issue: 1, Jan. 1981

[9] Cantoni, A., Godara, L.C., "Fast Algorithms for Time Domain Broadband Adaptive Array Processing", *Aerospace and Electronic Systems, IEEE Transactions on,* On page(s): 682 - 699, Volume: AES-18 Issue: 5, Sept. 1982

[10] Carlson, B. D., "Covariance matrix estimation errors and diagonal loading in adaptive arrays," *IEEE Trans. Aerosp. Electron. Syst.*, vol. 24, July, 1988.

[11] Chandran, Sathish. *Advances in Direction-of-arrival Estimation*. Boston: Artech House, 2006. Print.

[12] Cormen, Thomas H., Charles E. Leiserson, and Ronald L. Rivest. *Introduction to Algorithms*. Cambridge, MA: MIT, 1990. Print.

[13] Farina, A. "Single Sidelobe Canceller: Theory and Evaluation," *Aerospace and Electronic Systems, IEEE Transactions on* , vol.AES-13, no.6, pp.690-699, Nov. 1977

[14] Frost, O.L., III; , "An algorithm for linearly constrained adaptive array processing," *Proceedings of the IEEE* , vol.60, no.8, pp. 926- 935, Aug. 1972

[15] Gabriel, W.F.; , "Adaptive arrays—An introduction," *Proceedings of the IEEE* , vol.64, no.2, pp. 239- 272, Feb. 1976

[16] Godara, L.C., "Application of antenna arrays to mobile communications. II. Beam-forming and direction-of-arrival considerations", *Proceedings of the IEEE,* On page(s): 1195 - 1245, Volume: 85 Issue: 8, Aug 1997

[17] Goldstein, J.S., Reed, I.S., "Performance measures for optimal constrained beamformers", *Antennas and Propagation, IEEE Transactions on,* On page(s): 11 - 14, Volume: 45 Issue: 1, Jan 1997

[18] Goldstein, J.S., Reed, I.S., "Theory of partially adaptive radar", *Aerospace and Electronic Systems, IEEE Transactions on,* On page(s): 1309 - 1325, Volume: 33 Issue: 4, Oct. 1997

[19] Golub, Gene Howard, and Loan Charles F. Van. *Matrix Computations*. Baltimore, MD: Johns Hopkins UP, 1996. Print.

[20] H. Schrank and C. Hemmi, "Bandwidth of the Array Factor for Phase-Steered Arrays," *IEEE Antennas and Propagation Magazine,* Vol. 35 No. 1, February 1993

[21] Haykin, Simon S. *Adaptive Filter Theory*. Upper Saddle River, NJ: Prentice Hall, 2001. Print.

[22] Hunger, Raphael. *Floating Point Operations in Matrix-Vector Calculus*. Tech. Technische Universitat Munchen, 2007. Print.

[23] Jacob Benesty; Jingdong Chen; Yiteng (Arden) Huang; Jacek Dmochowski; , "On Microphone-Array Beamforming From a MIMO Acoustic Signal Processing Perspective," *Audio, Speech, and Language Processing, IEEE Transactions on* , vol.15, no.3, pp.1053-1065, March 2007

[24] Jian-Ren Wang; Ucci, D.R.; , "Main-lobe interference canceler," *Antennas and Propagation Society International Symposium, 1992. AP-S. 1992 Digest. Held in*

Conjuction with: URSI Radio Science Meeting and Nuclear EMP Meeting., IEEE, vol., no., pp.1027-1030 vol.2, 18-25 Jul 1992

[25] J.R. Guerci, Space-Tme Adaptive Processing for Radar, Artech House, Boston, 2003.

[26] Krim, H.; Viberg, M.; , "Two decades of array signal processing research: the parametric approach," *Signal Processing Magazine, IEEE* , vol.13, no.4, pp.67-94, Jul 1996

[27] K. Takao, M. Fujita, and T. Nishi, "An adaptive antenna array under directional constraint", *IEEE Trans. Antennas Propagat.*, vol. AP-24, pp.662 - 669 , 1976.

[28] L.E. Brennan and I.S. Reed "Theory of adaptive radar", IEEE Trans. Aerospace and Electronic Systems, vol. AES-9, 1973 .

[29] Lei Zhang; Wei Liu; Langley, R.J.; , "A Class of Constrained Adaptive Beamforming Algorithms Based on Uniform Linear Arrays," *Signal Processing, IEEE Transactions on* , vol.58, no.7, pp.3916-3922, July 2010

[30] Lin, H. "Design of element placement in adaptive arrays," *Antennas and Propagation Society International Symposium, 1980* , vol.18, no., pp. 383- 386, Jun 1980

[31] Liu, Wei, and Stephan Weiss. *Wideband Beamforming: Concepts and Techniques*. Chichester, West Sussex, U.K.: Wiley, 2010. Print.

[32] Longyang Huang, Bin Shen, Mengxing Li, Zemin Liu, "An Efficient Subband Method for Wideband Adaptive Beamforming", *Advanced Communication Technology, 2008. ICACT 2008. 10th International Conference on,* On page(s): 1489 - 1492, Volume: 3 Issue: , 17-20 Feb. 2008

[33] Manolakis, Dimitris G., Vinay K. Ingle, and Stephen M. Kogon. *Statistical and Adaptive Signal Processing: Spectral Estimation, Signal Modeling, Adaptive Filtering, and Array Processing.* Boston: Artech House, 2005. Print.

[34] Monzingo, Robert A., and Thomas W. Miller. *Introduction to Adaptive Arrays*. New York: Wiley, 1980. Print.

[35] Muralidhar Rangaswamy; , "Adaptive radar signal processing - the problem of exponential computational cost," *Integration of Knowledge Intensive Multi-Agent Systems, 2003. International Conference on* , vol., no., pp. 264- 269, 30 Sept.-4 Oct. 2003

[36] Nitzberg, R.; , "Performance of Digital Implementations of an Adaptive Processor," *Aerospace and Electronic Systems, IEEE Transactions on* , vol.AES-19, no.2, pp.168-173, March 1983

[37] Oppenheim, Alan V., Alan S. Willsky, and Ian T. Young. *Signals and Systems*. Englewood Cliffs, NJ: Prentice-Hall, 1983. Print.

[38] Reed, I.S.; Mallett, J.D.; Brennan, L.E. , "Rapid Convergence Rate in Adaptive Arrays," Aerospace and Electronic Systems, IEEE Transactions on , vol.AES-10, no.6, pp.853-863, Nov. 1974

[39] Richards, M. A. *Fundamentals of Radar Signal Processing*. New York: McGraw-Hill, 2005. Print.

[40] Roy, R.; Paulraj, A.; Kailath, T.; , "Direction-of-arrival estimation by subspace rotation methods - ESPRIT," *Acoustics, Speech, and Signal Processing, IEEE International Conference on ICASSP '86.* , vol.11, no., pp. 2495- 2498, Apr 1986

[41] Roy, T.; Meena, D.; Prakasam, L.G.M.; , "FPGA based Digital Beam Forming for Radars," *Radar Conference, 2009 IEEE* , vol., no., pp.1-5, 4-8 May 2009

[42] Skolnik, Merrill I. *Radar Handbook*. New York: McGraw-Hill, 2008. Print.

[43] S.P. Applebaum. *"Adaptive Arrays."* Syracuse University Research Corporation, Rep. SU-SEL-66-12, Tech Repon 67M-6, December 1966

[44] Takao, K.; Fujita, M.; Nishi, T.; , "An adaptive antenna array under directional constraint," *Antennas and Propagation, IEEE Transactions on* , vol.24, no.5, pp. 662- 669, Sep 1976

[45] Takao, K.; Komiyama, K.; , "An Adaptive Antenna for Rejection of Wideband Interference," *Aerospace and Electronic Systems, IEEE Transactions on* , vol.AES-16, no.4, pp.452-459, July 1980

[46] T. J. Shan and T. Kailath "Adaptive beamforming for coherence signals and interference", *IEEE Trans. Acoust., Speech, Signal Process.*, vol. ASSP-33, pp.527 1985

[47] Viikari, V.., Raisanen, A.V., "Antenna Pattern Correction Technique Based on Signal-to-Interference Ratio Optimization", *Antennas and Wireless Propagation Letters, IEEE,* On page(s): 267 - 270, Volume: 6 Issue: , 2007

[48] Ward, J.; Compton, R.T., Jr.; , "Sidelobe level performance of adaptive sidelobe canceller arrays with element reuse," *Antennas and Propagation, IEEE Transactions on* , vol.38, no.10, pp.1684-1693, Oct 1990

[49] Wei Liu, Renbiao Wu, Langley, R.J., "Design and Analysis of Broadband Beamspace Adaptive Arrays", *Antennas and Propagation, IEEE Transactions on,* On page(s): 3413 - 3420, Volume: 55 Issue: 12, Dec. 2007

[50] Widrow, B.; Mantey, P.E.; Griffiths, L.J.; Goode, B.B.; , "Adaptive antenna systems," Proceedings of the IEEE , vol.55, no.12, pp. 2143- 2159, Dec. 1967

[51] White, W.D., "Wideband Interference Cancellation in Adaptive Sidelobe Cancellers", *Aerospace and Electronic Systems, IEEE Transactions on,* On page(s): 915 - 925, Volume: AES-19 Issue: 6, Nov. 1983

[52] Zahm, C.L.; , "Application of Adaptive Arrays to Suppress Strong Jammers in the Presence of Weak Signals," *Aerospace and Electronic Systems, IEEE Transactions on* , vol.AES-9, no.2, pp.260-271, March 1973

[53] Zulch, P., Goldstein, J.S., "Performance Metric Issues for Space Time Adaptive Processing Methods", *Aerospace Conference, 2008 IEEE,* On page(s): 1 - 8, Volume: Issue: , 1-8 March 2008

[54] Picciolo, Michael L. *Robust Adaptive Signal Processors.* Dissertation. Virginia Polytechnic Institute and State University, 2003.

[55] Mathews, Ben. *New Cyclostationary Auxiliary Vector Selection Algorithm for Adaptive Beamforming.* Thesis. Virginia Polytechnic Institute and State University, 2005.

[56] Schoenig, Gregory N. *Constribution to Robust Adaptive Signal Processing with Application to Space-Time Adaptive Radar.* Dissertation. Virginia Polytechnic Institute and State University, 2007.

APPENDIX A

HOW THE NARROWBAND ASSUMPTION BREAKS DOWN

This appendix addresses the use of phase shifters for beam forming in phased array radars. It starts out by justifying why phase shifters may be used for a narrowband signal and then analyzes when a signal may no longer be considered narrowband. The paper concludes by solving for the losses associated with applying phase shifters to medium band signals. For the purposes of this paper, narrowband signals contain only a single frequency, medium band signals contain the range of frequencies for which a certain loss is acceptable, and wideband signal contain frequencies outside of that range.

This paper is based around the architecture shown in Figure 1 with a signal, x(t), being received by an array at an angle, θ. The first element will not have any delay since all elements are referenced relative to when this element starts to receive the signal. If the noise in all channels is ignored, the second element's received signal is the same as that of the first, except it is delayed. The delay for the i^{th} is as follows:

$$\tau = (i-1)\frac{d}{c}sin\theta \tag{A.1}$$

where d is the distance between adjacent elements, c is the speed of light, and θ is the angle of arrival of the signal relative to the boresight of the array, also known as the normal.

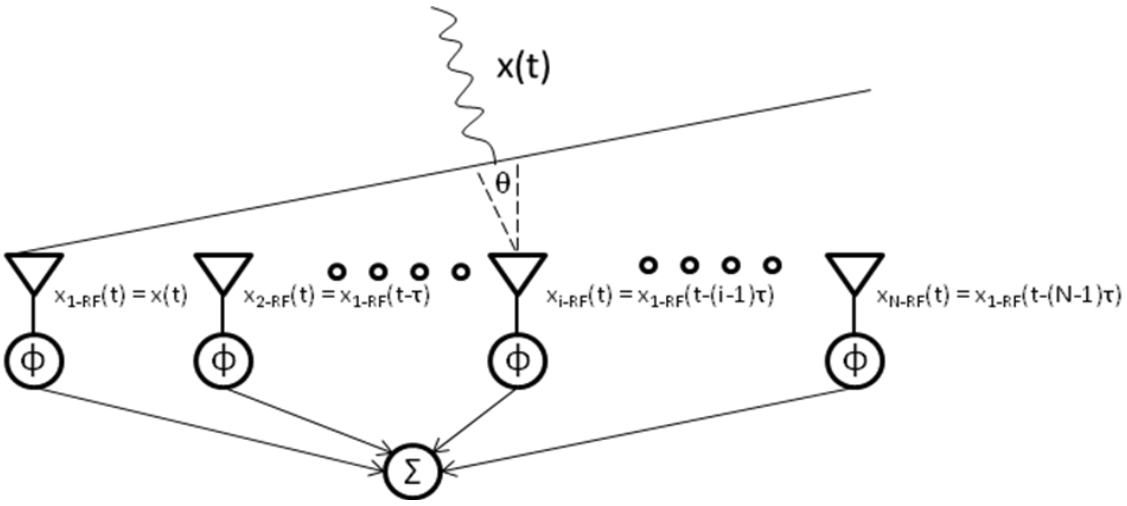

Figure A-1 - Diagram of Phased Array

A.1 DERIVATIONS

A.1.1 Implementing beam forming with phase shifters

For the case when x(t) is a narrowband signal, the bandwidth will be zero and x(t) will be a sinusoid at the radio frequency. Below, the signals received by the first and i^{th} elements are shown in the frequency domain to aid in analysis.

$$X_1(j\omega) = \mathcal{F}\left\{e^{j2\pi f_{RF}t}\right\} \tag{A.2}$$

$$X_i(j\omega) = \mathcal{F}\{x_1(t-\tau)\} = X_1(j\omega)e^{-j\omega\tau} \tag{A.3}$$

We know the value of τ and can use it in (A.3):

$$X_i(j\omega) = X_1(j\omega)e^{-j2\pi f(i-1)\frac{d}{c}sin\theta}$$

$$X_i(j\omega) = X_1(j\omega)e^{-j2\pi f(i-1)\frac{d}{\lambda f}sin\theta} \tag{A.4}$$

Equation (A.4) can be further simplified because the distance, d, is fixed at half the radio frequency wavelength and the radio frequency is the only frequency received.

$$X_i(j\omega) = X_1(j\omega)e^{-j2\pi f(i-1)\frac{\lambda_{RF}}{2\lambda f}sin\theta} = X_1(j\omega)e^{-j\pi(i-1)sin\theta} \tag{A.5}$$

$$x_i(t) = \mathcal{F}^{-1}\{X_i(j\omega)\} = \mathcal{F}^{-1}\left\{X_1(j\omega)e^{-j\pi(i-1)sin\theta}\right\} = x_1(t)e^{-j\pi(i-1)sin\theta} \tag{A.6}$$

Equation (A.6) shows that the signal received by the ith element is the same as the signal received at the first element multiplied by a complex scalar, or by shifting its phase. This implies that a beam can be formed by the array if this phase shift is applied incrementally across so that the signals in all elements may be constructively added. It is well known and stated in Schrank that the antenna pattern, or array factor, of an array of this type is:

$$AF(\theta) = \frac{\sin\left[N\pi\frac{d}{\lambda}(\sin\theta - \sin\theta_0)\right]}{N\sin\left[\pi\frac{d}{\lambda}(\sin\theta - \sin\theta_0)\right]} \tag{A.7}$$

where θ_0 is the steering angle.

A.1.2 Applying a Phase Shift to a Wideband Signal

The previous section showed that an incremental phase shift across the elements of a phased array can form and steer a beam. While this property is not unique to only one frequency of the array, it causes problems when more than one frequency is present in the signal of interest. Consider a multi-frequency signal that is approaching the array at an angle θ. A phase shift, ψ, can be found which will steer the array to that angle for the center frequency. For a particular element, this phase shift is the real part of the exponent in (A.6). This phase shift is only relevant to the frequency it was designed for. Equation (A.8) shows that if ψ is solved for a certain frequency and angle, f_0 and θ_0, then a change in frequency must be accompanied by a change in angle for ψ to remain constant.

$$\psi = -\pi(i-1)\frac{f}{f_0}\sin(\theta_0) = -\pi(i-1)\frac{f+\Delta f}{f_0}\sin(\theta_0+\Delta\theta) \tag{A.8}$$

Equation (A.9) simplifies (A.8) for a constant phase shift and groups the frequency terms and angle term separately.

$$-\pi(i-1)\sin(\theta_0) = -\pi(i-1)\frac{f_0+\Delta f}{f_0}\sin(\theta_0+\Delta\theta)$$

$$\sin(\theta_0) = \frac{f_0+\Delta f}{f_0}\sin(\theta_0+\Delta\theta)$$

$$\frac{f_0}{f_0+\Delta f} = \frac{\sin(\theta_0+\Delta\theta)}{\sin(\theta_0)} = \frac{\sin(\theta_0)\cos(\Delta\theta)+\cos(\theta_0)\sin(\Delta\theta)}{\sin(\theta_0)}$$

$$\frac{f_0}{f_0+\Delta f} = \cos(\Delta\theta) + \cot(\theta_0)\sin(\Delta\theta) \tag{A.9}$$

One may assume that the change in frequency is small compared to the carrier and that the change in angle is small enough to use the small angle approximation. With this assumption (A.9) reduces to the equation shown in Skolnik's *Radar Handbook*.

$$\frac{f_0}{f_0+\Delta f} \cong 1 + \cot(\theta_0)\,\Delta\theta$$

$$f_0 \cong f_0 + \Delta f + f_0\cot(\theta_0)\,\Delta\theta + \Delta f\cot(\theta_0)\,\Delta\theta$$

$$-\Delta f \cong f_0\cot(\theta_0)\,\Delta\theta + \Delta f\cot(\theta_0)\,\Delta\theta$$

$$\frac{-\Delta f}{f_0+\Delta f} \cong \cot(\theta_0)\,\Delta\theta$$

$$\Delta\theta \cong \frac{-\Delta f}{f_0}\tan(\theta_0) \tag{A.10}$$

Equations (A.8) through (A.10) show that a fixed phase shift solved to steer a certain frequency to an angle will steer a different frequency to a different angle. The change in angle, $\Delta\theta$, is solved by (A.10) relative to the original frequency, original angle, and change in frequency. This is the fundamental problem with a wideband array. This phenomenon becomes problematic when the angle adjustment for a certain frequency is outside of the main beam of the array factor in (A.7). This issue will be discussed further in the next section.

A.1.3 Errors in the Estimated Change in Angle

Equation (A.10) is an approximation of the change in steering angle due to a frequency change. The figure below shows how well this approximation reflects the true value. The true value of the change in steering angle is solved using Newton's Method to solve (A.9). Figure A-2 shows that the estimate works well for very small changes in steering angle while the small angle approximation is valid. However, it is important to keep in mind that wideband beam forming cannot use this assumption and (A.10) will not work; it overestimates angle shift and suggests the array has less bandwidth than it really does. Equation (A.10) was derived in this paper to aid in an understanding of the narrowband problem, but the true angle change using Newton's method will be used for any wideband analysis that follows.

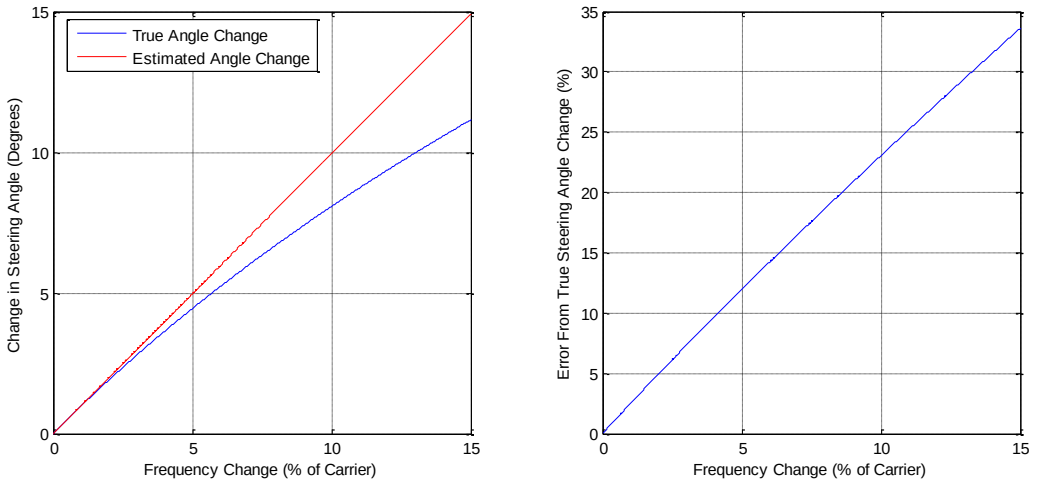

Figure A-2 - (a) Comparison of Change in Steering Angle (b) Percent Error from True value

A.1.4 Derivation of Array Bandwidth

Equation (A.7) is the array factor, or gain pattern, of an array with N elements. The beamwidth is going to be determined by the number of elements; more elements

results in a narrower beam. The definition of array bandwidth is the range of frequencies that will not be steered outside of this beamwidth using a single fixed phase shifter. The bandwidth of the array is a function of the number of elements. This section is going derive a useful estimate of the bandwidth of an array.

Equation (A.8) is used below to find the half power points of the array factor. For large values N and a constant frequency, equation ten can be approximated by the function below.

$$AF(\theta) = \frac{\sin\left[N\pi\frac{d}{\lambda}(\sin\theta - \sin\theta_0)\right]}{N\sin\left[\pi\frac{d}{\lambda}(\sin\theta - \sin\theta_0)\right]} \cong \frac{\sin\left[N\pi\frac{d}{c}f_0(\sin\theta - \sin\theta_0)\right]}{N\pi\frac{d}{c}f_0(\sin\theta - \sin\theta_0)} = 0.707 \tag{A.11}$$

One can use an iterative method to find that (A.11) reaches the half power point of 0.707 when $N\pi\frac{d}{c}f_0(\sin\theta - \sin\theta_0) \cong 0.442\pi$ which results in the following equality.

$$(sin\theta - sin\theta_0) \cong \frac{0.442c}{Ndf_0} \tag{A.12}$$

If (A.12) is solving for a boresight beamwidth, the small angle approximation and the symmetry of the array factor may be used to arrive at the following result:

$$(\theta - \theta_0) \cong \frac{0.442c}{Ndf_0}$$

$$Beamwidth = 2(\theta - \theta_0) \cong \frac{0.884c}{Ndf_0} \tag{A.13}$$

The next step is to again use (A.12), but fix θ to θ_0 and allow for the frequency to vary as follows:

$$AF(f) = \frac{\sin\left[N\pi\frac{d}{c}\sin\theta_0(f - f_0)\right]}{N\sin\left[\pi\frac{d}{c}\sin\theta_0(f - f_0)\right]} \cong \frac{\sin\left[N\pi\frac{d}{c}\sin\theta_0(f - f_0)\right]}{N\pi\frac{d}{c}\sin\theta_0(f - f_0)} = 0.707 \tag{A.14}$$

Just like with (A.12), equation (A.14) is at its half power point when the argument $N\pi\frac{d}{c}\sin\theta_0\,(f - f_0) \cong 0.442\pi$.

$$(f - f_0) \cong \frac{0.442c}{Nd\sin\theta_0} \tag{A.15}$$

$$\text{Bandwidth} = 2(f - f_0) \cong \frac{0.884c}{Nd \sin\theta_0} \cong \frac{Beamwidth * f_0}{\sin\theta_0} \quad \text{(A.16)}$$

Equation (A.16) is a good rule of thumb to relate the bandwidth to the beamwidth and is the result found by Schrank. One needs to note that when the antenna is steered to boresight, it has an infinite bandwidth since no phase shift is needed. Even though no phase shift is needed for a boresight steering angle, equation (A.16) uses the beamwidth of a boresight steering angle as a mathematical convenience.

A.1.5 Analysis of the Bandwidth Estimate

Much like (A.10), equation (A.16) is only an estimate and is useful for quick analysis. It makes some assumptions that may not necessarily be true, but Figure A-3 below shows that (A.16) is actually a very accurate way to predict the bandwidth for large values of N. Figure A-3 is a plot of the error between the result from (A.16) and the true value when one solves (A.14) iteratively. When there are less than ten elements in the array, there can be an error from 0.5% - 10%. Beyond this, the error is below 0.5% and is tolerable.

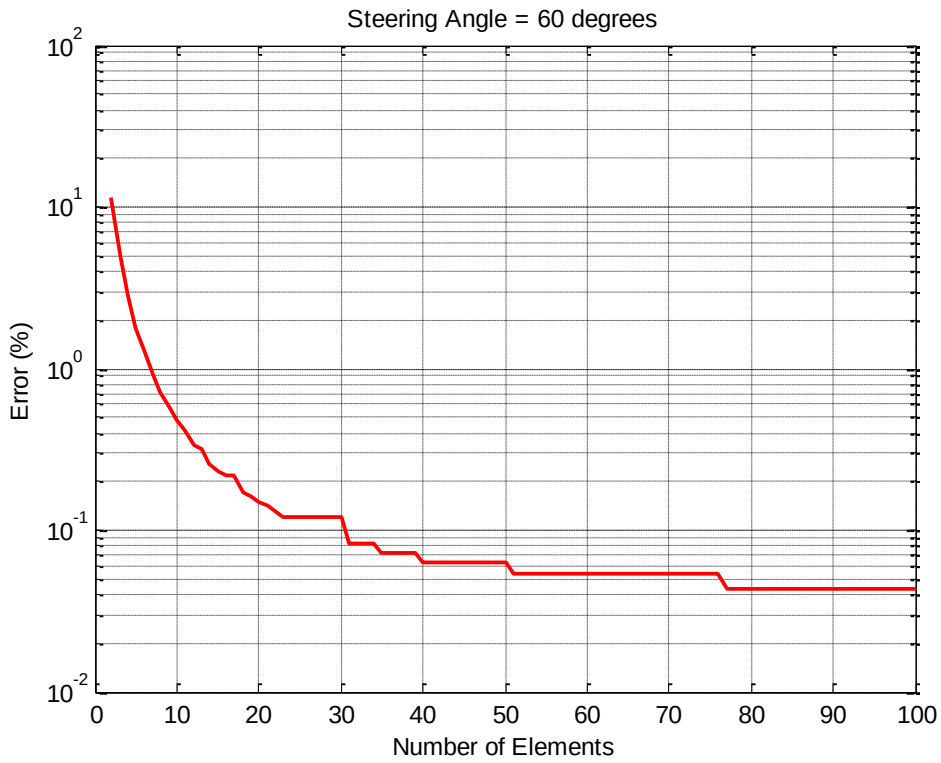

Figure A-3 - Percent Error of Estimated Array Bandwidth

One final thing to note about (A.16) is that it was derived to solve for the half power bandwidth. For some applications, it may be unacceptable to incur a 3 dB loss for parts of the signal and a new equation will need to be used. A procedure similar to that of finding (A.16) could be done for every conceivable loss bandwidth; however, one can also use a computer simulation to iteratively solve (A.14).

A.2 SIMULATIONS

A.2.1 Graphical Interpretation of the Problem

It is useful to think of the losses associated with narrowband beam forming in terms of the array factor, or antenna pattern of the phased array. For this example, assume there is a linear phased array with 100 elements that is designed to work at 3.0 GHz with phase shifters. According to (A.16), this array should have a 3 dB bandwidth

of 61.2 MHz, or 2.0% of its carrier frequency. If half of this frequency change is used to find the change in angle using (A.9), one will find that the phase shifter will steer this frequency to 59 degrees. The figure below shows the antenna pattern for this array and one will notice that the lower frequency of the bandwidth, denoted by the red dot, falls on the -3 dB point of the array factor.

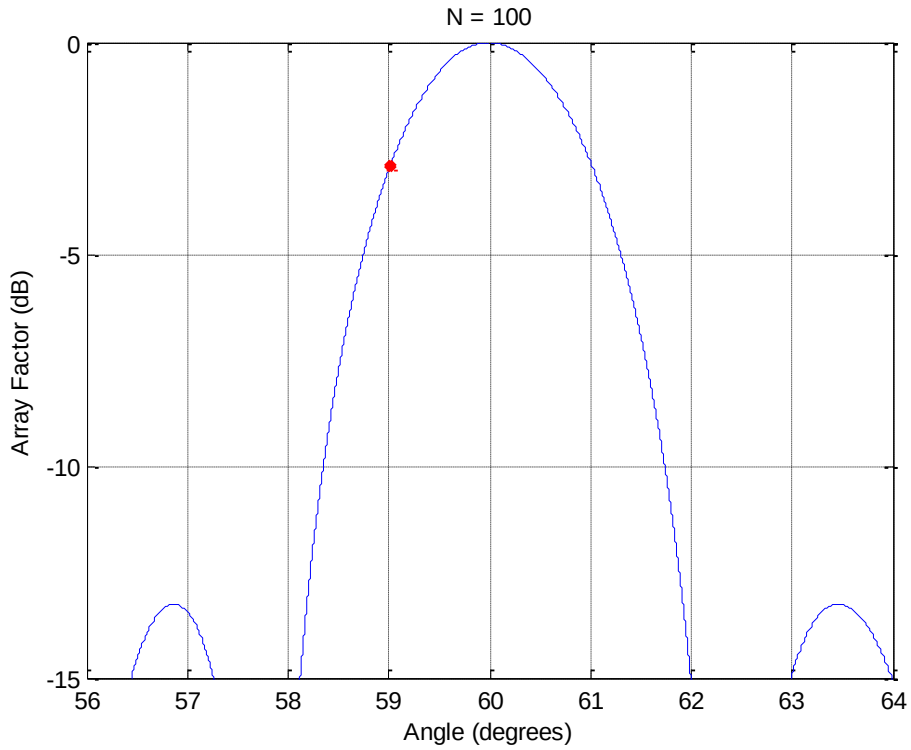

Figure A-4 - Received Power of -3 dB Frequency

A.2.2 How the Phenomenon Changes Signals

In addition to seeing a graphical representation of what is happening with off frequencies in a phase shifting arrays, it is also interesting to see the affect on the received signals. Figure A-5 shows a linear frequency modulated pulse at baseband that lasts 1 microsecond and sweeps from DC to half the bandwidth solved in the last section. It uses the same 100 element array and the signal is received at 60 degrees. One can see

that the high frequency components of the signal are attenuated due to the loss generated from the antenna pattern and are about 3 dB from the maximum signal strength.

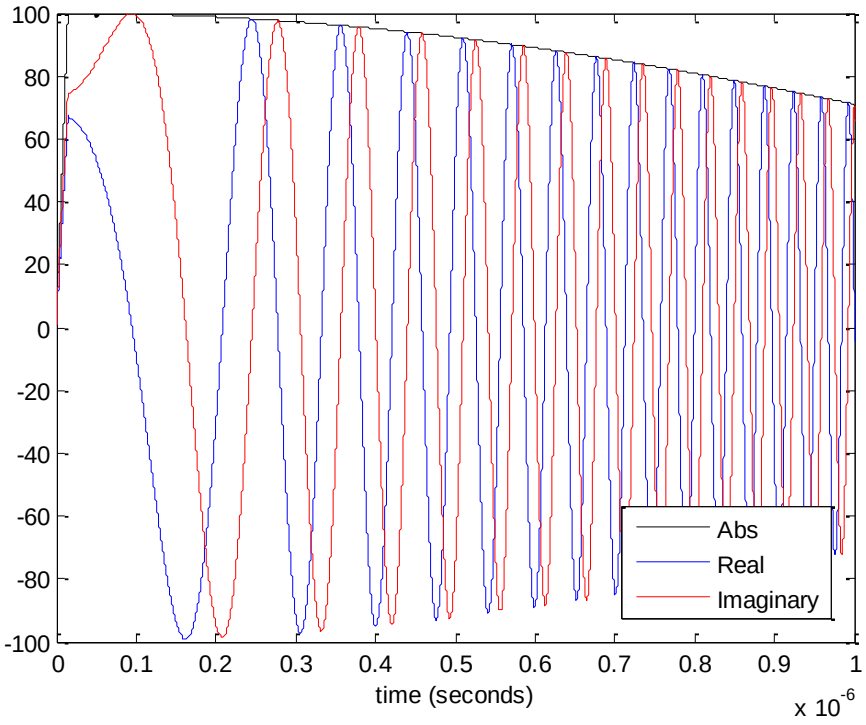

Figure A-5 Wideband Signal Received by Phase Shifting Array

A.2.3 Optimal Steering Angle for a Range of Frequencies

The final figure depicting how a wideband signal is affected by phase shifters is Figure A-6 which is a plot of several narrowband signals and their responses to certain phase shifts. The center frequency of the array in this simulation is 3.0 GHz, and narrowband signals from 2.0 to 4.0 GHz are applied to the array. The signal at each frequency is subjected to a phase shift consistent with steering angles from -90 to 90 degrees. The results plotted are the power received at given frequencies and angles. The signals of interest happen to be arriving from 30 degrees, so the center frequency obviously has its maximum received signal when the array is steered to 30 degrees.

However, one can see that a different steering angle, and thus phase shift, is needed as the frequency moves away from the center frequency.

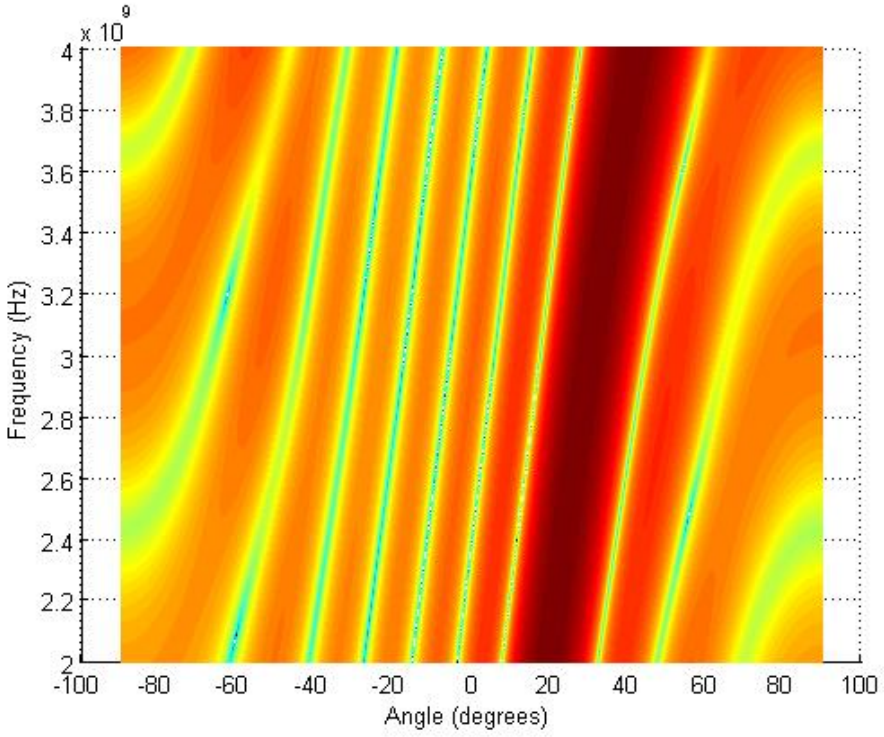

Figure A-6 - Angular Response for a 2 GHz Frequency Range

A.2.3 Bandwidth vs Attenuation

The equations used in this paper were derived to solve for the bandwidth that corresponds to a 3 dB loss in signal strength at the most extreme frequencies of the signal. This may not be an acceptable loss for some systems or may be too harsh a restriction. Below in Figure 7, the bandwidths are shown corresponding to a range of losses for various arrays.

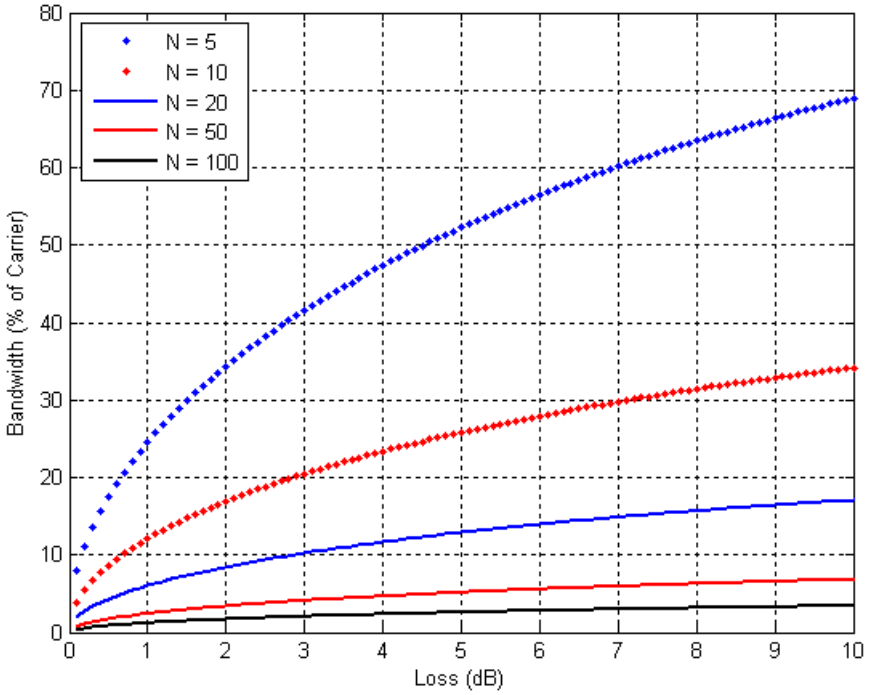

Figure A-7 - Loss vs. Bandwidth for Various Arrays

A.3 CONCLUSION

This appendix showed that phase shifters are an inadequate approach to beam forming for in arrays receiving multi-frequency signals. The phase shifters will steer different frequency components of the signal to different angles of arrival that may be outside the beam of the antenna. Analysis was done to show when this loss became too great and when another approach to beam forming would be needed. These results were then demonstrated in a series of simulations. Although phase shifters are not suitable for wideband beam forming, there are methods available to do this which are the subject of later papers.

APPENDIX B

ESTIMATION OF SIGNAL PARAMETERS VIA ROTATIONAL INVARIANCE TECHNIQUES

This thesis was about SABC technique which assumes that techniques may be used to solve for the angle of arrival of sources of interference. There are various methods to solve such as maximum likelihood estimation and multiple signal classification. However, the former has poor resolution and the latter is inconvenient for computational reasons. SABC instead uses Estimation of Signal Parameters via Rotational Invariance Techniques (ESPRIT) because it has fine resolution and is more practical computationally than MUSIC. This appendix first reviews the theory behind ESPRIT, then details the computational considerations.

B.1 THEORY OF ESPRIT

Consider a linear array with M elements uniformly spaced a distance of $d = \frac{\lambda_c}{2}$, where λ_c is the wavelength of f_c, the center frequency. If there are J sources of interference present, then the signal in element m can be written as:

$$x_m(t) = \sum_{j=1}^{J} s_j(t) e^{-j2\pi f_c (m-1)\frac{d}{c}\sin\theta_j} + n_m(t) \qquad \text{(B.1)}$$

where $s_j(t)$ is the signal of the j[th] source of interference, $n_m(t)$ is the noise in the m[th] element, and θ_j is the angle of arrival of the j[th] source of interference. Equation (B.1) can be written in vector form as shown in (B.2).

$$\mathbf{x}(t) = A\mathbf{s}(t) + \mathbf{n}(t) \tag{B.2}$$

where **x**(t) is an [Mx1] vector of the element's signals, A is a [MxJ] matrix of [Mx1] steering vectors, **s**(t) is a [Jx1] vector of the interference sources, and **n**(t) is an [Mx1] vector of noise signals. One may now solve for the covariance of the elements.

$$\begin{aligned} R &= E\left[\mathbf{x}(t)\mathbf{x}(t)^H\right] = AE\left[\mathbf{s}(t)\mathbf{s}(t)^H\right]A^H + \sigma_n^2 I \\ &= ASA^H + \sigma_n^2 I \end{aligned} \tag{B.3}$$

In (B.3), the sources of interference are assumed to be uncorrelated so S is just a diagonal matrix of the powers of the sources and σ_n^2 is the power of the noise. The covariance matrix has the following eigendecomposition:

$$R = V_s \Lambda_s V_s^H + V_n \Lambda_n V_n^H \tag{B.4}$$

where V_s and V_n are the matrices of eigenvectors of the signals and noise, and Λ_s and Λ_n are diagonal matrices of the eigenvalues of the signals and noise respectively. Since A and V_s occupy the same vector space, A can be mapped to V_s as is shown below:

$$V_s = AT \tag{B.5}$$

We may now define two new matrices $J_1 \triangleq \left[I_{M-1}\mathbf{0}\right]$ and $J_2 \triangleq \left[\mathbf{0}\, I_{M-1}\right]$, where I_{M-1} is an [(M-1)x(M-1)] identity matrix and **0** is an [(M-1)x1] zero vector. These two matrices may be used to transform V_s into two new matrices that are shown in (B.6) and (B.7).

$$V_{s1} = J_1 V_s = J_1 AT = A_1 T \tag{B.6}$$

$$V_{s2} = J_2 V_s = J_2 AT = A_2 T \tag{B.7}$$

It can be shown that:

$$A_2 = A_1 \Phi \tag{B.8}$$

where

$$\Phi = \begin{bmatrix} e^{-j2\pi f_c \frac{d}{c} \sin\theta_1} & 0 & \cdots & 0 \\ 0 & e^{-j2\pi f_c \frac{d}{c} \sin\theta_2} & & 0 \\ \vdots & & \ddots & 0 \\ 0 & 0 & 0 & e^{-j2\pi f_c \frac{d}{c} \sin\theta_J} \end{bmatrix}.$$

The matrix Φ is useful because the angles of the diagonal elements contain the information about the angles of arrival of the interference sources. This matrix is not directly measurable; however, by solving for the eigenvector matrix of the covariance matrix one may solve the relationship between V_{s1} and V_{s2}.

$$V_{s2} = V_{s1} \Gamma \tag{B.9}$$

With substitution, (B.9) becomes:

$$A_2 T = A_1 T \Gamma \tag{B.10}$$

and can be solved for Γ as shown below:

$$\Gamma = T^{-1} A_1^{-1} A_2 T = T^{-1} \Phi T \tag{B.11}$$

Therefore, if one performs an eigendecomposition on Γ, the eigenvalues will correspond to the diagonal elements of Φ and the angle information about the interference sources may be obtained.

B.2 COMPUTATIONAL COST OF ESPRIT

The first row of Table 4-1 made a claim about how many FLOPs were needed for ESPRIT; this section shows how that result was found. Table B-1 shows the particular steps needed for this ESPRIT algorithm and the FLOPs needed for each step. In this table $\widehat{M}$ is the number of elements used for the ESPRIT algorithm, J is the number of sources of interference, and K is the number of samples used to form the covariance matrix. It should be noted that the number of elements used must be greater than the number of sources of interference. The first two rows of the table involve forming the covariance matrix of the elements used. The third row shows how many FLOPs are needed to do a singular value decomposition of the covariance matrix for only the singular values and the V matrix according to Golub [19]. Next, the matrices V_1 and V_2 are formed from the multiplications of the J matrices defined in B.1. The rest of the rows show how many FLOPs are needed to solve for Γ, its eignenvalues, and the angles that correspond to these eigenvalues. Row five is accomplished with an algorithm in Golub [19]. Row six requires fewer FLOPs than row three because only eigenvalues, and thus only one matrix need to be solved by the SVD.

Table B-1: FLOPs needed for the ESPRIT algorithm.

$\hat{R} = \hat{X}\hat{X}^H$	$2\hat{M}^2K - \hat{M}^2$
$\hat{R} = \frac{1}{K}\hat{R}$	$\hat{M}K$
Solve for Σ *and* V *with SVD of* $\hat{R}$	$12\hat{M}^3$
$V_1 = J_1V_s;\ \ V_2 = J_2V_s$	$4\hat{M}^2J - 2\hat{M}J$
$\Gamma = V_1^{\dagger}V_2$	$2\hat{M}J^2 + 11J^2$
Solve for eigenvalues with SVD of Φ	$\frac{8}{3}J^3$
$\theta_j = a\sin\left(\frac{a\tan(\sigma_j)}{\pi}\right)$ *for* $j = 1:J$	$3J$
Total	$12\hat{M}^3 - \hat{M}^2 + 3\hat{M}K + 4\hat{M}^2J + \frac{8}{3}J^3 + 11J^2 + 3J - \hat{M}J$